INTERNATIONAL ATOMIC ENERGY AGENCY
UNITED NATIONS EDUCATIONAL, SCIENTIFIC AND CULTURAL ORGANIZATION
INTERNATIONAL CENTRE FOR THEORETICAL PHYSICS
I.C.T.P., P.O. BOX 586, 34100 TRIESTE, ITALY, CABLE: CENTRATOM TRIESTE

SMR.703 - 1

WORKING PARTY ON:
MECHANICAL PROPERTIES OF INTERFACES

23 AUGUST - 3 SEPTEMBER 1993

"Basic and Introductory Lectures on Fracture"
(Part I)

"Physics of Fracture"

Robb THOMSON
United States Department of Commerce
National Institute of Standards and Technology
Materials Science and Engineering Laboratory
Building 223
Gaithersburg, MD 20899
U.S.A.

SOLID STATE PHYSICS, VOLUME 39

Physics of Fracture

ROBB THOMSON

National Bureau of Standards
Washington, D.C. 20234

I. Introduction

Thirty years before the date of this article, one of the founding editors of this series proposed and elaborated the concept of the imperfection in a nearly perfect solid[1] as a way of understanding the structure-sensitive properties of crystalline matter. His synthesis has since proven to be one of the bases upon which much of modern materials science rests. Included in the original list of fundamental imperfections was the dislocation, which was originally proposed by Orowan *et al.* in 1934[2–4] to explain the plastic mechanical properties of a solid. We suggest that the crack should be added to this list, and argue that the crack and dislocation taken together comprise what might be termed a "complete set" for understanding the mechanical failure of crystalline materials.

The argument follows from the fact that materials failure exhibits a bipolar character; i.e., materials are classifiable in terms of their relative brittleness or ductility. A material at the extreme ductile pole flows plastically like taffy when stressed above its elastic limit, and finally separates by necking, as depicted in Fig. 1. Pure copper single crystals are excellent prototypes of this extreme pole. The necking failure in this crystalline case involves only dislocation processes, and is often termed plastic rupture. At the opposite pole of brittle failure, the material is perfectly elastic up to a critical stress at which it cleaves catastrophically (Fig. 2). Ordinary silicate glasses are the most widely known examples of brittle fracture, but, because it is crystalline, silicon at room temperature is perhaps a better prototype. At this pole, no dislocation activity

[1] F. Seitz, *in* "Imperfections in a Nearly Perfect Solid" (R. Smoluchowski, ed.), p. 3. Wiley, New York, 1952.
[2] E. Orowan, *Z. Phys.* **89**, 605, 634 (1934).
[3] M. Polanyi, *Z. Phys.* **89**, 660 (1934).
[4] G. I. Taylor, *Proc. R. Soc. London Ser. A* **145**, 362 (1934).

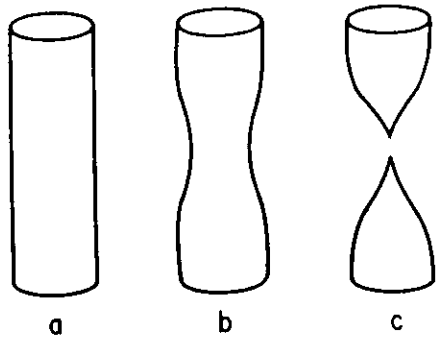

FIG. 1. A rod of ideally ductile material when pulled develops a region of plastic instability which finally thins uniformly down to a sharp point.

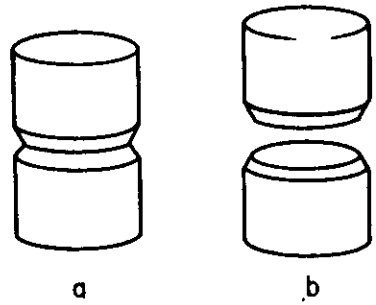

FIG. 2. An ideally brittle material when pulled separates suddenly by cleavage with no prior or simultaneous deformation. A notch is shown which localizes the plane of fracture.

at all is observable at failure, and the fracture is due to the propagation of a single atomically sharp cleavage crack right through the specimen.

The conceptual importance of the two types of defects operating at these opposite poles derives from the fact that the material in each case fails at an average stress level which is often many orders of magnitude less than the theoretical strength of the material, expressed in terms of its constituent atomic bonds. This low failure stress at the two polar extremes thus constitutes a fundamental problem in mechanical failure. The reader is reminded that, in the case of the dislocation, this problem is solved in principle, because the dislocation is a lattice defect whose atomically sized core contains stresses equal to the theoretical shear strength of the constituent atomic bonds. Under a modest external stress, the dislocation translates through the crystal, shearing bonds as it goes, in a progressive fashion. When it traverses a crystal from one side to another, a shear of one atom spacing results. Generation of new dislocations in the local region of the macroscopic neck in the sample then

explains its final separation. Similarly, the atomically sharp cleavage crack (Fig. 3) possesses a core of atomic size at its tip where the stresses are magnified to the tensile strength of the bonds, and when the crack passes through the crystal, again the bonds are broken progressively until the entire crystal cleaves into two halves. Thus the dislocation and crack are twin lattice defects which jointly provide an answer to this first fundamental problem of materials failure.

Fortunately for materials technology, however, the vast majority of materials are situated at neither pole, and are much stronger than pure single crystal copper, and much tougher than untreated silicate glass. (The concept of "toughness" will be defined more carefully later, but for the present it can be taken as simply the energy absorbed from the external stressing machine as the crack propagates.)

Materials of high strength and toughness have been the goals for a large portion of materials research for many years, and the detailed understanding of these properties is still elusive. Qualitatively, however, materials are tough and strong because of the rich variety of interactions dislocations have with themselves, with cracks, and with other imperfections, and perhaps the greatest conceptual difficulty of the subject is connected with the collective character of this interaction. Thus the understanding of the two complementary material properties of strength and toughness constitutes a second major fundamental problem in materials science of very great proportion, which is yet largely unsolved. In this article, we shall be primarily concerned with toughness and the properties of cracks, which constitutes only half of the total problem associated with mechanical failure, though the problem of strength is closely related to and overlaps that of toughness.

It is possible to get close to the heart of the problem of toughness by focusing on the structure of the underlying cracks in a solid. In the next section, where some of the background phenomenology of fracture will be

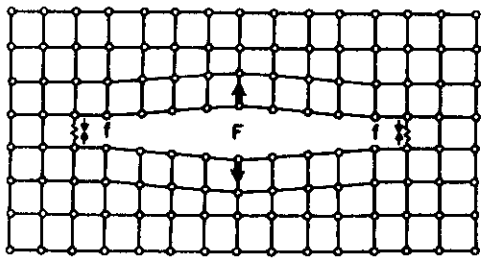

FIG. 3. Diagram of a crack in a two-dimensional square lattice with external forces exerted at the center of the crack. Bonds at the two crack tips are nonlinear. The nonlinear attractive forces at the tip are labeled f and the external applied forces at the center of the crack are labeled F.

displayed, the ductile/brittle duality will be found to extend or persist well into the middle ground of the ductile/brittle axis. It persists in the sense that even though a failure may appear macroscopically to be cracklike, on closer microscopic examination, the "crack" will be found to be quite blunt and irregular in shape, without the characteristic atomically sharp tip of the cleavage crack. On the other hand, a crack showing considerable toughness may consist of a sharp underlying cleavage crack, but be associated with large numbers of dislocations. On moving from relatively ductile to relatively brittle materials, the shape of the underlying crack changes from a blunt notch or rounded hole which expands by purely plastic means (i.e., dislocation formation from the material ahead of the crack, or from corners on the crack surface, either of which usually leads to necking on a microscale) to a sharp crack which advances by cleavage. This change in mechanism when induced in a given specimen or structure usually has dramatic, tangible, and even practical consequences, as for example when a material becomes embrittled by external chemical attack.

A valuable key in the approach to the toughness problem is to distinguish between an intrinsically brittle material and an intrinsically ductile one in terms of the atomic structure of their cracks. We show that the first class of materials can sustain an atomically sharp crack stably in the lattice without breakdown by dislocation generation, while the second class cannot. In those materials where the sharp crack is stable, cleavage crack growth is possible; in the opposite case, only tougher ductile crack growth is possible. This distinction between intrinsic brittle or ductile cracks may depend upon external conditions, as well as on the material itself. This distinction will be modified as we develop it, for example, by considering a middle ground where the crack is only barely stable, and by considering the effects of dislocations generated in the bulk material; but without undercutting its overall usefulness in sorting out the enormously complex phenomenology of fracture.

After establishing the basic distinction between intrinsically ductile and intrinsically brittle materials, the study of toughness then proceeds to develop the dislocation interactions with the two types of cracks and from this to establish the fracture criterion. Unfortunately, much of this analysis, especially for ductile cracks, still remains to be done, and even in the case of the brittle crack, is only in semiquantitative form. But the central role of the structure of cracks also emphasizes a familiar type of problem to physicists, namely the atomic structure of defects. In the case of the crack, the severe nature of the distortion of the lattice by the defect puts the quantitative study of the structure of cracks still largely in the "research to be done" category.

The previous paragraph is couched in theoretical terms. But the science of fracture at the time of writing is entering a period of intense development on the experimental side as well, which is generating a theory–experiment

confrontation and consequent flowering of our understanding, reminiscent of the period 1955–1965 in dislocation research. This experimental development has largely been due to the work by Hockey in brittle materials, and Ohr, Wilsdorf, Neuman, their co-workers, and others in ductile materials; usually working with thin films in electron microscopes. In a sense, then, this article is able to point to some guiding principles, and initial theoretical and experimental findings whose major purpose will be to point with hope toward the future.

In an article like this, it will be necessary to establish some background information. Therefore, in the next section, a series of microphotographs will be presented to provide the reader with a necessary observational perspective. In Part III, the required results from the elastic analysis of cracks and dislocations will be presented. In Part IV, a central theorem of Eshelby on the force exerted on elastic singularities will be used to derive the forces on cracks and dislocations and the interactions between them. Then, in Parts V and VI, the central theme of the structure and properties of sharp cracks in lattices, including interactions with external chemical environments, will be addressed. In Part VII, the idea of dislocation shielding of static and moving cracks is presented along with the simple available models for fracture toughness and the available experimental evidence.

We shall not attempt to cover the more applied aspects of fracture, partly because it would be unsuitable in an article emphasizing the physical fundamentals of fracture, but also because the more important applications still await an adequate description in terms of fundamental ideas. Hydrogen embrittlement and fatigue crack initiation are just two examples where a final description is probably still well in the future, even though some of the fundamental tools are coming to hand. Nor shall we have space to consider fracture in polymers, where the effects of crazing bring up a different set of phenomena that are now being successfully tackled.

Finally, we note here that the subject of fracture is one involving a number of disciplines. We shall, of course, repeatedly delve into physics, chemistry, and materials science. However, fracture science also deeply involves continuum mechanics. The reason is easily seen from inspection of Fig. 3: A crack requires an external force for its existence. If this force disappears, in principle the lattice will simply heal itself. Hence, the manner in which this force manifests itself at the crack tip is a continuum mechanics problem that will involve the way the force is applied to the external surfaces of the body, and may involve sophisticated mathematical descriptions of deforming media. Fortunately, we shall find it possible to condense most of the mechanical aspects of the problem into a local parameter at the crack tip called the local stress intensity factor. However, the reader should be aware that there are classes of problems such as propagation of cracks through plastic media, or the role of plastic instability in the propagation of ductile fracture, where continuum plasticity approaches must be used.

II. Observational Background and Initial Concepts

A casual observation of the fracture of any practically useful engineering material shows a very complex phenomenon. This section will thus be devoted to a demonstration of some of this complexity, and will also demonstrate the observational basis for the scientific approach which we have outlined in the Introduction, but which must be firmly established on an observational basis. At the same time, the reader will appreciate from a perusal of the fractographs which we will display here the limitations of making quantitative predictions of fracture toughness for engineering materials.

1. Macroscopic Fractographic Observations

Before displaying the rather sobering complexity which we have alluded to above, Fig. 4[5] illustrates the beautifully symmetric brittle fractures which are possible in a material such as glass. The figure shows a hertzian crack with cylindrical symmetry produced by an indentation at one point on the surface of the glass. The fact that the glass is completely isotropic results in a highly symmetric fracture mode and a highly regular overall configuration. A BB pellet stopped by ordinary plate glass will display such a hertzian crack. At the opposite extreme, Fig. 5[6] illustrates the chisel point which is formed when a highly ductile metal is pulled to ultimate fracture. Each of these two examples is of course a direct illustration of the two poles of fracture shown schematically in Figs. 1 and 2 of the Introduction.

FIG. 4. A Hertzian crack produced in the upper surface of a block of glass by a round indenter (after Roesler[5]).

[5] F. C. Roesler, *Proc. Phys. Soc. B* **69**, 981 (1956).
[6] H. G. F. Wilsdorf, *Mater. Sci. Eng.* **59**, 1 (1983).

FIG. 5. A chisel point formed in a rod specimen of gold after necking and rupture. Original specimen was 0.15 cm in diameter (courtesy of H. Wilsdorf[6]).

2. MICROSCOPIC OBSERVATIONS

On a microscopic level the rough surface typical of a high-toughness metal still displays a high complexity. The surface is highly dimpled on a micrometer level and below, as shown in Fig. 6. These dimples have been shown to be caused by the formation of holes which form ahead of a main crack as shown in Fig. 7. As the crack grows, the holes enlarge by plastic means and coalesce with the main crack and with other holes in the vicinity. In these cases the growth and coalescence of the voids with the main crack are really a manifestation of the necking process on a microscale. As shown in Fig. 6, the larger voids are found to be nucleated at the site of precipitated particles in the

FIG. 6. Ductile fracture surface, showing the final dimpled structure of hole growth. Precipitate particles are visible in some of the dimples which served as nucleation sites for the holes (courtesy of C. Interrante).

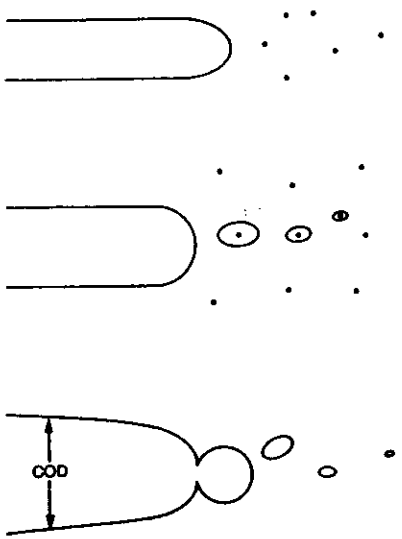

FIG. 7. Schematic drawing of the development of a ductile fracture from a blunt crack embedded in a material containing inclusions. Microcracks are nucleated at the inclusions, which are blunted in turn. (COD is an abbreviation for crack opening displacement.)

matrix. The precipitate particles may fail on their interface with the matrix, or brittle precipitates may cleave. In either case, they are left behind in the holes, as shown in Fig. 6.

In a brittle ceramic, or in a steel in an embrittled condition (such as when under hydrogen or other chemical attack, or when the temperature is low and the strain rate high), the fracture morphology is different. Figure 8[7] shows an intergranular brittle fracture in which the crack proceeds without any obvious void formation, and a very clean form of separation at the grain boundaries occurs. Transgranular brittle fracture can also occur, often mixed with the intergranular variety. This example shows how important the metallurgical and ceramic microstructural variables such as grain-boundary segregation and second-phase coarsening are to fracture toughness.

3. PROTOTYPE FRACTURES

In the next set of observations, the phenomena characteristic of more ideal conditions are illustrated. Figure 9 shows the results of Hockey[8] for cracks in silicon. Figure 9a shows a completely brittle cleavage crack at low temperatures in which no dislocation activity is observable. Figure 9b shows that the cracks in silicon are nearly completely reversible. This crack presumably has grown beyond its final position, with a network of misfit dislocations appearing between the initial and final positions of the crack after regression has occurred. Figure 9c shows a crack grown in silicon above the ductile transition temperature, in which significant dislocation activity in the presence of the crack tip is visible. It is not clear whether these dislocations are formed out of the crack after it stops, or whether they have been carried along by the crack from the deformation zone in which the crack itself was formed. Figure 10 shows the electron channeling pattern of a transgranular cleavage surface in embrittled steel, which illustrates that dislocations are generally present even in very brittle fracture in steels, except at high crack speed.

Figure 11[9] shows the crack configuration of iron–2.6 at.% silicon. The crack is wedge-shaped just as one would expect if dislocations were emitted on

[7] E. Fuller, unpublished photograph of a crack in Si_3N_4 at high temperature.

[8] B. Lawn, B. Hockey, and S. Wiederhorn, *J. Mater. Sci.* **15**, 1207 (1980).

FIG. 8. Brittle crack in a ceramic.[7] The crack has opened along the grain boundaries of the material, giving rise to a very irregular morphology. Such forms of brittle fracture are also observed in metals.

[9] H. Vehoff and P. Neumann, *Acta Metall.* **28**, 265 (1980).

FIG. 9. (a) An electron microscograph of a fully brittle crack in Si. In the photograph, the crack is seen edge on. In (b) a brittle crack has regressed from its initial position, leaving a network of misfit dislocations on the closed portion of the cleavage plane. (c) Cracks formed in Si at 500 °C are associated with dislocations as shown (see Lawn *et al.*[8]). (Courtesy of B. Hockey.)

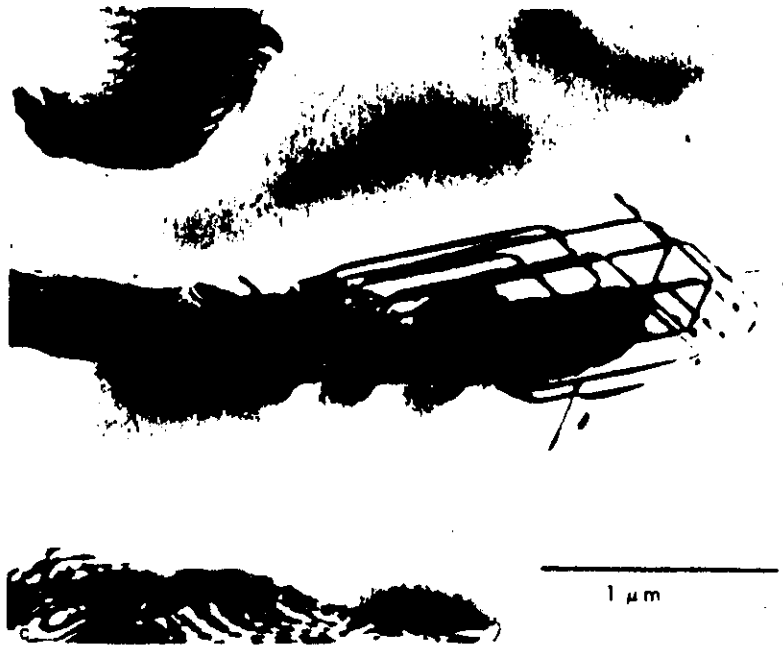

FIG. 9. (*Continued*).

slip planes intersecting the crack tip (see also Fig. 43). In this case the material "slides off" on its slip plane which is at an oblique angle to the plane of the crack. When hydrogen is introduced into the system (Fig. 11a) the angle is made more acute, showing that cleavage and emission take place simultaneously.

Figure 12 shows the experimental configuration used by Ohr and co-workers.[10] When a region in the very thin section near the hole is imaged in the microscope, the results are shown in Fig. 13.[11] In this case the crack spews out screw dislocations on its cleavage plane. The crack has a substantial region near its tip (termed an elastic enclave or dislocation free zone) where no dislocations are present. Similar experiments have been performed in a variety of other metals (see Table I).

A more typical form of purely ductile failure is shown in Fig. 14,[12] where experiments performed by Wilsdorf,[6] again in thin foils, exhibit a more normal

[10] S. Ohr, J. Horton, and S. Chang, *in* "Defects, Fracture, and Fatigue." (G. C. Sih and J. W. Provan, eds.), p. 3. Nijhoff, The Hague, 1983.
[11] S. Kobayashi and S. Ohr, *Scripta Metall.* **15**, 343 (1981).
[12] R. Lyles and H. G. F. Wilsdorf, *Acta Metall.* **23**, 269 (1975).

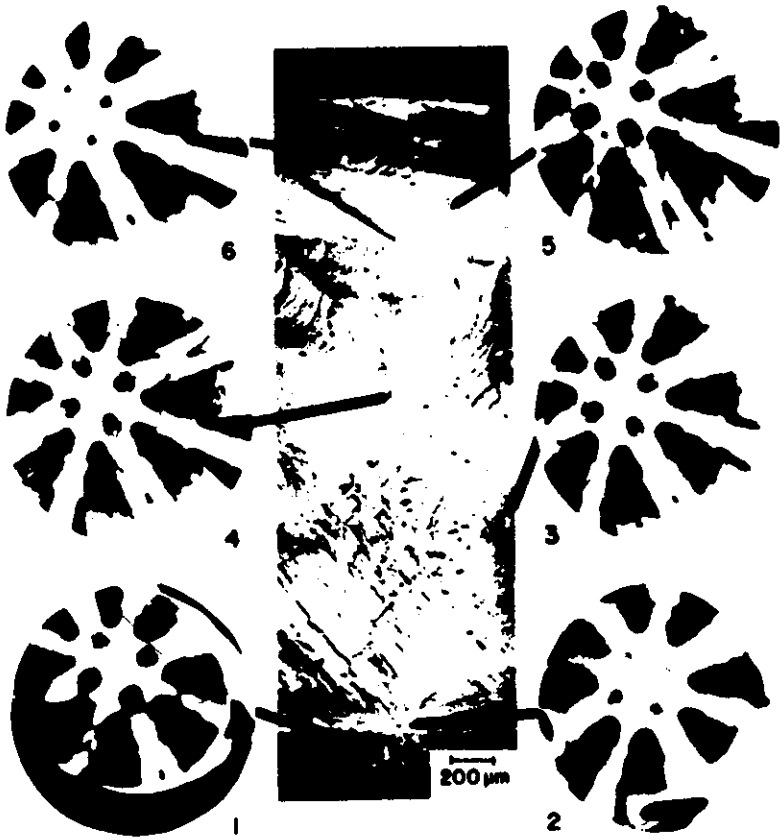

FIG. 10. Electron channeling patterns from portions of a cleavage crack in hydrogen embrittled steel. A blurred pattern indicates lattice plane rotations caused by presence of dislocations. In the figure, the crack accelerates from its initial position at rest in the region of pattern 1 to a high velocity near pattern 6. At the high velocity (an appreciable fraction of the sound velocity), there is no measurable increase in the dislocation density above that of the initial material. (Courtesy of W. Gerberich and K. A. Peterson.)

failure by hole growth and coalescence. The event shown in the figure is the final result of the chisel necking shown in Fig. 5. In this case the foil thins by plastic processes and small holes form in the dislocation cell walls, which then grow to a size equal to the film thickness and the large holes shown in the figure then become visible. These holes are crystallographic in shape corresponding to the slip planes in the material. A mixed form of growth seems to take place in which some dislocations are emitted from the crack tip itself, while others are generated at sources in the medium very close to the crack tip. Although these films are very thin, the hole formation and growth processes illustrated

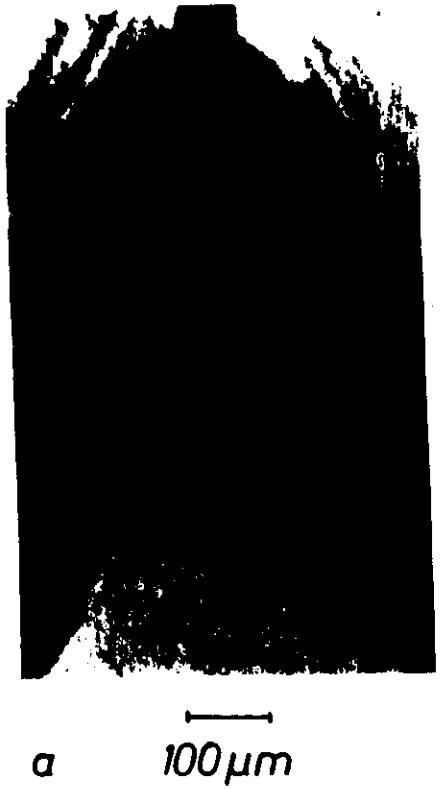

FIG. 11. In (a) sharp cracks are formed in a hydrogen atmosphere in Fe (+ Si). In (b) the crack opens entirely by dislocation slide-off at the crack tip. In both cases, dislocations are emitted from the crack tip, and form slip bands. In (a), cleavage must also be present. The angle of the wedge opening in (b) is defined by the intersection angle of the two slip planes with the crack plane (after Vehoff and Newmann[9]).

are thought to be analogous to those taking place in bulk samples such as in Figs. 6 and 7. In Fig. 14, of course, the void generation takes place in the dislocation cell walls rather than at precipitate particles, perhaps corresponding to the smaller holes formed in Fig. 6. It is in fact generally observed on close examination that the large voids formed at large precipitated second-phase particles are often connected by void sheets composed of very small voids, and the question of whether these sheets are created at small precipitates or are generated at dislocation cell boundaries has not been fully sorted out.[6,13]

[13] A. Thompson and P. Weirauch, *Scripta Metall.* **10**, 205 (1976).

FIG. 11. (*Continued*).

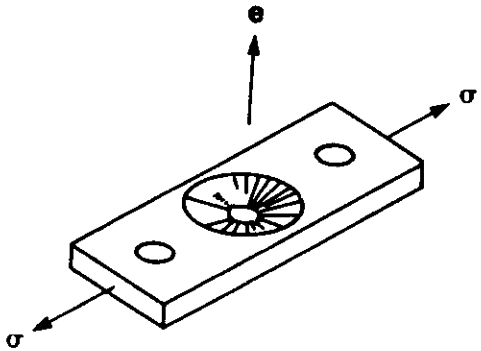

FIG. 12. Specimen geometry used in electron microscope fracture experiments by Ohr and co-workers.[10] The crack grows out of the thinned region nearest the hole in the center.

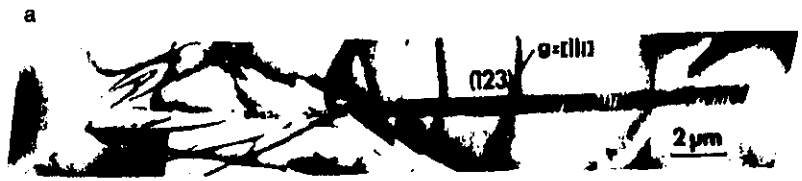

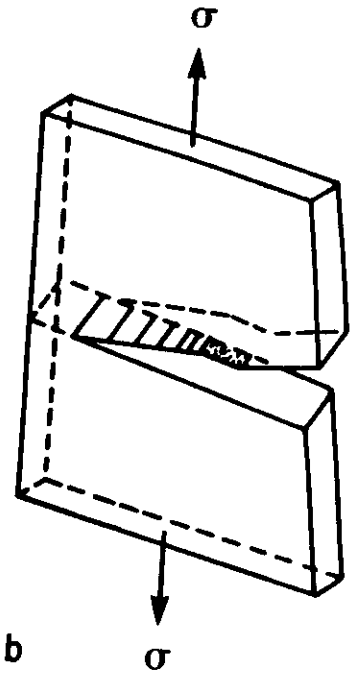

FIG. 13. (a) Dislocations emitted from the tip of a crack in a foil of copper. The crack has grown from the left. Immediately ahead of the crack is a region free of dislocations. The pile-up of dislocations is seen extending on the cleavage-slip plane to the right. In (b) the crack dislocation geometrical configuration is illustrated (after Kobayashi and Ohr[11]).

FIG. 14. Side view of a growing fracture in a thin film of gold. Holes are shown nucleating ahead of the crack (see Lyles and Wilsdorf[12]). (Courtesy of H. G. F. Wilsdorf.)

4. Fracture Mode and Crack Dislocations

The previous fractographs indicate that real cracks are three-dimensional defects whose fracture planes may be very rough surfaces, that even brittle fractures may take place on the three-dimensional network of a grain boundary structure, and that interaction with various kinds of imperfections in a material is common. Nevertheless, for analytical purposes, it is desirable to idealize a crack line as a one-dimensional line defect on a flat cleavage plane. There are, then, three modes of cracks corresponding to the different orientations of the external stress with respect to the fracture plane. These three modes are analogous to the two different classes of dislocations: screw and edge. In the case of the crack, a cut is made in the medium which becomes the cleavage plane, and simple shear or tensile stresses are exerted on the external surfaces of the specimen. In Mode I the stress is a tensile stress with principal axis normal to the cleavage plane, as shown in Fig. 15a. This mode is the only one leading to physical fracture, because, unless the external stress physically separates the two surfaces on the cleavage plane, then rewelding would occur even after the stress is applied. In Mode II the stress is a shear parallel to the cut in the x_1 direction (we use the coordinate system of Fig. 16a). In Mode III the stress is a shear parallel to the cut in the antiplane or x_3 direction. Mode III is important because antiplane strain is associated with a particularly simple analysis, and we shall make extensive use of this analysis in order to describe results for cracks in a generic sense. Even in the case of simple two-dimensional cracks, mixed cases are common. For example, a crack may be produced which is primarily Mode II or III, but with enough Mode I present to separate the cleavage plane.

We note here an idea originally proposed by Friedel[14] that the displacement on the cleavage plane of a crack may be represented by a distribution of dislocations of appropriate Burgers vector. Such a representation can be used analytically to describe the stress field of a cleavage crack (see Part III).

5. The Observational Basis for Fracture Science

From the selected illustrations above, an observational basis can be constructed for our approach to fracture, as follows.

(a) In practice, cracks are most often flaws of a complex three-dimensional form which sometimes only vaguely approximate the three idealized modes of

[14] J. Friedel, "Les Dislocations," p. 214. Gauthier-Villars, Paris, 1956; "Dislocations," p. 320. Pergamon, London, 1964. See also B. A. Bilby and J. D. Eshelby, *in* "Fracture" (H. Liebowitz, ed.), Chap. I, p. 99. Academic Press, New York, 1968.

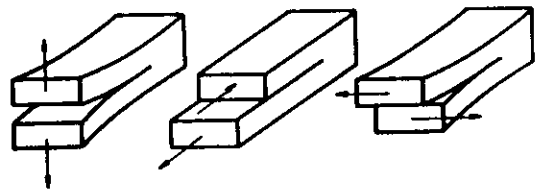

FIG. 15. The three modes of fracture. In each case, the crack is formed by making a planar slit in the material, with the crack line along the edge of the cut. In Mode I, the opening mode, the force is exerted normal to the cleavage plane. In Mode II, the force is in the plane of the crack normal to the crack line. In Mode III, or antiplane strain, the force is in the plane along the crack line. Modes II and III are shear cracks.

Fig. 15. However, because of the necessity of developing models which can be analyzed and described in accessible mathematics, we are led to the study of these idealized modes.

(b) In some solids, the crack is capable of cleavage advance without intrinsic generation of dislocations (Fig. 9). (By intrinsic is meant generation from the crack tip itself, independent of external sources.) In others, when the crack is stressed, dislocations are emitted from the tip without cleavage (Figs. 11 and 13). Crack advance in the second case takes place by ledge formation or slide-off at the crack tip, Fig. 11. The shape of the crack in the cleavage case is atomically sharp at its tip (Fig. 9). When the crack advance is controlled entirely by dislocation emission, the shape is that of a wedge whose opening angle is equal to the angle between the operating slip planes (Fig. 11; see also Fig. 43).

(c) The ubiquitous presence of dislocation sources in nearly all materials and the stress concentration around the crack tip assures that dislocations, sometimes in copious numbers, are generated which accompany the fracture process (Figs. 9 and 10). Only in exceptional cases, such as in Si at low temperatures, or in fast fracture when the crack outruns its dislocation cloud, are ideal brittle fractures observed. Since dislocations and cracks are singularities in an elastic medium (if the crack tip has a sharp angle), their stress fields give rise to strong crack–dislocation interactions which play a central role in determining the overall toughness.

(d) The effect of plasticity external to the crack is to blunt the crack by means of the steps formed on the cleavage surfaces when dislocations are annihilated there. The final macroscopic shape of the crack blunted by dislocation absorption will be determined by the combined effect of the available slip systems, stress distribution around the crack, the characteristics of the sources such as operating stress, etc., and the mobility and mean free

path of the dislocations. A variety of final shapes is thus possible, but in general the shape of the crack will not be dominated by crystallographic features as in the case for the cleaving or emitting crack. Further, such a crack (we shall often refer to blunted cracks as notches), of itself, will not advance solely by dislocation absorption under continued stressing, but will simply increase its effective radius at the tip by indefinite plastic blunting. In practice, however, inhomogeneities in the material cause microcracking to occur ahead of the main crack with subsequent hole growth (Fig. 7). Blunting of the main crack stops when a void is absorbed, and "crack" advance takes place by accretion of the voids to the main crack. The void formation and accretion also limit the necessary region of plastic activity to that surrounding the blunted crack tip; so that fracture can occur without raising the stress of the entire specimen to the plastic yield value.

We are thus led to propose three prototype cracks: cracks which cleave, cracks which emit dislocations, and plastically blunted notches which merely activate external plastic flow in the surrounding medium. The physical mechanisms in each case are quite distinct, and each type tends to correspond to a particular geometry. Mixed cases are to be expected, however. Thus, external dislocation sources usually are activated by cleavage cracks, even though the crack advances by cleavage and no hole growth is observed (Figs. 9c and 10). Likewise, in cases where the fracture is predominantly by plastic hole growth, significant portions of transgranular or grain boundary cleavage facets may be observable in the fractured surfaces. Also the initial stages of hole formation normally involve cleavage, and the whole question of how the cleavage (or emission) events are affected by the alteration of crack shape caused by dislocation absorption is unanswered. Finally, mixed cleavage–emission is possible in cases where a crack is balanced on the borderline between cleavage and emission (Fig. 11a).

The correlation between these three prototype cracks, which are classified according to their atomic structures and the mechanisms of their advance, with the overall fracture toughness and the brittle/ductile polarity, becomes the central task of fracture science. Qualitatively, the brittle pole is associated with the cleavage crack, while the emitting crack and the plastically blunted crack are forms of ductile fracture.

The crucial physical implication of this line of thought is that the structure of the underlying crack and its immediate environment determines the overall mechanical response. The atomic structure of the tip will dictate whether the crack is a cleaver or an emitter, and the properties of the dislocations and their sources in the medium and their interactions with the crack will determine whether the core crack can ever be stressed sufficiently so that cleavage or emission is possible.

Thus, the balance achieved regarding the brittle/ductile polarity in any fracture event is determined partly by the bonding of the atoms of the solid, partly by the lattice structure, partly by the microstructure of the material, and partly by the external environment. A material may change from ductile hole growth to brittle cleavage by modifying these factors in various ways. For example, for any given material, a variety of chemical species can be embrittling agents. Hydrogen in steels and water in glass are examples. Toughness is also a function of strain rate and temperature, and steels typically undergo a dramatic ductile-to-brittle transition along the axes of these parameters.

III. The Elastic Fields of Cracks and Dislocations

6. Introduction

Many scientists view elasticity as a field essentially completed by the end of the 19th century. However, in this article the mathematics of elasticity will play a much more important role than that of an ancient formalism to be briefly revisited. Rather, cracks and dislocations, viewed as interacting singularities in the elastic field, will lead to new insights into the toughness of materials, and much of the mathematics required will be unfamiliar to most readers with a nodding acquaintance with the elements of classical elasticity. For full-scale numerical calculations in a particular crystal, anisotropic elasticity is the mode of choice, and a brief review of some aspects of anisotropic theory will be given. However, we shall find the more analytic results possible in isotropic theory to be more useful in this article for developing the physical insight which is our main purpose.

The basic reference for this section is the treatise on elasticity by Muskhelishvili[15] because it contains an authoritative treatment of two-dimensional elasticity, complex potentials, conformal mapping, and Muskhelishvili singular integrals. However, it does not address cracks or fracture problems. For collateral reading on fracture, the reader is referred to the excellent articles by Bilby and Eshelby,[16] Rice,[17] Sih and Libowitz,[18]

[15] N. Muskhelishvili, "Some Basic Problems in Mathematical Theory of Elasticity." Noordhoff, Leyden, 1977.
[16] B. Bilby and J. Eshelby, *in* "Fracture" (H. Liebowitz, ed.), Chap. 1, p. 99. Academic Press, New York, 1968.
[17] J. Rice, *in* "Fracture" (H. Liebowitz, ed.), Chap. 2, p. 191. Academic Press, New York, 1968.
[18] G. Sih and H. Liebowitz, *in* "Fracture" (H. Liebowitz, ed.), Chap. 2, p. 67. Academic Press, New York, 1968.

and Goodier[19] in the series *Fracture*, edited by Liebowitz on the elastic (and plastic) treatment of cracks. Bilby and Eshelby,[16] in a *tour de force*, present cracks entirely in terms of dislocation pileup theory, treating the crack as a distribution of virtual "crack" dislocations in the sense proposed by Friedel.[14] Many reflections of their work will be found in our treatment. Rice[17] has used the Muskhelisvili integral equation in deriving crack stress fields, and because of the similarity of his treatment to ours, his article is especially recommended.

7. General Equations and Boundary Conditions[15]

Local static equilibrium at a point in an elastic medium requires that the net force density at the point be equal to zero,

$$f_i = \sigma_{ij,j} = 0, \tag{7.1}$$

where σ_{ij} is the stress tensor, the summation convention over repeated indices is assumed, and the comma represents differentiation. Hooke's law connects the stress with the local derivatives of the displacement (strain), and in an isotropic medium is given by

$$\sigma_{ij} = \lambda u_{l,l}\delta_{ij} + \mu(u_{i,j} + u_{j,i}). \tag{7.2}$$

λ and μ are elastic coefficients, and $u_i(x_1, x_2, x_3)$ is the displacement function.

In any elastic problem, boundary values of σ_{ij} on the external (and internal) surfaces of the body must be specified in order to generate unique solutions. If a surface is free of externally applied forces, the fact that a free surface exists implies that forces, F_i, cannot be transmitted across it. Thus,

$$F_i = \sigma_{ij}n_j = 0. \tag{7.3}$$

n_j is the normal vector at the surface pointing from the negative to positive sides of the surface. Equation (7.3) represents the force per unit area transmitted across the surface from its positive side toward (the material on) its negative side.

In the crack problem (Fig. 16), two general approaches are possible. In the first (Fig. 17a), forces are applied to the external surfaces which give rise to a stress distribution in the body, $\sigma_{ij}^{(0)}(\mathbf{x})$. Then a cut is made in the medium which defines the cleavage surface of the crack. Since the cleavage surfaces are free surfaces in the above sense, Eq. (7.3) is satisfied on them. If $g_{ij;l}(\mathbf{x}, \mathbf{x}')$ is a Green's function for a dipole force at $\mathbf{x}'$ on the cleavage surfaces (an equal and opposite force is exerted on each of the cleavage surfaces facing one another across the cut), then the total stress in the body in its final stressed and cracked

[19] J. N. Goodier, *in* "Fracture" (H. Liebowitz, ed.), Chap. 2, p. 2. Academic Press, New York, 1968.

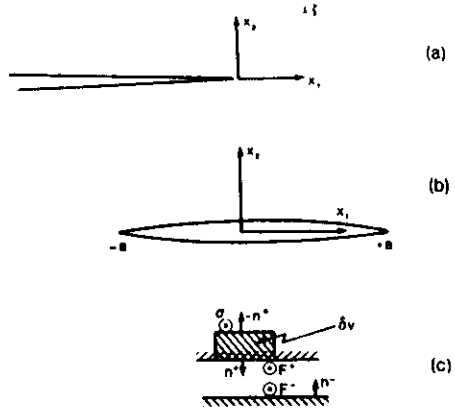

FIG. 16. Two crack-coordinate configurations for use in this article. In (a), the crack extends indefinitely along the negative x_1 axis. In (b), the crack is finite in length, and again lies along the x_1 axis from $-a \leq x_1 \leq +a$. Dislocations may be present at position ζ_i in the complex plane. (c) Construction for Eq. (8.9). An equal and opposite force distribution is exerted on the two surfaces of the cleavage planes in Mode III. These externally applied forces on an element of volume at the upper surface are shown balanced by internally generated stresses, which cancels the total force on the volume element shown.

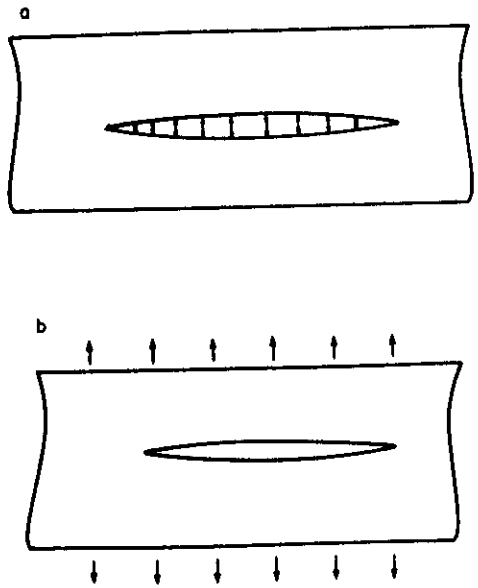

FIG. 17. Two ways of creating a crack in a medium are illustrated. The stresses may be exerted on the external surfaces as shown in (a), or as a pressure acting within the crack as shown in (b). Under conditions described in the text, the stresses near the crack tips are equivalent.

state is

$$\sigma_{ij} = \sigma_{ij}^{(0)} - \int g_{ij;l}\sigma_{lk}^{(0)} n_k \, ds. \tag{7.4}$$

The integral serves the purpose of simply nullifying the forces which were exerted by the initial stresses across the cleavage surface before the cut was made.

In the second approach (Fig. 17b), after the cut is made, forces are exerted on the crack surfaces which force them open, thereby generating stresses in the medium. If $-\sigma_{lk}^{(0)} n_k$ are these forces, then

$$\sigma_{ij} = -\int g_{ij;l}\sigma_{lk}^{(0)} n_k \, ds \tag{7.5}$$

is the stress in the body. n points from the medium across the surface to the vacuum.

There is thus a basic equivalence between these two approaches, and they will be referred to in the following as Problem 1 and Problem 2. For example, in Mode I, a standard problem is to exert forces on the upper and lower surfaces of the specimen as shown in Fig. 17a, giving rise to a constant stress throughout the body $\sigma_{ij}^{(0)} = \sigma_{22}^{(0)}$. In Problem 2, if this same constant force is applied on the surface of the crack, then the only difference between the final stress as given in Eqs. (7.4) and (7.5) is the constant term $\sigma_{22}^{(0)}$ in Eq. (7.4). Near the crack tips, where most of our concern lies, the stress is highly concentrated, and the constant term can be neglected. Thus, which fracture problem is addressed in any situation is usually a matter of mathematical convenience.

Two-dimensional analysis has a special place in the treatment of fracture problems. The reason is simply that 3D treatments of cracks are usually enormously difficult, and nearly always numerical. Thus, the 3D literature is sparce and recommended for the specialist only. But, as with dislocations, much can be accomplished in 2D, where the crack line is straight (taken along the x_3 axis) and infinite in length. In addition, in 2D, it is required that $u_{i,3} = 0$ everywhere. Substitution of this requirement into Eq. (7.1) with Eq. (7.2) shows that the solutions break into two separate cases,

$$\nabla^2 u_3 = u_{3,11} + u_{3,22} = 0, \tag{7.6}$$

$$(\lambda + \mu)u_{j,ji} + \mu u_{i,jj} = 0, \qquad i,j = 1,2. \tag{7.7}$$

These two cases correspond to the two independent shear and longitudinal polarization solutions for sound waves, and are called antiplane strain, and plane strain, respectively. Equation (7.6) corresponds to screw dislocations and Mode-III cracks, and Eq. (7.7) to edge dislocations and to mode I and II cracks.

In usual treatments of elasticity, the so-called compatibility conditions on the strain are introduced. Since we shall be dealing with dislocations, where these conditions are violated, however, it will be easier simply to monitor the single-valuedness of the displacement directly in discussion of solutions, rather than to introduce these considerations as special added equations to the basic equilibrium equations (7.6) and (7.7), which are of course the field equations of elasticity.

There are several approaches to the solution of any boundary-value problem, and, in the case of 2D elasticity, Green's functions, conformal mapping, and a singular integral method generalized from the Hilbert transform have been most effectively used. In any given case, one or another of these techniques can be employed, depending on the ease and directness of the relevant mathematics. In cases where the Green's functions can be found easily, that is often the method of choice, but for slit cracks, the singular integral method has been developed by the Russian school associated with Muskhelishvili into an elegant and powerful approach which we shall use, and from which the elastic Green's functions can be derived. On the other hand, conformal mapping can be a powerful tool for application to more general crack shapes such as wedges, which are also important. The mathematics for both these latter approaches will be found in the Appendix. Elasticity is complicated by the tensor character of the variables, and, like electromagnetism, is generally simplified by the introduction of elastic potentials. In spite of the fact that these potentials were discovered in the 19th century, they are not familiar to nonspecialists, and the elastic equations expressed in terms of these potentials are also developed in the Appendix.

In 2D the variables u_i and σ_{ij} will only be functions of the complex variables $z = x_1 + ix_2$ and $\bar{z} = x_1 - ix_2$, and it is natural to invoke complex function theory. In antiplane strain, where only u_3 is nonzero, this is a particularly straightforward procedure, and it will be discussed first. The reader is reminded, however, since elasticity is a linear theory, that the total solution in mixed cases is a simple superposition of plane and antiplane solutions.

8. Antiplane Strain. The Mode-III Crack

Since the field equation for antiplane strain, Eq. (7.6), is Laplace's Equation, a solution can be given in terms of any analytic complex function η of z, such that

$$u_3 = u_3(x_1, x_2) = (2/\mu)\,\mathrm{Im}(\eta(z)). \tag{8.1}$$

η will be called the antiplane strain elastic potential and the factor 2 is used to achieve symmetry with certain expressions to be derived in plane strain. The

only nonzero stress components, σ_{31} and σ_{32}, can be written in terms of η by Eq. (7.2) as

$$\sigma(z) = \sigma_{32} + i\sigma_{31} = 2\eta'(z), \tag{8.2}$$

where the prime denotes differentiation. As shown in the Appendix, σ is not a true vector, because $\bar{\sigma}/i$ is the quantity which transforms as a vector (see Eq. A.23). In polar coordinates,

$$\begin{aligned} \sigma_{r_3} &= \sigma_{31}\cos\theta + \sigma_{32}\sin\theta = \mathrm{Im}(\sigma e^{i\theta}), \\ \sigma_{\theta_3} &= -\sigma_{31}\sin\theta + \sigma_{32}\cos\theta = \mathrm{Re}(\sigma e^{i\theta}). \end{aligned} \tag{8.3}$$

Singular solutions for a dislocation or a line force at the origin are given by

$$\eta = (\mu b/4\pi)\ln z. \tag{8.4}$$

The real part of b represents a dislocation, and the imaginary part gives the strength of a line force. $\mathrm{Re}(b)$ is given by the multivaluedness of η at the origin,

$$\mathrm{Re}(b) = \frac{2\,\Delta\eta}{i\mu} = \frac{2}{i\mu}\oint \eta'\,dz. \tag{8.5}$$

In the same way, the strength of the line force is given by integration of σ_r around the origin.

Suitable elastic potentials for the crack problem are found by satisfying the boundary conditions on the open cleavage surface in Problem 1. If a cleavage plane lies along the negative x_1 axis, with the crack line coinciding with the x_3 axis, as in Fig. 16a, then

$$\sigma_{32}(x_1, 0) = 0, \qquad x_1 < 0. \tag{8.6}$$

A suitable solution is

$$\begin{aligned} \eta &\propto \sqrt{z}, \\ \eta' &= K_{\mathrm{III}}/2\sqrt{2\pi z}. \end{aligned} \tag{8.7}$$

In this solution, the cleavage surface is a branch line and $\sigma \to 0$ at infinity. The crack tip is a branch point in the function η. This simple result is a clue that crack problems in general will lead to square-root-like functions, with branch lines coincident with the cleavage plane. The discontinuity in the potential function on the cleavage surface corresponds to the discontinuities in both displacement and σ_{31} there. (Note that σ_{31} need not be zero on the open surface along $-x_1$.) The constant K is a measure of the strength of the singularity at the crack tip.

In Fig. 16b a more general finite crack is shown lying along the x_1 axis from $-a \le x_1 \le a$. Again, a complex potential η is sought having a branch line on the cleavage surface. In Problem II, equal and opposite external forces per unit

area, $F_{\mathrm{III}}(x_1)$, are exerted on the cleavage plane, as shown in Fig. 16c, thereby generating an internal stress σ_{32}. On an element of volume at the upper surface in Fig. 16c, zero net force requires that $\sigma_{32}(-n_2^+) + F_{\mathrm{III}} = 0$, with $n_2^+ = -1$. $\sigma_{32}^+ = -F_{\mathrm{III}}(x_1)$ on the upper surface. By the same reasoning $\sigma_{32}^- = -F_{\mathrm{III}}(x_1)$ on the lower surface, because equal and opposite forces are exerted on the lower surface. Thus the boundary condition at the cleavage surface is given by

$$[\sigma_{32}]^+ = [\sigma_{32}]^- = -F_{\mathrm{III}}(x_1), \tag{8.8}$$

where F_{III} is an arbitrary real function of x_1. In terms of the potential function η Eq. (8.8) is written

$$\{[\eta']^+ + [\eta']^-\} = -F_{\mathrm{III}}(x_1). \tag{8.9}$$

Note that in Eq. (8.9) the imaginary parts of η' on the opposite sides of the crack surface are of opposite sign, because F_{III} is real.

Equation (8.9) and the boundary-value problem it represents conform to the discussion of the Muskhelishvili singular integrals in the Appendix (Subsection 3). Specifically, Eq. (8.9) is of the form specified for $h(t)$ in Eq. (A.40), and the solution for η' according to that equation is

$$\eta'(z) = -\frac{1}{2\pi\sqrt{z^2 - a^2}}\int_{-a}^{a} \frac{F_{\mathrm{III}}(t)\sqrt{a^2 - t^2}}{t - z}\,dt. \tag{8.10}$$

The polynomial is set to zero in Eq. (A.41) in order for the stress at infinity to be zero. The solution in Eq. (8.10) is singular at $z = (\pm a, 0)$. Near $z = a$, the solution has the form

$$\begin{aligned} 2\eta'(\zeta) = \sigma(\zeta) &= \frac{K_{\mathrm{III}}}{\sqrt{2\pi\zeta}} + O\left(\frac{\zeta}{a}\right)^{1/2}; \qquad \zeta = z - a, \\ K_{\mathrm{III}} &= \frac{1}{\sqrt{\pi a}}\int_{-a}^{a} F_{\mathrm{III}}(t)\left(\frac{a + t}{a - t}\right)^{1/2} dt, \\ K_{\mathrm{III}} &= F_{\mathrm{III}}\sqrt{\pi a}; \qquad F_{\mathrm{III}} = \text{const.} \end{aligned} \tag{8.11}$$

This solution corresponds to the "second problem." When a constant stress F_{III} is added at infinity ("first problem"), the singularities at the crack tips are the same as in Eq. (8.11), and thus the constant K_{III} is also the same.

The relations in Eq. (8.11) give the central results for the region near a crack tip, showing that a $1/\sqrt{z}$ stress singularity exists there, with a strength K, called the stress intensity factor. K is linear in the external driving stress, and depends upon the crack geometry, as well as the specimen shape and the way the external stress is applied. This latter point is seen from the second equation of (8.11), where K depends upon the initial stress distribution on the cleavage surface.

The reader will note that Eq. (8.10) has the form of a Green's function solution [Eq. (7.5)], where the Green's function for the finite crack is

$$\eta' = -\int F_{III}(t)g(t,z)\,dt,$$
$$g(t,z) = \frac{1}{2\pi}\left(\frac{a^2-t^2}{z^2-a^2}\right)^{1/2}\frac{1}{t-z}. \tag{8.12}$$

9. Plane Strain and Plane Stress

The plane-strain equations are given by Eq. (7.7), and in terms of the Goursat potential functions, the field equations (7.7) become

$$\sigma_{11}+\sigma_{22} = 2[\varphi'(z)+\overline{\varphi'(z)}],$$
$$\sigma_{22}-\sigma_{11}+2i\sigma_{12} = 2[\bar{z}\varphi''(z+\psi'(z)], \tag{9.1}$$
$$2\mu u = 2\mu(u_1+iu_2) = \kappa\varphi(z) - [z\overline{\varphi'(z)}+\overline{\psi(z)}].$$

These equations are derived in Appendix Subsection 1 [see Eqs. (A.12)-(A.15)].

For cases where the specimen is a plate whose thickness is small compared with all other dimensions in the problem, these same Eqs. (9.1) are also valid, when κ has the appropriate value. This case is called plane stress, and all future equations are valid for both plane strain and plane stress when

$$\kappa = \begin{cases} 3-4\nu\text{: plane strain,} & \sigma_{33} = \nu(\sigma_{11}+\sigma_{22}); \\ (3-\nu)/(1+\nu)\text{: plane stress,} & \sigma_{33} = 0. \end{cases} \tag{9.2}$$

In the fracture problem of Fig. 16, the boundary conditions pertain to σ_{22} and σ_{21}; so it is convenient to recombine Eq. (9.1) so that these quantities are displayed conveniently:

$$\sigma_{11}+\sigma_{22} = 2[\varphi'(z)+\overline{\varphi'(z)}],$$
$$\sigma_{22}-i\sigma_{12} = \varphi'+\overline{\omega'}+(z-\bar{z})\overline{\varphi''}$$
$$2\mu u = \kappa\varphi-(z-\bar{z})\overline{\varphi'}-\bar{\omega}, \tag{9.3}$$
$$\omega = z\varphi'+\psi.$$

In these equations, the new function ω has replaced ψ for convenience in the following analysis, because of the appearance of the term $(z-\bar{z})$, which is zero on the x_1 axis.

For a crack lying on the x_1 axis, $-a < x_1 < a$ (Fig. 16b), in Problem II, the internal stresses on the left-hand side of the second part of Eq. (9.3) are balanced at the crack surface by an externally applied force distribution which we shall call F, and following the reasoning leading up to Eq. (8.10), the boundary condition on the crack faces where $(z-\bar{z}) = 0$ is written

$$-\bar{F} = [\varphi'(t)+\overline{\omega'(t)}]^+,$$
$$-\bar{F} = [\varphi'(t)+\overline{\omega'(t)}]^-, \tag{9.4}$$
$$F = F_I + iF_{II}.$$

As before, + and − superscripts relate to the limiting values of φ' and $\overline{\omega'}$ on the upper and lower crack surface. In the notation adopted for the externally applied forces, F_I relates to a force in the x_2 direction producing a Mode-I opening of the crack, and F_{II} relates to a force in the x_1 direction producing a pure Mode-II crack. The use of the real variable t denotes that the variable is taken along the cut, $-a < x_1 < a$.

In the form of Eq. (9.4), the Muskhelishvili analysis cannot be used because its right-hand side contains the nonanalytic function $\bar{\omega}'$. That is, $\bar{\omega}$ is not a function of z, but of $\bar{z}$. It is, however, possible to rewrite Eq. (9.4) in terms of analytic functions of z, through the function $\omega^*(z)$ defined by

$$\omega^*(z) = \overline{\omega(\bar{z})}. \tag{9.5}$$

On the real axis, $[\omega^*(t)]^+ = [\overline{\omega(t)}]^-$ and Eq. (9.4) becomes

$$[-\bar{F}]^+ = [\varphi'(t)]^+ + [\omega'^*(t)]^-;$$
$$[-\bar{F}]^- = [\varphi'(t)]^- + [\omega'^*(t)]^+. \tag{9.6}$$

Subtraction of these two equations shows that $[\varphi'(z)-\omega^{*\prime}(z)]$ is a function with no discontinuity on the crack surface, and hence is analytic everywhere. From Liouville's theorem it is therefore zero, because the constant allowed by Liouville's theorem would not fit the requirement in problem 2 that the stresses are zero at ∞. Hence, $\varphi'(z) = \omega^{*\prime}(z)$, and the sum of the equations [Eq. (9.6)] has the form

$$-\bar{F} = [\varphi'(t)]^+ + [\varphi'(t)]^-. \tag{9.7}$$

The analysis of the Appendix Subsection 3 now applies, and the result from Eq. (A.41) is

$$\varphi'(z) = -\frac{1}{2\pi\sqrt{z^2-a^2}}\int_{-a}^{a}\frac{\bar{F}\sqrt{a^2-t^2}}{t-z}\,dt$$
$$F(t) = F_I(t)+iF_{II}(t). \tag{9.8}$$

Investigation of the singularity at $z = a$ leads to

$$\varphi'(\zeta) = \frac{\bar{K}}{2\sqrt{2\pi\zeta}}+O(\sqrt{\zeta/a}), \tag{9.9}$$
$$K = K_I + iK_{II},$$
$$K = \frac{1}{\sqrt{\pi a}}\int_{-a}^{a}F(t)\left(\frac{a+t}{a-t}\right)dt, \tag{9.10}$$

in complete analogy to the antiplane-strain case. When F_I and F_{II} are constants,

$$K = F\sqrt{\pi a}. \tag{9.11}$$

In this notation, Eqs. (9.9) and (9.10) contain both Mode I and Mode II as their real and imaginary parts, respectively. As noted earlier, Mode-III stresses when they exist are simply added in linear fashion to these equations.

As in the antiplane-strain case, Eq. (9.8) provides an expression for the Green's function for the plane-strain crack, because Eq. (9.8) is in the form of a Green's-function-type integral, with a set of forces, σ, distributed in equal and opposite amounts on the opposing crack surfaces,

$$\varphi'(z) = -\int \bar{F}(t)g(t,z)\,dt,$$
$$g(t,z) = \frac{1}{2\pi}\left(\frac{a^2 - t^2}{z^2 - a^2}\right)^{1/2}\frac{1}{t - z}. \tag{9.12}$$

Finally, it is noted that the potential function $\varphi'(z)$ possesses the same simple form in plane strain as does the η' and stress in antiplane strain. The stresses themselves, however, are quite complicated, and obtained from Eq. (9.3) after a quite tedious manipulation, and this fact demonstrates the great usefulness of the elastic potentials. In the interest of completeness, the stresses are given below:

Equations for Mode I:

$$\left.\begin{matrix}\sigma_{xx}\\ \sigma_{yy}\\ \sigma_{xy}\end{matrix}\right\} = \frac{K_I}{(2\pi r)^{1/2}}\begin{cases}\cos(\theta/2)[1 - \sin(\theta/2)\sin(3\theta/2)]\\ \cos(\theta/2)[1 + \sin(\theta/2)\sin(3\theta/2)];\\ \sin(\theta/2)\cos(\theta/2)\cos(3\theta/2)\end{cases}$$

$$\left.\begin{matrix}\sigma_{rr}\\ \sigma_{\theta\theta}\\ \sigma_{r\theta}\end{matrix}\right\} = \frac{K_I}{(2\pi r)^{1/2}}\begin{cases}\cos(\theta/2)[1 + \sin^2(\theta/2)]\\ \cos^3(\theta/2)\\ \sin(\theta/2)\cos^2(\theta/2)\end{cases};$$

$$\sigma_{zz} = \nu'(\sigma_{xx} + \sigma_{yy}) = \nu'(\sigma_{rr} + \sigma_{\theta\theta}), \tag{9.13}$$

$$\sigma_{xz} = \sigma_{yz} = \sigma_{rz} = \sigma_{\theta z} = 0;$$

$$u_z = -(\nu''z/E)(\sigma_{xx} + \sigma_{yy}) - (\nu''z/E)(\sigma_{rr} + \sigma_{\theta\theta});$$

$$\left.\begin{matrix}u_x\\ u_y\end{matrix}\right\} = \frac{K_I}{2E}\left(\frac{r}{2\pi}\right)^{1/2}\begin{cases}(1+\nu)[(2\kappa - 1)\cos(\theta/2) - \cos(3\theta/2)]\\ (1+\nu)[(2\kappa + 1)\sin(\theta/2) - \sin(3\theta/2)]\end{cases};$$

$$\left.\begin{matrix}u_r\\ u_\theta\end{matrix}\right\} = \frac{K_I}{2E}\left(\frac{r}{2\pi}\right)^{1/2}\begin{cases}(1+\nu)[(2\kappa - 1)\cos(\theta/2) - \cos(3\theta/2)]\\ (1+\nu)[-(2\kappa + 1)\sin(\theta/2) + \sin(3\theta/2)]\end{cases}$$

Equations for Mode II:

$$\left.\begin{matrix}\sigma_{xx}\\ \sigma_{yy}\\ \sigma_{xy}\end{matrix}\right\} = \frac{K_{II}}{(2\pi r)^{1/2}}\begin{cases}-[\sin(\theta/2)][2 + \cos(\theta/2)\cos(3\theta/2)]\\ \sin(\theta/2)\cos(\theta/2)\cos(3\theta/2)\\ [\cos(\theta/2)][1 - \sin(\theta/2)\sin(3\theta/2)]\end{cases};$$

$$\left.\begin{matrix}\sigma_{rr}\\ \sigma_{\theta\theta}\\ \sigma_{r\theta}\end{matrix}\right\} = \frac{K_{II}}{(2\pi r)^{1/2}}\begin{cases}[\sin(\theta/2)][1 - 3\sin^2(\theta/2)]\\ -3\sin(\theta/2)\cos^2(\theta/2)\\ \cos(\theta/2)[1 - 3\sin^2(\theta/2)]\end{cases};$$

$$\sigma_{zz} = \nu'(\sigma_{xx} + \sigma_{yy}) = \nu'(\sigma_{rr} + \sigma_{\theta\theta}), \tag{9.14}$$

$$\sigma_{xz} = \sigma_{yz} = \sigma_{rz} = \sigma_{\theta z} = 0;$$

$$u_z = -(\nu''z/E)(\sigma_{xx} + \sigma_{yy}) = -(\nu''z/E)(\sigma_{rr} + \sigma_{\theta\theta}).$$

$$\left.\begin{matrix}u_x\\ u_y\end{matrix}\right\} = \frac{K_{II}}{2E}\left(\frac{r}{2\pi}\right)^{1/2}\begin{cases}(1+\nu)[(2\kappa + 3)\sin(\theta/2) + \sin(3\theta/2)]\\ -(1+\nu)[(2\kappa - 3)\cos(\theta/2) + \cos(3\theta/2)]\end{cases};$$

$$\left.\begin{matrix}u_r\\ u_\theta\end{matrix}\right\} = \frac{K_{II}}{2E}\left(\frac{r}{2\pi}\right)^{1/2}\begin{cases}(1+\nu)[-(2\kappa - 1)\sin(\theta/2) + 3\sin(3\theta/2)]\\ (1+\nu)[-(2\kappa + 1)\cos(\theta/2) + 3\cos(3\theta/2)]\end{cases};$$

Equations for Mode III:

$$\sigma_{xx} = \sigma_{yy} = \sigma_{rr} = \sigma_{\theta\theta} = \sigma_{zz} = 0, \qquad \sigma_{xy} = \sigma_{r\theta} = 0;$$

$$\left.\begin{matrix}\sigma_{xz}\\ \sigma_{yz}\end{matrix}\right\} = \frac{K_{III}}{(2\pi r)^{1/2}}\begin{cases}-\sin(\theta/2)\\ \cos(\theta/2)\end{cases};$$

$$\left.\begin{matrix}\sigma_{rz}\\ \sigma_{\theta z}\end{matrix}\right\} = \frac{K_{III}}{(2\pi r)^{1/2}}\begin{cases}\sin(\theta/2)\\ \cos(\theta/2)\end{cases}; \tag{9.15}$$

$$u_z = (K_{III}/2E)(r/2\pi)^{1/2}[2(1+\nu)\sin(\theta/2)];$$

$$u_x = u_y = u_r = u_\theta = 0.$$

For all modes:

$\kappa = (3 - \nu)/(1 + \nu)$, $\nu' = 0$, $\nu'' = \nu$ (for plane *stress*);

$\kappa = (3 - 4\nu)$, $\nu' = \nu$, $\nu'' = 0$ (for plane *strain*).

10. Dislocation Stress Fields

One of the central themes of this article will be the interaction of dislocations with cracks, and in order to study this it will be necessary to develop analytic expressions for the potential function of a dislocation in the presence of a crack. There are a variety of ways for doing this. One is by means

of the conformal mapping for the known image solutions of dislocations in the presence of an infinite free surface.[20] This is the only method practicable for wedge cracks and other complicated crack shapes. For slit cracks, however, a simpler approach is to use the general Green's-function expressions already developed for slit cracks, Eqs. (8.12) and (9.12).

In both antiplane strain and plane strain, the solution is obtained by breaking η', φ', and ω' each into two parts, that given by the dislocation potential in an infinite homogeneous medium, and that required to satisfy the boundary condition at the crack cleavage surface.

a. Antiplane Strain

In antiplane strain, η' is thus given by

$$\begin{aligned} \eta' &= \eta'_0 + \eta'_1, \\ \eta_0 &= \mu b/4\pi(z - \zeta). \end{aligned} \tag{10.1}$$

The origin is at the tip of the semi-infinite crack shown in Fig. 16a and the screw dislocation is at ζ. The solution η'_0 produces a nonzero force on the open cleavage surface, and η'_1 corresponds to additional forces exerted on the crack plane to ensure that $\sigma_{ij}n_j = 0$ here. Thus, $\eta'_1(a)$ is calculated from Eq. (8.10) when that equation is modified to represent the crack configuration of Fig. 16a, i.e., translate the origin to the right-hand side of the crack and take $a \to \infty$:

$$\eta'_1(z) = \frac{i}{\pi\sqrt{z}} \int_{-\infty}^{0} \frac{\sqrt{t}\,\mathrm{Re}[\eta'_0(t)]}{t - z}\,dt. \tag{10.2}$$

In Eq. (8.10) we have taken $F_{III} = -2\,\mathrm{Re}[\eta'_0(t)]$ with the substitution for η'_0 from Eq. (10.1). Straightforward integration of Eq. (10.2) leads to the total stress

$$\begin{aligned} 2\eta' = \sigma &= \frac{\mu}{4\pi\sqrt{z}} \sum_j \left(\frac{b_j}{\sqrt{z} - \sqrt{\zeta_j}} - \frac{b_j}{\sqrt{z} - \sqrt{\bar{\zeta}_j}} \right) + \frac{K_{III}}{\sqrt{2\pi z}} \\ &= \frac{\mu}{4\pi} \sum_j \left\{ \frac{b_j}{z - \zeta_j} \left[\left(\frac{\zeta_j}{z} \right)^{1/2} + 1 \right] + \frac{b_j}{z - \bar{\zeta}_j} \left[\left(\frac{\bar{\zeta}_j}{z} \right)^{1/2} - 1 \right] \right\} + \frac{K_{III}}{\sqrt{2\pi z}}. \end{aligned} \tag{10.3}$$

In this equation, the total stress is the linear sum of a set of dislocations situated at ζ_j, and the crack K field is also added from Eq. (8.7) in order to obtain a general result.

Physically, this expression is interesting because of the appearance of the term in $\bar{\zeta}_j$, which corresponds to images of the dislocations at ζ_j. Because of the cancelling effect of these images, the dislocation part of the stress field at infinity decays more strongly than the normal $1/z$ dislocation field. Of course, the overall field is dominated at long range by the K_{III} field.

[20] G. Hirth and J. Lothe, "Theory of Dislocations," 2nd Ed. McGraw-Hill, New York, 1982.

The most important result from Eq. (10.3), however, is that the stress singularity in the tip region is also of the $1/\sqrt{z}$ variety, but with a different strength than the long-range K_{III}. Thus, from the limiting form of σ near the origin, the local stress intensity factor, k, is defined by the relations

$$\begin{aligned} \sigma_{z\to 0} &= k_{III}/\sqrt{2\pi z}, \\ k_{III} &= K_{III} - \frac{\mu}{2} \sum_j \left(\frac{b_j}{\sqrt{2\pi\zeta_j}} + \frac{b_j}{\sqrt{2\pi\bar{\zeta}_j}} \right). \end{aligned} \tag{10.4}$$

The important physical meaning of Eq. (10.4) is that the dislocations *shield* the crack from the externally applied stress field for positive Burgers vectors. Dislocations with negative Burgers vectors are antishielding dislocations because they enhance the effect of the external field. Note from Eq. (10.4) that k_{III}, like K_{III}, is always a real quantity.

b. Plane Strain

In plane strain, the procedure is exactly the same as the antiplane case, except that two potentials are required, φ and ω. As before,

$$\begin{aligned} \varphi' &= \varphi'_0 + \varphi'_1, \\ \omega' &= \omega'_0 + \omega'_1. \end{aligned} \tag{10.5}$$

φ'_0 and ω'_0 represent the potential functions for "free" edge dislocations. These functions are not exhibited in the traditional dislocation texts, but the reader can verify with Eq. (9.3) that the following expressions reproduce the edge-dislocation stress fields as published, for example, in Hirth and Lothe:[20]

$$\begin{aligned} \varphi'_0 &= \frac{2A}{z - \zeta}, \\ \omega'_0 &= \frac{2\bar{A}}{z - \zeta} - \frac{2(\zeta - \bar{\zeta})}{(z - \zeta)^2} A, \\ A &= \frac{\mu b}{2\pi i(\kappa + 1)}. \end{aligned} \tag{10.6}$$

These solutions satisfy the Burgers circuit condition and have zero line-force term at the origin. The appearance of the second term in ω'_0 arises because of the necessary translational symmetry of the stress fields of a dislocation in expressions like Eq. (9.3).

The terms φ_1' and ω_1' are once more chosen to satisfy the boundary condition $\sigma_{ij}n_j = 0$ on the crack surface in Eq. (9.3). They can again be regarded as due to additional forces exerted on the crack surfaces which accomplish this goal, and which give rise to new stresses calculated from Eq. (9.8). Fortunately, the analysis is simplified, because

$$\varphi_1'(z) = \omega_1'^*(z). \tag{10.7}$$

The reason is that φ_1' and ω_1' are potentials which are derived from ("external") forces exerted on the crack surfaces, and the same reasoning leading up to Eq. (9.7) applies in this case as well. The function $\bar{F}$ to be used in Eq. (9.8) is given by

$$-\bar{F} = 2\varphi_0'(t) \tag{10.8}$$

from Eq. (9.3) because $z = \bar{z}$. Thus, with the obvious modification of Eq. (9.8) for a semi-infinite crack (translate origin to the right-hand crack tip and let $a \to \infty$),

$$\varphi_1' = \omega_1'^* = \frac{i}{\pi\sqrt{z}}\int_{-\infty}^{0}\frac{\sqrt{t}\,\varphi_0'(t)}{t - z}dt. \tag{10.9}$$

The easiest way to evaluate Eq. (10.9) is to integrate in the complex plane, ζ, with the expanded contour shown in Fig. 18, in which t is the real axis:

$$\oint_\infty = \int_c + \oint_z + \oint_{\zeta_0} + \oint_{\bar{\zeta}_0} = 0. \tag{10.10}$$

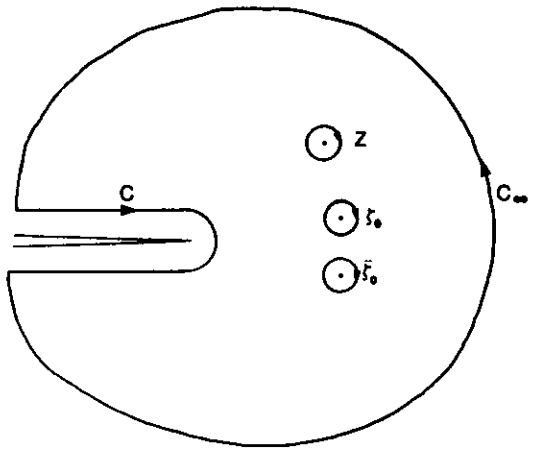

FIG. 18. Expanded contour of integration of Eq. (10.10) along the negative real axis. The expanded contour surrounds the negative real axis, C, continues at infinity with C_∞, and encloses the poles at z, ζ_0, and $\bar{\zeta}_0$.

The final result for the total φ' corresponding to a collection of dislocations in the presence of a crack is

$$\begin{aligned}\varphi' &= \varphi_0' + \varphi_1' \\ &= \sum_j A_j\left\{\frac{1}{z - \zeta_j}\left[\left(\frac{\zeta_j}{z}\right)^{1/2} + 1\right] + \frac{1}{z - \bar{\zeta}_j}\left[\left(\frac{\bar{\zeta}_j}{z}\right)^{1/2} - 1\right]\right\} \\ &\quad + \sum_j \frac{\bar{A}_j(\zeta_j - \bar{\zeta}_j)}{2(z - \bar{\zeta}_j)^2}\left[\left(\frac{\bar{\zeta}_j}{z}\right)^{1/2} + \left(\frac{z}{\bar{\zeta}_j}\right)^{1/2} - 2\right] \\ &\quad + \frac{\bar{K}}{2\sqrt{2\pi z}}; \qquad K = K_I + iK_{II};\ A_j = \mu b_j/2\pi i(\kappa + 1).\end{aligned} \tag{10.11}$$

For ω',

$$\begin{aligned}\omega' &= \sum_j \bar{A}_j\left\{\frac{1}{z - \zeta_j}\left[\left(\frac{\zeta_j}{z}\right)^{1/2} + 1\right] + \frac{1}{z - \bar{\zeta}_j}\left[\left(\frac{\bar{\zeta}_j}{z}\right)^{1/2} - 1\right]\right\} \\ &\quad - \sum_j \frac{A_j(\zeta - \bar{\zeta}_j)}{2(z - \zeta_j)^2}\left[\left(\frac{\zeta_j}{z}\right)^{1/2} + \left(\frac{z}{\zeta_j}\right)^{1/2} + 2\right] + \frac{K}{2\sqrt{2\pi z}}.\end{aligned} \tag{10.12}$$

As in the antiplane-strain case, the relevant expression for the crack part of the potentials, in Eq. (9.9) have been added to Eqs. (10.11) and (10.12), and the additive property of stresses has been used to write an expression for a collection of dislocations of Burgers vectors b_j at positions ζ_j. These equations for the potentials φ and ω exhibit some similarities to the antiplane-strain case, Eq. (10.3), but contain extra terms. As in the antiplane-strain case, the dominant term at infinity in these equations is the K term. The far-field stresses of the dislocations are also again degraded by the image terms in the crack surface, although these image terms are considerably more complicated than in the earlier case.

The limiting functional form of Eqs. (10.11) and (10.12) at infinity and at the origin again provides the basis for the physical picture in which the dislocations shield or antishield the crack. The relation between local and applied stress intensity factors is then given by

$$\begin{aligned}\varphi_{z\to 0} &= \bar{k}/2\sqrt{2\pi z} \\ \bar{k} &= \bar{K} - \frac{\mu}{2i(1 - \nu)}\sum_j\left(\frac{b_j}{\sqrt{2\pi\zeta_j}} + \frac{b_j}{\sqrt{2\pi\bar{\zeta}_j}} + \frac{\pi\bar{b}_j(\zeta_j - \bar{\zeta}_j)}{(2\pi\bar{\zeta}_j)^{3/2}}\right).\end{aligned} \tag{10.13}$$

The reader is reminded of the complex number character of k, K, and b_j; $k = k_I + ik_{II}$; $b = b_1 + ib_2$, etc. [As noted earlier, these equations are valid for plane stress when the substitution $\nu \to \nu/(1 + \nu)$ is made.]

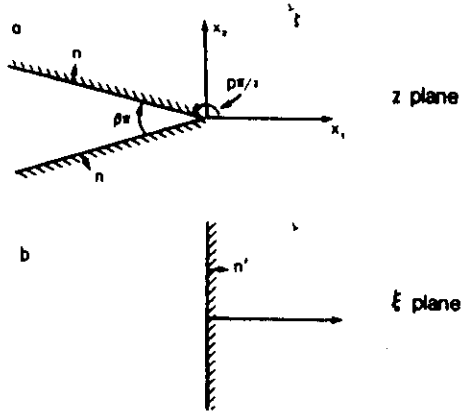

FIG. 19 Wedge configuration. In (a) the wedge parameters are shown in the z plane. In (b) the wedge is transformed to the imaginary axis of the ξ plane.

A somewhat different treatment from that given here for dislocation-crack stresses is given by Hirth and Wagoner,[21] and an elegant method for deriving the image stress of dislocations in the presence of cracks [contained in Eqs. (10.11), (10.12), and (10.3)] has been derived by Rice and Thomson.[22] The method here is quite similar to, and was suggested by, a development in unpublished lecture notes of J. R. Rice.

11. Wedge Cracks

Although in most crack problems, the slit-crack analysis is adequate because dislocation processes at the crack tip modify its shape, dislocation interactions with other shapes are important. In particular, the wedge configuration is the result of continued dislocation emission (see Fig. 11), and will be dealt with here. The analysis will follow that of Chang *et al.*,[23] but Sinclair[24] has also discussed the dislocation-wedge configuration, numerically. As mentioned earlier, the only analytic method suitable for this case is conformal mapping as presented in the Appendix (Subsection 2). The geometry is shown in Fig. 19.

In antiplane strain, the relevant equations are Eqs. (A.27) and (A.28). The boundary condition, of course, is that $\sigma_{ij}n_j = 0$, which transforms into the ξ plane as

$$\mathrm{Im}[\sigma_T(re^{\pm i\pi/2})] = 0. \tag{11.1}$$

The transformation law is

$$z = \xi^p, \qquad 1 < p < 2, \tag{11.2}$$

where p is geometrically related to the wedge geometry as shown in Fig. 19, and points on the wedge are transformed onto the imaginary axis of the plane. Equation (A.28) becomes

$$\sigma_T(\xi) = \frac{2}{p(\bar{\xi}\xi)^{(p-1)/2}}\frac{d\eta(\xi)}{d\xi}, \qquad e^{i\alpha} = \left(\frac{z'(\xi)}{\bar{z}'(\xi)}\right)^{1/2} = \left(\frac{\xi^{p-1}}{\bar{\xi}^{p-1}}\right)^{1/2}. \tag{11.3}$$

α, as explained in the Appendix, is the local rotation at a point.

Since $\xi\bar{\xi}$ is a real quantity everywhere, the boundary condition on the x_2 axis in the plane is then

$$\mathrm{Im}[\eta'(\xi)]_{\mathrm{Im\,axis}} = 0. \tag{11.4}$$

A second boundary condition, of course, is that the solution represent a dislocation at $z = \zeta$ in the z plane; that is $u(z)$ must be double valued at ζ with strength given by the Burgers vector

$$\Delta u(z = \zeta) = b. \tag{11.5}$$

These two boundary conditions, of course, are reminiscent of the similar problem of the image solution for a dislocation in an infinite free surface, and indeed the function,

$$\eta(\xi) = \frac{A}{2}\ln\left(\frac{\xi - \zeta^{1/p}}{\xi - \bar{\zeta}^{1/p}}\right) \tag{11.6}$$

satisfies Eq. (11.4). The constant $\zeta^{1/p}$ is chosen so that $\eta(z)$ is singular at $z = \zeta$. In the z plane, Eq. (11.5) is satisfied if A takes the form

$$\eta(z) = \frac{\mu b}{4\pi}\ln\left(\frac{z^{1/p} - \zeta^{1/p}}{z^{1/p} - \bar{\zeta}^{1/p}}\right), \qquad \sigma(z) = 2\eta'(z). \tag{11.7}$$

This function is the same as the crack solution [Eq. (10.3)] when $p = 2$.

The dislocation interaction with a wedge is only complete when a term corresponding to a K term in Eq. (10.3) is added. When the wedge (assumed semi-infinite in extent) is present without a dislocation, Eq. (11.4) is still valid,

[21] J. Hirth and R. Wagoner, *Int. J. Solids Struct.* **12**, 117 (1976).
[22] J. Rice and R. Thomson, *Philos. Mag.* **29**, 73 (1974).
[23] S. Chang, S. Ohr, and R. Thomson, to be published (1986).
[24] J. Sinclair, *Nucl. Metall.* **20**, 388 (1976).

and the simplest function satisfying Eq. (11.4) is

$$\eta' = \frac{p}{2}\Lambda_{III}; \qquad \eta = \frac{p}{2}\Lambda_{III}\xi, \qquad \xi \text{ plane};$$
$$\eta' = \frac{\Lambda_{III}}{2z^{1-1/p}}; \qquad \eta = \frac{p}{2}\Lambda_{III}z^{1/p}, \qquad z \text{ plane}. \tag{11.8}$$

This solution has the same meaning and limitations as the infinite crack solution [Eq. (8.8)] has. That is, Λ_{III}, as a measure of the strength of the wedge-tip singularity, must be specified by other considerations, such as those discussed in Part III,3. Note that for $p = 2$, $\Lambda_{III} = K_{III}/\sqrt{2\pi}$.

In antiplane strain, the total potential function for dislocations and "loaded" wedge is given by the linear superpositions

$$\eta(z) = \sum_j \frac{b_j}{4\pi} \ln\left(\frac{z^{1/p} - \zeta_j^{1/p}}{z^{1/p} + \zeta_j^{1/p}}\right) + \frac{p}{2}\Lambda_{III}z^{1/p} \tag{11.9}$$

12. Anisotropic Elasticity

General methods have been developed for anisotropic elastic problems and have been applied primarily to dislocations. An excellent recent review of these techniques is provided by Bacon *et al.*[25] For two-dimensional problems, this theory is based on the methods originated by Eshelby *et al.*,[26] which are briefly summarized below. In the general tensor notation for Hooke's law,

$$\sigma_{ij} = c_{ijkl}u_{k,l}. \tag{12.1}$$

The equations of equilibrium are

$$\sigma_{ij,j} = 0 = c_{ijkl}u_{k,lj}. \tag{12.2}$$

If all derivatives with respect to x_3 are zero, then a solution of the equations is of the form

$$u_k = A_k f(p_1x_1 + p_2x_2). \tag{12.3}$$

Substitution of Eq. (12.3) into (12.2) yields a set of homogeneous algebraic equations in the coefficients,

$$c_{ijkl}p_ip_lA_k = 0. \tag{12.4}$$

In this notation, $p_3 = 0$, and because of the arbitrary form of the function f, it is permissible to set $p_1 = 1$. With this convention, the determinant for the coefficients in Eq. (12.4) when set to zero yields a sixth-order polynomial in p_2, which will yield complex roots. Because the c_{ijkl} in Eq. (12.2) are all real, the roots of the determinantal equation appear in complex-conjugate pairs. Thus, there are three independent values of p_2, for which it has been customary to introduce a notation with Greek indices, $p_{2\alpha}$, in which the summation convention does *not* apply to repeated Greek indices. With these conventions, the general solution has the form

$$u_k = \sum_{\alpha=1}^{3} A_k f_k(x_1 + p_{2\alpha}x_i). \tag{12.5}$$

Since u_k is real, the two f's corresponding to complex conjugate p's are also paired, so that the final solution is

$$u_k = \sum_{\alpha=1}^{3} \mathrm{Re}\, A_k f_\alpha(x_1 + p_{2\alpha}x_2). \tag{12.6}$$

Thus there are three arbitrary solutions, f_α, of a complex variable $z_\alpha = [x_1 + \mathrm{Re}(p_{2\alpha})x_2] + i\,\mathrm{Im}(p_{2\alpha})x_2$, and the usual complex function theory can be employed.

In particular, the stresses are given by the relations

$$\sigma_{i1} = 2\,\mathrm{Re}\left(-\sum_{\alpha=1}^{3} p_\alpha L_{i\alpha} f'_\alpha(z_\alpha)\right),$$
$$\sigma_{i2} = 2\,\mathrm{Re}\left(\sum_{\alpha=1}^{3} L_{i\alpha} f'_\alpha(z_\alpha)\right). \tag{12.7}$$

f' denotes differentiation with respect to $z_\alpha = x_1 + p_2x_2$. This theory has been applied to the crack problem by a number of authors, with results as reviewed by Bacon *et al.*[25]

A general warning must be made in applying this formalism in certain cases. In the isotropic case, the solutions become highly degenerate, and isotropic results are not always the limit of the corresponding anisotropic expressions. For example, in the isotropic case, antiplane strain separates from plane strain, and in plane strain, the solution [Eq. (12.3)] is not the most general solution of Eq. (12.2). Additional functions are required. Thus, in plane-strain isotropic problems it is best to revert to the Airy stress-function analysis or its complex-variable variant as done in this section.

IV. The Elastic Forces on Cracks and Dislocations

13. Introduction

Since the problem of fracture entails the traversal of a crack and its associated dislocated deformation zones through a solid, the problem of the

[25] D. J. Bacon, D. M. Barnett, and R. D. Scattergood, *Prog. Mater. Sci.* **23**, 51 (1980).
[26] J. Eshelby, W. Read, and W. Shockley, *Acta Metall.* **1**, 251 (1953).

equilibrium configuration and dynamics of the assemblage requires an analysis couched in terms of the various forces on and between the constituent defects. Historically, the elastic force on a dislocation segment was worked out many years ago by Peach and Koehler,[27]

$$d\mathbf{f} = (\boldsymbol{\sigma} \cdot \mathbf{b}) \times d\mathbf{l} \tag{13.1}$$

in terms of the external stress field σ, the Burgers vector b, and the line segment dl. A fundamental result of Peach and Koehler's analysis is that the self-stress of the dislocation does not exert a force on itself. Likewise, for the elastic sharp crack, Irwin[28] derived a similarly classic result for the force per unit length on a Mode-I crack in two-dimensional isotropic elasticity, in terms of the stress intensity K, Poisson ratio ν, and Young's modulus E,

$$f = K_I^2(1 - \nu^2)/E. \tag{13.2}$$

This force is traditionally called the energy release rate in the mechanics literature, and is known by the letter G. However, here we adopt a more comfortable physical notation.

When cracks and dislocations are combined together, as in nearly all fracture events, one could proceed by simply combining these two results in an *ad hoc* manner to find the individual forces on cracks and/or dislocations, because from Part III, the stress fields and local stress intensity factors are known. However, there is a more powerful, general, and elegant approach which follows from the basic theorem of Eshelby[29] on the force exerted on an elastic singularity, expressed in terms of the energy momentum tensor for the elastic field. This second approach has the added advantage that it can be written in terms of the complex potentials, which are much simpler to work with than the full stress tensors as in Eq. (13.1). With it, we shall also make direct contact with the J integral of Rice,[30–32] which is the standard continuum-mechanics approach to cracks in a deformation field. Clearly, then, we shall prefer this latter path, and will display the Peach–Koehler and Irwin results as special cases. The point of view and results of this section largely stem from two papers involving the author.[33,34]

[27] M. O. Peach and J. S. Koehler, *Phys. Rev.* **80**, 436 (1950).
[28] G. R. Irwin, *J. Appl. Mech.* **24**, 361 (1957).
[29] J. D. Eshelby, *Solid State Phys.* **3**, 79 (1956).
[30] J. Rice, *J. Appl. Mech.* **35**, 13 (1968).
[31] J. R. Rice, *in* "Fracture" (H. Liebowitz, ed.), Chap. 2, p. 191. Academic Press, New York, 1968.
[32] J. Rice, *Mech. Fract. ASME Winter Annu. Meet.*, 1976; *AMD* **19**, 33 (1976).
[33] R. Thomson and J. Sinclair, *Acta Metall.* **30**, 1325 (1982).
[34] I. H. Lin and R. Thomson, *Acta Metall.* **34**, 187 (1986).

14. The Force on an Elastic Singularity: Eshelby's Theorem

To derive this theorem, following Eshelby,[29] we suppose the finite elastic body possesses a set of stress singularities, as shown in Fig. 20, and that the external surface of the body is subjected to a specified set of external forces. A strain-energy density function is assumed to exist, and since, except at the singularities, the medium is elastic, this function is given by

$$W = \tfrac{1}{2}\sigma_{ij}u_{i,j}. \tag{14.1}$$

In this and the following equations through (14.8), the full three-dimensional elastic notation will be used. If all the singularities move a constant distance δx from their initial positions x_p to $x_p + \delta x$, the energy change is calculated in three stages:

In Stage 1, the energy change, $\delta U^{(1)}$, arises from integrating the strain-energy density function over the solid. In this stage, when the sources translate, the stresses and displacements constituting the elastic solution are assumed to move rigidly with them in space. Thus, after the displacements occur, the new value of the strain-energy function is

$$W^{(1)}(x) = W(x) - \frac{\partial W}{\partial x_k}\delta x_k. \tag{14.2}$$

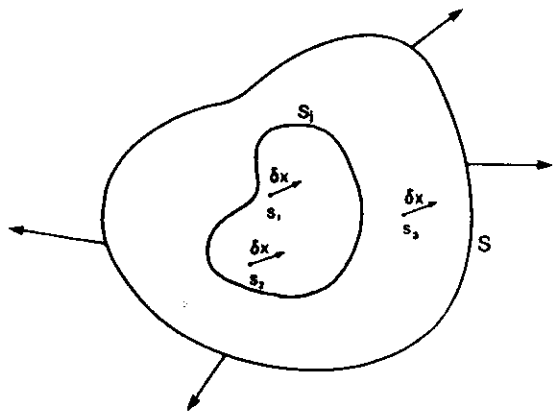

FIG. 20. Figure for deriving Eshelby's theorem. A body is contained within an external surface S, and is subject to external stresses. Strain singularities exist at $s_1, s_2, s_3, \ldots$, which are translated by δx to new positions. S_f is an inner surface enclosing singularities s_1 and s_2.

The total energy change integrated over the body is thus by Gauss's theorem

$$\delta U^{(1)} = -\int \frac{\partial W}{\partial x_k}\delta x_k\, dV = -\int W\, dS_k\, \delta x_k. \tag{14.3}$$

In the second stage, the boundary condition on the surface of the body when the sources translate is considered. In Stage 1, just above, when the elastic solutions translate rigidly with the sources, the stresses at the boundary translate in the same way. However, although the stress originally on the boundary satisfied the required boundary condition,

$$\sigma_{ij}n_j = F_i, \tag{14.4}$$

on the boundary, where n is the normal to the boundary, after the rigid translation of the elastic solution, the new stresses and displacements on the boundary no longer satisfy Eq. (14.4). In Stage 2, an additional surface stress is generated, such that when it is added to the translated stress, the total stress satisfies the required condition [Eq. (14.4)], on the surface. The added stress, $\Delta\sigma_{ij}$, generates a new set of displacements at the surface after the translation has taken place. Thus, if $u^{(0)}$ is the initial displacement before the sources are displaced, the changes generated in displacements during Stage 2 are

$$\Delta u_i = u_i^{\text{final}} - \left(u_i^{(0)} - \frac{\partial u_i^{(0)}}{\partial x_j}\delta x_j\right). \tag{14.5}$$

The work done on the body by the total stress acting over (Δu_i) is then, to first order ($\sigma + \Delta\sigma \sim \sigma$),

$$\begin{aligned}\delta U^{(2)} &= \int \sigma_{ij}^{(0)}\Delta u_j\, dS_j \\ &= \int \sigma_{ij}^{(0)}\left(u_i^{\text{final}} - u_i^{(0)} + \frac{\partial u_i}{\partial x_k}\delta x_k\right)dS_j.\end{aligned} \tag{14.6}$$

The third contribution is the energy change in the external loading machinery caused by the total change in displacement at the surface, $u^{\text{final}} - u^{(0)}$. This is the total change in displacement from that before the source translates to that after the end of Stage 2, when the boundary conditions are satisfied

$$\delta U^{(3)} = -\int \sigma_{ij}^{(0)}\,(u_i^{\text{final}} - u_i^{(0)})\, dS_j. \tag{14.7}$$

Addition of Eqs. (14.3), (14.6), and (14.7) gives the final result

$$f_k = -\frac{\partial U}{\partial x_k} = \int (W\delta_{ik} - \sigma_{ij}u_{i,k})\, dS_j. \tag{14.8}$$

f_k is the force on the singularity in the Lagrangian sense because it represents the negative of an energy derivative.

A subtlety arises when applying Eq. (14.8) to a crack. The slit comprising the cleavage plane of the crack is, of course, a part of the external surface of the body. However, since on the free surface of the slit, Eq. (14.4), is satisfied, the second term in Eq. (14.8) is zero. Also, by symmetry, W on the lower surface is equal to W on the upper. Because of the change in sign of dS_i when comparing the upper to the lower surface, the contribution of the first term is thus zero also. Hence, in making a contour around a crack, the contour may end on the crack cleavage surface.

The integration in Eq. (14.8) is over the actual external surface of the body, and may enclose a number of singularities. The force in this case represents the total force on the entire set of singularities. If instead, the force on a single singularity, or subset of the original group, is desired, the following strategem can be adopted. An inner boundary, S_i, is drawn surrounding the singularities in question (Fig. 20), and the remainder of the body then serves as an "external driving system" on the inner surface. In carrying out Stage 2 of the argument, however, a subtle point must be observed. The boundary conditions are established on the *real* surfaces of the body, and the Δu_i as calculated in Eq. (14.5) are the Δu_i on the inner integration path S_i which are induced by satisfying the boundary conditions on the external surface S. The rest of the argument then follows as before. In this case, of course, the force on the singularities within S_i is not only a function of the external driving stresses, but also of the remaining singularities outside S_i.

An important property of the integral in Eq. (14.8) is that, within certain limits, it is independent of the shape of the surface. Consider two surfaces enclosing a collection of singularities, such that the volume between the two surfaces contains no additional singularities. Then the difference in the integration over the two surfaces is

$$f_k^{\text{I}} - f_k^{\text{II}} = \oint (W\delta_{ik} - \sigma_{ij}u_{i,k})\, dS_j, \tag{14.9}$$

where the integral now encloses the volume between the two surfaces. Using Gauss's law for the enclosed volume, the equation of equilibrium, $\sigma_{ij,j} = 0$, and remembering that within V there are no additional singularities, then

$$f_k^{\text{I}} - f_k^{\text{II}} = \int_V (W_{,k} - \sigma_{ij}u_{i,kj})\, dV. \tag{14.10}$$

The general definition of the strain-energy density is

$$W = \int \sigma_{ij}\, d\epsilon_{ij}; \qquad \epsilon_{ij} = \tfrac{1}{2}(u_{i,j} + u_{j,i}). \tag{14.11}$$

By the chain rule of differentiation, and provided that σ_{ij} is only a function of the strain function ε_{ij}, which does not depend upon position (i.e., the medium is elastically homogeneous), then

$$W_{,k} = \epsilon_{ij,k}\frac{d}{d\epsilon_{ij}}\int \sigma_{ni}\,d\epsilon_{ni} = \sigma_{ij}u_{j,ki}, \tag{14.12}$$

and the integral in Eq. (14.11) is zero. Hence Eq. (14.8) depends only on the number, type, and configuration of singularities enclosed in the contour for a homogeneous medium, and does not depend upon the shape of the contour. In more physical terms, if f_k in Eq. (14.8) is the Langrangian force on the singularities, it cannot depend upon the shape of the contour on which the elastic fields are evaluated.

This corollary is very evocative of the Cauchy residue theory in two dimensions, and indeed it has been shown[33] that for general anisotropic media Eq. (14.8) can be written in two dimensions as

$$f_i = -4\pi\,\mathrm{Im}\left(\sum_{\alpha=1}^{3}(\pm p_\alpha L_{ki}A_{k\alpha})\sum_{R\alpha}\mathrm{Res}[f'_\alpha(z_\alpha)]^2\right). \tag{14.13}$$

This equation is written in the notation of Stroh[35,36] explained in Part III,12, and $\sum_{R\alpha}$ is a sum over the enclosed residues. The $\pm$ sign is the sign of $\mathrm{Im}(p_\alpha)$. The Peach–Koehler and Irwin relations are also examples of the same proposition that forces on defects depend only on functions evaluated at the singularities.

15. Antiplane Strain. Mode-III and Screw Dislocations

In isotropic elasticity, the general equation (14.13) degenerates into noninteracting antiplane- and plane-strain parts. The antiplane-strain part then corresponds[35,36] to

$$\begin{aligned} p_3 &= i, \\ L_{k3} &= \tfrac{1}{2}\delta_{k3}, \\ A_{k3} &= -\delta_{k3}/2\mu, \\ f'_3(z) &= \sigma(z), \end{aligned} \tag{15.1}$$

[35] A. N. Stroh, *Philos. Mag.* **3**, 625 (1958).
[36] A. N. Stroh, *J. Math. Phys.* **41**, 77 (1972).

where $\sigma(z)$ is the complex stress defined in Eq. (8.2). Then Eq. (14.13) becomes

$$\begin{aligned} \bar{f} &= \frac{\pi}{\mu}\sum_{R\alpha}\mathrm{Res}(\sigma^2), \\ f &= f_1 + if_2. \end{aligned} \tag{15.2}$$

Alternatively, one can derive Eq. (15.2) directly from Eq. (14.8) using the complex function notation of Part III, by substitution for σ_{ij} and u_i in antiplane strain, and using the Cauchy residue theorem. Note the complex vector notation introduced for the force f.

The simple Irwin and Peach–Koehler relations are recovered from Mode-III cracks and screw dislocation by taking a contour surrounding only one defect in each case. For a Mode-III crack at the origin, from Eq. (8.11), $\sigma = K_{\mathrm{III}}/\sqrt{2\pi z}$, and

$$\bar{f}_c = K_{\mathrm{III}}^2/2\mu. \tag{15.3}$$

This equation is the Mode-III form of the Irwin relation. Note that the force is real, so the crack opens only in the x_1 direction.

For a dislocation, the self-stress is of the form $1/z$, which contributes no residue. Thus the self-force is zero. If an analytic external stress σ_0 is added to the dislocation stress, so that

$$\sigma = \sigma_0(z) + \mu b/2\pi z, \tag{15.4}$$

then the force on the dislocation becomes

$$\bar{f} = b\sigma_0, \tag{15.5}$$

which is again the Peach–Koehler result.

More substantive results are obtained when the crack coexists with one or more dislocations. For this purpose the stress field of Eq. (10.3) is required. Using this expression in Eq. (15.2), the force on the crack is

$$\begin{aligned} \bar{f}_c &= k_{\mathrm{III}}^2/2\mu, \\ k_{\mathrm{III}} &= K_{\mathrm{III}} - \frac{\mu}{2}\sum_j\left(\frac{b_j}{\sqrt{2\pi\zeta_i}} + \frac{b_i}{\sqrt{2\pi\bar{\zeta}_j}}\right). \end{aligned} \tag{15.6}$$

Thus the force is the expected Irwin relation, but using the local k field of the crack, as defined in Eq. (10.4). Note again that the force is always real, that is, $\bar{f}$ is an extension force along the x_1 direction. In antiplane strain, there is no force tending to carry the crack away from its initial cleavage plane.

The force on a dislocation at ζ with Burgers vector b in the presence of the crack and other dislocations at ζ_j with Burgers vector b_j as shown in Fig. 21 is

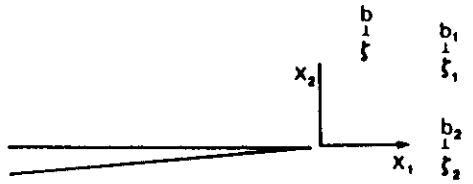

FIG. 21. Crack-dislocation configuration. In this section, the crack is assumed to lie along the negative real axis. Dislocations are located at points ζ_j. When a reference dislocation is needed, as for example when a force is calculated on it, it is referred to without subscript. Subscripts are given to all other dislocations.

evaluated in terms of the residue at ζ, and is given by

$$\bar{f}_d = \frac{K_{III}b}{\sqrt{2\pi\zeta}} - \frac{\mu b^2}{4\pi}\left[\frac{1}{2\zeta} + \frac{1}{\zeta-\bar{\zeta}} - \left(\frac{\bar{\zeta}}{\zeta}\right)^{1/2}\frac{1}{\zeta-\bar{\zeta}}\right] + \sum_j{}' \frac{\mu b b_j}{4\pi}\left[\frac{1}{\zeta-\zeta_j} - \frac{1}{\zeta-\bar{\zeta}_j} + \left(\frac{\zeta_j}{\zeta}\right)^{1/2}\frac{1}{\zeta-\zeta_j} + \left(\frac{\bar{\zeta}_j}{\zeta}\right)^{1/2}\frac{1}{\zeta-\bar{\zeta}_j}\right]. \quad (15.7)$$

The prime on the summation is to remind one that the reference dislocation at ζ is not included.

Three types of terms are contained in Eq. (15.7). The first is the K field, or direct crack interaction and depends on the distance from the crack as $1/\sqrt{\zeta}$. The second is a self-image force on the dislocation in the open surface of the crack, because it depends only on b and varies with distance from the tip as $1/\zeta$. Further, the self-image force *in the radial direction* from the crack is simply

$$(f_r^d)_{image} = -\mu b^2/4\pi|\zeta|, \quad (15.8)$$

which is exactly the same as if, at the crack line, an infinite open surface were erected perpendicular to the radius to the dislocation. This is a result first obtained by Rice and Thomson.[37] The third group of terms is the contribution to the force from the dislocation–dislocation interactions. They have the expected $1/(\zeta - \zeta_j)$ terms, but are modified by the factors $\sqrt{\zeta/\zeta_j}$, because, if the reference dislocation is near the crack tip, even if $K_{III} = 0$, it will sense a stress concentration there contributed by the stresses of the dislocations at ζ_j. These are, of course, the K-field contributions due to the dislocations which lead to the local k concept in Eq. (15.6). In addition to the direct dislocation–dislocation terms, there are also contributions from dislocations at the image points, $\bar{\zeta}_j$, and caused by the open surface on the cleavage plane. Note particularly that the sign of the force is linear in b in the first term, bilinear in the third term, and is quadratic in the second. That is, the force is repulsive or attractive, depending on b or b_i in the first or third terms, but always attractive for the self-image term.

[37] J. Rice and R. Thomson, *Philos. Mag.* **29**, 73 (1974).

An interesting variation of Eq. (15.7) can be written in terms of the local k_{III}, namely

$$\bar{f}_d = \frac{k_{III}b}{\sqrt{2\pi\zeta}} + \frac{\mu b^2}{4\pi}\left[\frac{1}{2\zeta} - \frac{1}{\zeta-\bar{\zeta}} + \left(\frac{\zeta}{\bar{\zeta}}\right)^{1/2}\frac{1}{\zeta-\bar{\zeta}}\right] + \sum{}' \frac{\mu b b_j}{4\pi}\left[\frac{1}{\zeta-\zeta_j} - \frac{1}{\zeta-\bar{\zeta}_j} + \left(\frac{\zeta}{\zeta_j}\right)^{1/2}\frac{1}{\zeta-\zeta_j} + \left(\frac{\zeta}{\bar{\zeta}_j}\right)^{1/2}\frac{1}{\zeta-\bar{\zeta}_j}\right]. \quad (15.9)$$

Thus, Eq. (15.7) is a form which best expresses the force when the dislocation is near the outer edge of the dislocation distribution, while Eq. (15.9) is a better approximation when near the inner edge.

When the contour is taken around all dislocations and the crack, then the result is simply

$$\mathrm{Re}(\bar{f}_{tot}) = K_{III}^2/2\mu. \quad (15.10)$$

Thus the elastic force on the entire collection of crack plus dislocations is simply that for a crack characterized by the far field K. When the distribution is symmetric about the real axis, then $\mathrm{Im}(f_{tot}) = 0$.

A simple relation can be written when all the dislocations are lined up on the x_1 axis in a one-dimensional distribution. Then Eq. (15.7) becomes

$$\bar{f}_d = \frac{K_{III}}{\sqrt{2\pi x}} - \frac{\mu b^2}{4\pi x} + \sum_j{}' \frac{\mu b b_j}{2\pi(x - x_j')}\left(\frac{x_j'}{x}\right)^{1/2}, \quad (15.11)$$

$$K_{III} = k_{III} + \sum_j \frac{\mu b_j}{\sqrt{2\pi x_j}}.$$

The simplicity of this result lends itself to use in pileup problems in later sections.

16. Plane Strain: Edge Dislocations and Mode-I and Mode-II Cracks

The Mode-I and Mode-II case is not a straightforward limit of the anisotropic results as in antiplane strain, because the isotropic solutions of the field equations are not of the form of Eq. (12.13). It is then necessary to revert to the potential functions developed in Parts III,9 and 11. With the use of the strain-energy function in its plane-strain form,

$$W = \tfrac{1}{2}\sigma_{ij}u_{i,j} = \tfrac{1}{2}[\sigma_{11}u_{1,1} + \sigma_{12}(u_{2,1} + u_{1,2}) + \sigma_{22}u_{2,2}], \quad (16.1)$$

direct substitution of the stresses and displacements, Eq. (9.3), into (14.8) can

be shown to yield[34]

$$\bar{f} = \frac{2\pi(1-\nu)}{\mu} \sum_{\text{Res}} [2\,\text{Res}(\varphi'\omega' - \varphi^2 - z\varphi'\varphi'') + \text{Res}(\varphi^2)]. \tag{16.2}$$

In terms of the φ and ψ, $\bar{f}$ has the simpler form

$$\bar{f} = \frac{2\pi(1-\nu)}{\mu} \sum_{\text{Res}} [2\,\text{Res}(\varphi'\psi') + \overline{\text{Res}(\varphi'^2)}]. \tag{16.3}$$

Similar equations have also been derived by Budiansky and Rice,[38] and by Chang.[39]

For the crack alone, the force corresponds to the residue at the origin, and carrying out a limit analysis of Eqs. (12.6) and (12.7) at the origin, the force on the crack is

$$\bar{f}_c = \frac{1-\nu}{2\mu}\left(k\bar{k} + \frac{k^2 - \bar{k}^2}{2}\right), \qquad k = k_I + ik_{II}. \tag{16.4}$$

The k here is the local k at the crack tip. In terms of components,

$$(f_c)_1 = \frac{1-\nu}{2\mu}(k_I^2 + k_I^2) = \frac{1-\nu^2}{E}(k_I^2 + k_{II}^2), \tag{16.5}$$

$$(f_c)_2 = -\left(\frac{1-\nu}{\mu}\right)k_I k_{II}. \tag{16.6}$$

E is Young's modulus. Equation (16.5) is the Irwin relation for Modes I and II.

Unlike Mode III, there is in Eq. (16.6) a component of the force along the imaginary axis, the meaning of which is somewhat obscure. Strictly speaking, Eq. (16.6) is the force of translating the crack rigidly in the X_2 direction, which is not a normal physical motion for the crack. However, cracks do branch away from their original cleavage planes, as shown in Fig. 22. One might suppose that Eq. (16.6) would form a reasonable estimate of this branching force, since the force on the crack is the same as the force on the virtual or "crack" dislocations which are equivalent to the crack, and these dislocations are highly concentrated at the tip. But a more careful analysis of the branching force shows that such is not the case, and that the branching force is actually composed of a linear combination of the terms k_I^2, k_{II}^2, and $k_I k_{II}$ in an approximate treatment carried out by Cottrell and Rice.[40] The reader is

[38] B. Budiansky and J. Rice, *J. Appl. Mech.* **40**, 201 (1973).
[39] S. J. Chang, *Int. J. Fract.* **16**, R79 (1980).
[40] B. Cottrell and J. R. Rice, *Int. J. Fract.* **16**, 155 (1980).

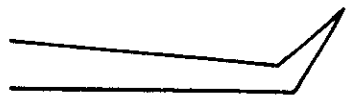

FIG. 22. Branching motion of a crack in which the crack abruptly changes cleavage plane.

referred to these authors for an excellent discussion of the branching force, and for citations to the further literature on the subject.

The relation between K and k in the analysis leading to Eq. (16.4) yields again the complex number form of the shielding relations for Modes I and II:

$$\bar{K} = \bar{k} + \frac{\mu}{2i(1-\nu)} \sum_j \left(\frac{b_j}{\sqrt{2\pi\zeta_j}} + \frac{b_j}{\sqrt{2\pi\bar{\zeta}_j}} + \frac{\pi\bar{b}(\zeta_j - \bar{\zeta}_j)}{(2\pi\bar{\zeta}_j)^{3/2}} \right). \tag{16.7}$$

The force on the dislocation requires an evaluation of the residue at ζ_j, and is much more complicated than in antiplane strain. Again, as in Eq. (15.7), there are three separate contributions to this force, which will be denoted

$$f_d = f_{Kd} + f_{d^2} + f_{dd'}. \tag{16.8}$$

The first term is linear in the reference dislocation b, and linear in K. It corresponds to the direct interaction between the crack and the dislocation. The second term is proportional to b^2, and represents the self-image term. Finally, the third term is proportional to bb_j and represents the dislocation–dislocation interaction. These three terms will be addressed in turn.

The direct crack–dislocation force is

$$\bar{f}_{Kd} = \frac{1}{2i\sqrt{2\pi\zeta}}\left(Kb - \bar{K}\bar{b} + \frac{\bar{K}b(\zeta - \bar{\zeta})}{2\zeta} - \bar{K}b \right) - \frac{K\bar{b}}{2i\sqrt{2\pi\bar{\zeta}}}. \tag{16.9}$$

Since the dislocations in question are edge in character, it is convenient to rewrite Eq. (16.9) in terms of a coordinate system rotated so the slip plane lies along the real axis (Fig. 23). In this coordinate system

$$\bar{f}^{sp} = \bar{f}e^{i\alpha}; \qquad b^{sp} = be^{-i\alpha}; \qquad \text{etc.} \tag{16.10}$$

b^{sp} by definition is real, i.e., $b^{sp} = b_e$, and equal to the edge component of the dislocation. In this coordinate system,

$$\bar{f}^{sp}_{Kd} = \frac{b_e}{2\sqrt{2\pi r}}\left(\frac{Ke^{i\alpha} - \bar{K}e^{-i\alpha}}{i} e^{i(\alpha - \theta/2)} + \bar{K}\sin\theta\, e^{i(2\alpha - 3\theta/2)} + i\bar{K}e^{i(2\alpha - \theta/2)} + iKe^{i\theta/2} \right). \tag{16.11}$$

Note that the $\text{Re}(\bar{f}^{sp})$ is the slip force on the dislocation and $-\text{Im}(\bar{f}^{sp})$ is the climb force.

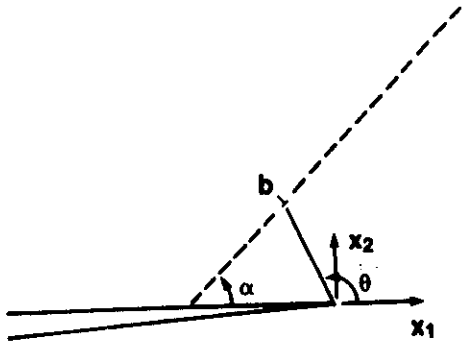

FIG. 23. Configuration of Mode-I and -II edge dislocation in slip-plane coordinates.

When the slip plane intersects the tip, then $\alpha = \theta$, and Eq. (16.11) simplifies to

$$\mathrm{Re}(\bar{f}^{sp}_{kd}) = \frac{b_e}{2\sqrt{2\pi r}}[K_I \sin\theta\cos\theta/2 + K_{II}(2\cos 3\theta/2 + \sin\theta\sin\theta/2)]. \tag{16.12}$$

For future reference, inspection of the angular parts of this equation indicates that dislocations are likely to be more strongly affected by K_{II} than by K_I. For rough estimation, Eq. (16.12) gives a good picture of the force on dislocations in the deformation zone, because generally speaking, it is those dislocations whose slip planes roughly intersect the crack tip which do the shielding. After they are left behind in the wake, for instance, they have little interaction with the crack tip, and their prime interaction is with themselves and possibly with the open cleavage surface.

The second term in Eq. (16.8) is the self-image term quadratic in b, and is given by

$$\bar{f}_{d^2} = -\frac{\mu}{4\pi(1-\nu)}\left\{\frac{b^2\sqrt{\bar{\zeta}}}{\zeta^{3/2}}\left[1+\left(\frac{\bar{\zeta}}{\zeta}\right)^{1/2}\right] + \frac{b\bar{b}}{4}\left[\frac{3}{\bar{\zeta}} + \frac{1}{2\sqrt{\zeta\bar{\zeta}}}\left(1-\frac{\bar{\zeta}}{\zeta}\right)\right.\right.$$
$$\left.\left. + \frac{3-\sqrt{\bar{\zeta}/\zeta}}{\sqrt{\zeta}(\sqrt{\zeta}+\sqrt{\bar{\zeta}})}\right] - \frac{\bar{b}^2}{4\bar{\zeta}}\left[1+\left(\frac{\bar{\zeta}}{\zeta}\right)^{1/2}\right]\right\}. \tag{16.13}$$

When slip-plane coordinates are used and $\theta = \alpha$, the result is

$$(\bar{f}^{sp}_{d^2})_{slip} = -\mu|b^2|/4\pi(1-\nu)r, \tag{16.14}$$

$$(\bar{f}^{sp}_{d^2})_{climb} = \frac{\mu b^2 \tan(\theta/2)(5+3\cos\theta)}{16\pi(1-\nu)r^2}. \tag{16.15}$$

The result Eq. (16.14) was first given by Rice and Thomson,[37] and has the same form as in antiplane strain. That is, Eq. (16.14) is the same as the simple image force on a dislocation at a distance r from an infinite surface.

The third term in Eq. (16.8) is bilinear in bb_j and is the dislocation–dislocation term. The general expression is

$$\frac{8\pi(1-\nu)}{\mu}\bar{f}_{dd'} = (bb_j + \bar{b}\bar{b}_j + b\bar{b}_j)\left\{\frac{1}{\xi_j}\left[\left(\frac{\zeta_j}{\zeta}\right)^{1/2}+1\right] + \frac{1}{\xi_j^*}\left[\left(\frac{\bar{\zeta}_j}{\zeta}\right)^{1/2}-1\right]\right\}$$
$$- \bar{b}\bar{b}_j\left\{\frac{1}{\bar{\xi}_j}\left[\left(\frac{\bar{\zeta}_j}{\bar{\zeta}}\right)^{1/2}+1\right] + \frac{1}{\bar{\xi}_j^*}\left[\left(\frac{\zeta_j}{\bar{\zeta}}\right)^{1/2}-1\right]\right\}$$
$$- 2b_j b i y\left\{\frac{1}{\xi^2}\left[\left(\frac{\zeta_j}{\zeta}\right)^{1/2}+1\right] + \frac{1}{\xi^{*2}}\left[\left(\frac{\bar{\zeta}_j}{\zeta}\right)^{1/2}-1\right]\right\}$$
$$+ \frac{bb_j i y_j}{\xi^2}\left[\left(\frac{\zeta_j}{\zeta}\right)^{1/2} + \left(\frac{\zeta}{\zeta_j}\right)^{1/2} + 2\right] \tag{16.16}$$
$$- \left(\frac{(b\bar{b}\bar{b}_j + b\bar{b}_j)iy_j}{\xi^{*2}} + \frac{4b\bar{b}_j y y_j}{\xi^{*3}}\right)\left[\left(\frac{\bar{\zeta}_j}{\zeta}\right)^{1/2} + \left(\frac{\zeta}{\bar{\zeta}_j}\right)^{1/2} - 2\right]$$
$$- \frac{\bar{b}\bar{b}_j i y_j}{\bar{\xi}^{*2}}\left[\left(\frac{\zeta_j}{\bar{\zeta}}\right)^{1/2} + \left(\frac{\bar{\zeta}}{\zeta_j}\right)^{1/2} - 2\right] - \frac{bb_j iy}{\zeta^{3/2}}\left(\frac{\sqrt{\zeta_1}}{\xi} + \frac{\sqrt{\bar{\zeta}_1}}{\xi^*}\right)$$
$$+ \frac{b\bar{b}_j y y_j}{\xi^{*2}}\left(\frac{1}{\sqrt{\zeta\bar{\zeta}_j}} - \frac{\sqrt{\bar{\zeta}_j}}{\zeta^{3/2}}\right),$$

$$\xi_j = \zeta - \zeta_j; \qquad \xi_j^* = \zeta - \bar{\zeta}_j; \qquad y = (\zeta - \bar{\zeta})/2i; \qquad y_j = (\zeta_j - \bar{\zeta}_j)/2i.$$

This complicated expression is a bizarre example of how difficult it can become to solve boundary-value problems in elasticity for any but the simplest situations. The various distances, ξ, ξ^*, etc., are diagrammed in Fig. 24.

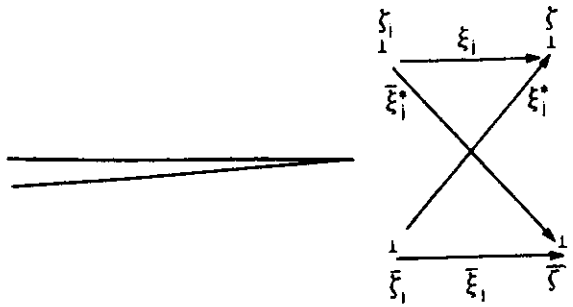

FIG. 24. Diagram of the distances ξ_j, ξ_j^*, $\bar{\xi}_j$, and $\bar{\xi}_j^*$ for a pair of dislocations at ζ and ζ_j for interpretation of Eq. (16.16).

17. The Wedge Case

When dislocations are in the elastic field of a wedge crack, then the equations for the potentials given in Part III,11 apply. For the Mode I–II case, the results become quite complicated, and the reader is referred to the paper by Sinclair[24] for numerical results. In Mode III, when the dislocation is on the x_1 axis, the results are (see Fig. 19).

$$\bar{f}_c = 0, \qquad p \neq 2,$$
$$\bar{f}_d = \frac{\Lambda b}{\zeta^{1-q}} - \frac{\mu b^2}{4\pi\zeta}\,\frac{1}{1+(\bar{\zeta}/\zeta)^q}, \tag{17.1}$$
$$q = 1/p.$$

These results for the dislocation reduce to the slit crack when $p = 2$. The curious result is that $f_c = 0$ when the wedge angle is finite. The analytic reason is that the singularity at the crack tip then differs from $1/\sqrt{r}$, and no residue exists. On the other hand, the wedge can certainly be extended, geometrically, into the medium, and when it does so, the external surfaces of the material extend, and work is done by the external stressing machines. So a paradox exists. The resolution is by means of the construction in Fig. 25, which shows that a self-similar translation of the wedge, *in which its elastic stress field is rigidly translated with it*, can only be produced by dislocation emission. That is,

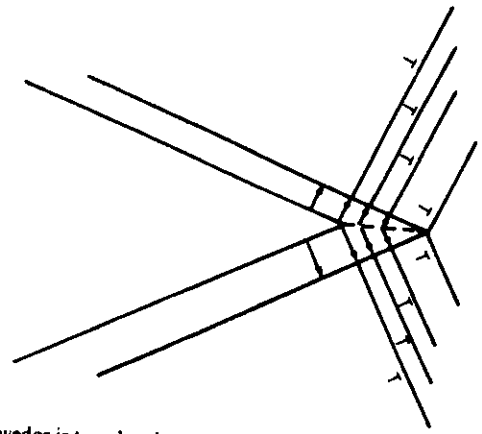

Fig. 25. When a wedge is translated to the right, the arrows show the displacement necessary, and indicate an accumulation of strain at the tip and along the sides. Thus, self-similar translation of the wedge and strain field is impossible elastically. When dislocation emission is allowed, such translation is possible.

if the wedge is cut open at its tip, and the faces forced into the wedge shape, elastically, then the stress field is not translationally invariant as the process continues as required in the Eshelby theorem. On the other hand, after emission of dislocations from the tip, the stress field of the wedge does so translate (when the dislocations move away!). But dislocation emission generates nonzero incompatibility, and is therefore nonelastic. If the work done on the dislocations as they are emitted is included in the analysis, then the work done as they emerge from the external surfaces is just that done by the external stressing machines, which resolves the paradox. In other words, there is no elastic force on the wedge as it translates, but there is on the dislocations. Closely coupled to this distinction between cracks and wedges is the fact that a Mode-I wedge does not disappear when the external stress is removed, even though the stress singularity does. By contrast, the cleavage crack, of course, has the basic property that, when the external stress is removed, the atom bonds zip together again and the crack disappears. Thus, the wedge is, fundamentally, a void (made by punching out dislocation loops or agglomeration of vacancies), whereas cleavage cracks are a logically distinct class of crystal lattice defect. This analytically derived distinction between cleavage cracks and wedges is, of course, intimately connected with the physical consequences for toughness to be discussed in later sections. (The dislocations in this discussion are, of course, "real" dislocations, as distinct from the virtual or "crack" dislocations introduced by Friedel and discussed in Part II,5.)

18. The J Integral

Equation (14.8) as applied to cracks was derived independently of Eshelby by Rice,[30–32] who called the right-hand side of Eq. (14.8) the J integral. J is used extensively in the fracture mechanics field for the analysis of fracture in plastic materials. Unlike our approach, which addresses plasticity in terms of the individual dislocations which are the seat of crystal placticity, J is calculated using continuum plasticity theory under the assumption that the medium obeys a nonlinear stress–strain law, which is a single-valued function of strain. From the definition of the strain-energy function, Eq. (14.11), W is then no longer a quadratic function of strain,

$$W = \tfrac{1}{2}c_{ijkl}\varepsilon_{ij}\varepsilon_{kl}, \tag{18.1}$$

but a more general nonlinear function of the strain. If this more general stress–strain law is a unique single-valued function of strain, then Eq. (14.12) is still valid, and the integral in Eq. (14.10) is still zero. Thus J is path independent.

The difference between J and f as we have used it is that in J there are no singularities representing the dislocations of the plastic zone, only a nonlinear stress–strain "constitutive law." Thus, unlike f, the contour path for J can be

shrunk through the deformation zone to the crack tip itself, for all of which contours, the value is an invariant. Further, outside the deformation zone, J is exactly the same as calculated for our $\bar{f}$, and *in this case*, from Eq. (15.10),

$$J_{III} = \mathrm{Re}(\bar{f}_{tot}) = K_{III}^2/2\mu. \tag{18.2}$$

Similar equations follow for Modes I and II,

$$J_{I,II} = \mathrm{Re}(\bar{f}_{tot}) = [(1 - \nu^2)/E](K_I^2 + K_{II}^2). \tag{18.3}$$

Note that we have followed tradition and defined J for the x_1 component of the force only.

Equations (18.2) and (18.3) follow only when a K field can be defined outside the deformation zone. That is, the boundaries of the specimen must be far away from the edge of the plastic zone surrounding the crack on a scale based on the size of the deformation zone. This case is called the "small-scale yielding" approximation. The major usefulness for J comes from its use when the small-scale yielding approximation is not valid (see Fig. 26). In this latter case, of course, J is still calculable by Eq. (14.8) even though no K field can be inferred. But the relation to the force has a less clear meaning—in our terms,

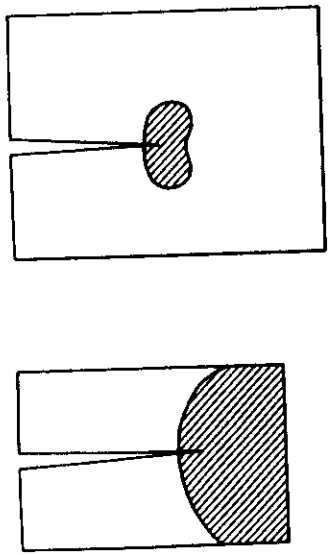

FIG. 26. Small-scale yielding. In (a), the deformation zone surrounding a crack (shown shaded) is small compared to all physical dimensions of crack size and specimen size. A K field outside the deformation zone is well defined. In (b), the deformation zone overlaps the specimen surfaces, and no K field can be defined at large distances from the crack. Nevertheless, J can be calculated in the latter case and is contour invariant.

the dislocations of the deformation zone may disappear in the boundary when the configuration is displaced if the deformation zone overlaps the boundary, for example.

The great value of J is associated with the fact that it is a characterizing parameter for a crack in a given material, and critical values of J can be measured for cracks at which catastrophic failure occurs, J_c. From its derivation, J_c is a parameter which depends only on the material properties such as yield stress, work hardening, etc., and can be used as a measure of the susceptibility of a material to failure under various conditions of stress and crack size. Moreover, J_c is a parameter which can be measured for specimens where the small-scale yielding assumption is no longer valid. Although there is some uncertainty about its physical meaning in this case, one would roughly expect from its contour invariance that the conditions at the crack tip which cause crack growth should continue to be approximately inferred by J_c even when not in small-scale yielding. Indeed, empirical explorations have shown that J_c is in fact an excellent fracture criterion in the large-scale or general yielding case as well as for small-scale yielding. (See the engineering references below.)

A more serious problem arises when a crack is stressed to the critical level and actually *moved*. As the crack moves, it leaves behind in its wake material which has gone through a stress cycle of loading followed by release. The J formalism is only valid if the release of stress follows the reversible stress–strain law used in deriving W in Eq. (14.11). Unfortunately, real materials exhibit considerable hysteresis if they are cycled into their plastic regimes, so that the J formalism is not valid for a crack which begins to move, and of course, most certainly not for one in something approaching steady-state or dynamic conditions. (Eshelby has described this condition on J in the classic words that the J_c concept is valid "so long as one does not call the material's bluff" by unloading it!) A great deal of work has been done to explore the practical limits of this difficulty for engineering purposes, and the limitations do not impose important constraints for crack initiation measurements and, surprisingly, not even for fatigue growth.[41,42] The reader is referred to the various volumes of the ASTM series for the details of the engineering applications, especially the article by Begley and Landes[43] and the book edited by Campbell *et al.*[44]

[41] C. Wutherichs, *Int. J. Fract.* **20**, R35 (1982).
[42] H. Heitmann, H. Vehoff, and P. Neumann, *Fatigue Eng. Matr. Str.*, in press (1986).
[43] J. Begley and J. Landes, Fracture toughness *ASTM Spec. Tech. Publ.* 560, p. 186; see other articles in this publication.
[44] J. Campbell, W. Gerberich, and J. Underwood, "Application of Fracture Mechanics for Selection of Metallic Structural Materials." ASM, Metals Park, Ohio, 1982.

For the purposes of this article, however, J and the continuum plastic approach have important limitations.[45] Perhaps the most important reason follows from a crucial theorem of Rice,[32,46] which states that if the stress field saturates near a crack tip, as it must in a plastic theory with a realistic finite plastic yield condition (which may incorporate strain hardening), then as the crack moves forward, all the energy supplied by the external loading machine is absorbed by the deforming region, and none is left over to provide energy to open the surface. We will return to this issue in Part VII, but this theorem is a fatal blow to the attempt to understand the conditions under which a crack will open (what we will call the fracture criterion) on the continuum level, because the energy supplied to open the bonds at the crack tip is the crucial event in the entire crack growth process. We will show that it is the local k which is important in this connection. That is, unlike J, which is a complete invariant, $\bar{f}$ gives a different value when the contour only encloses the local crack tip than when it encloses all the dislocations in the deformation zone, and it is this distinction which will allow a microscopic physical picture of the cracking process to be constructed.

19. The Griffith Relations

This section will be concluded with a review of the classic work of Griffith on the equilibrium of cracks in brittle materials.[47] This is the simplest example of crack equilibrium, a subject to which we return in Part VII.

It will be assumed that the crack of Fig. 16b is loaded in Mode I. Then, since there are no dislocations present, the elastic force on the crack, Eqs. (16.5) and (16.6), is

$$f_c = \frac{(1-\nu)}{2\mu} K_I^2. \tag{19.1}$$

Opposing this elastic force are resistive forces to crack opening provided by the material. In later sections, a variety of such forces will be considered, but there is always one contribution for a Mode-I crack, namely the simple surface tension of the opening surfaces at the crack tip. Working by simple analog to a soap bubble–like surface tension operating at the crack tip and neglecting for the moment the complexities of surface tension in a solid, the opposing force exerted on the crack by the crystal is simply

$$f_{crys} = -2\gamma. \tag{19.2}$$

[45] Fracture mechanics in design and service: A Royal Society discussion organized by H. Ford, P. Hirsch, J. Knott, A. Wells, and J. Williams. *Philos. Trans. R. Soc. London Ser. A* **299**, 3 (1981).
[46] J. Rice, *Proc. Int. Conf. Fract. Sendai* **1**, p. 309 (1966).
[47] A. A. Griffith, *Philos. Trans. R. Soc. London Ser. A* **221**, 163 (1920).

(Note there are two surfaces presented to the crack tip.)

When the elastic forces and surface tension forces are in balance, then the point of equilibrium is given by the critical value of K,

$$K_{Ic} = 2\sqrt{\gamma\mu/(1-\nu)}. \tag{19.3}$$

This equation is often called the Griffith relation, although it is not in the form given by him, since the stress intensity factor was introduced much later.

The point of equilibrium is actually unstable for the most usual form of crack loading (Problem 1), a fact most easily seen by working with the energy of the system. For Mode I, from Eqs. (9.10) and (18.4) the energy of the system with the double-ended crack of Fig. 16b is given by

$$U = 2\int_0^a (f_c + 2\gamma)\,da$$

$$= -[\pi F^2 a^2(1-\nu)/2\mu] + 4\gamma a. \tag{19.4}$$

This expression represents an inverted parabola as a function of the crack length, a, with its maximum at the Griffith stress, σ_G,

$$\sigma_G = 2\sqrt{\gamma\mu/\pi a(1-\nu)}. \tag{19.5}$$

This is the equation derived by Griffith[47] (as corrected—see Goodier[19]). With the assumed loading geometry, the crack is in unstable equilibrium at the Griffith point. With other forms of loading the specimen, for example by using a wedge at the crack mouth with a point-function opening force exerted at the mouth, the crack can be stable at the Griffith point. For these reasons, Eq. (19.3) is a more general and satisfactory way of expressing the crack equilibrium, because it is independent of the loading geometry. The reader will note that Eqs. (19.3) and (19.5) are equivalent through Eq. (9.10).

In the usual derivation of the Griffith equation (and in his original paper) a careful distinction is made between the elastic energy of the medium and the potential energy change of the external stressing machine. This subtlety is included in the Eshelby derivation of the force on the crack. Thus, f_c is not the derivative of the internal energy of the material with respect to crack position, but the derivative of the elastic energy of the total system, including energy changes of the external stressing machines, with respect to crack position.

The instability at the Griffith value is the physical reason why fracture is often catastrophic when a critical stress is reached on a crack and, of course, is the physical basis for the enormous practical importance of fracture control in actual materials. The instability in the other direction, i.e., crack closure, is not normally observed (except in polymers!) because the surfaces, once open, are subject to oxide formation, deformation, etc., so that crack closure with exact registry is difficult to effect. It is observed in brittle solids when sufficient care is taken, however. (See Fig. 9b.)

V. Atomic Structure of Cracks

20. Introduction

The discrete atomic nature of matter leads to chemical and other bonding effects at crack tips which generally go beyond simple continuum concepts. It will thus be necessary to develop descriptions of cracks in lattices. This general subject falls into two subheadings, the problems associated with cleavage (including the chemical effects) and the problems associated with the breakdown of the crack with emission of a dislocation. These two subjects will be treated consecutively in this and the following section. The mathematical framework will, however, be dealt with here. Although this discussion will address the properties of the ideal brittle crack, the ideas presented will be applicable to cracks shielded by dislocations in more general circumstances.

21. Lattice Statics

The mathematics of lattice statics for describing defects in lattices has recently been reviewed by Bullough and Tewary.[48] This method yields such a simple and accessible approach to the cracked lattice, that we will use it to discuss cracks in a simple 2D lattice in some detail. The discussion is based on the papers of Hsieh and Thomson,[49] Esterling,[50] and Thomson and Fuller.[51]

We imagine a lattice as shown in Fig. 3, which is bound by nearest-neighbor forces. The crack is defined by cutting a finite number $(2N + 3)$ of the bonds crossing the cleavage plane. An external force, F_0, is assumed to act on the two atoms at the center of the crack to hold the crack open, again as shown in Fig. 3. It is assumed that all the atoms of the crystal are bonded by springs, so that the system as a whole responds in a strictly linear manner to the imposition of the external force, $\mathbf{F}_0$. Finally, it is assumed that arbitrary bonding forces, f, are applied to the pair of atoms at each end of the cut, which for the moment will be viewed as "external" forces. The response of the system can then be written in the form

$$\mathbf{U}_i = \sum \ddot{G}_{ij}\mathbf{F}_j. \tag{21.1}$$

$\mathbf{U}_i$ is the displacement of the jth lattice point, and $\ddot{G}$ is the Green's tensor for the cracked lattice. $\ddot{G}$ is a function of N, the crystal structure, and the direction of the cleavage plane in the lattice. $\mathbf{u}$ and $\mathbf{F}$ are vectors. Equation (21.1) is a general lattice equation, and can be applied to any lattice or direction of crack. But in order to develop some simple illustrative results, we will restrict the following discussion to simple cubic lattices, with $\mathbf{u}$ and $\mathbf{F}$ in the x_2 direction, so that these quantities become simple scalars. Then, because of symmetry, with only the forces F_0 on the central pair and $-f_N$ on the atoms at the tip, when $N \gg 1$, the two equations from the set of Eq. (21.1) most important to us are those giving the displacement of the center of the crack, u_0, and the displacement at the tip u_N. Thus

$$\begin{aligned} u_0 &= G_{00}F_0 - 2G_{0N}f_N, \\ u_N &= G_{0N}F_0 - G_{NN}f_N, \end{aligned} \tag{21.2}$$

the distinction of capital and lowercase between F_0 and f_N is made to emphasize the point that F_0 is a "real" external force, while f_N will ultimately be interpreted as an atomic bond force.

The general formalism of Bullough and Tewary[48] for lattices has to be modified to obtain the relevant Green's tensor for the crack. In brief, for the crack, the G is obtained by calculating the displacement from the perfect lattice Green's tensor due to a unit force, when fictitious forces are simultaneously applied on the cleavage plane to annihilate the bonds there. The result is the cracked lattice Green's function, and details for finding it will be found in Hsieh and Thomson.[49] For present purposes, the coefficients, G_{00}, and G_{0N} and G_{NN} are simply taken as given constants.

The character of the crack solution is then easily seen by inspection of the first of Eqs. (21.2) when f is set to zero, viz. $u_0 = G_{00}F_0$. The displacement as a function of F_0 is simply a straight line with slope G_{00}, where the slope is a function of N. For different values of N, the solution is then a manifold, as shown in Fig. 27. If the force law is assumed to possess a critical range, as shown in Fig. 29a, then there exists a maximum value of displacement u_0 when the bond at the tip reaches the critical displacement. Thus, the portion of the line in Fig. 27 larger than this maximum value (above the upper limit curve) is not an allowed part of the solution. Likewise, when F_0 is decreased, there comes a point where the last open bonds on the cleavage surface at the tip snap back together, and again, portions of the line less than this value (below the lower limit curve) do not represent a solution. Thus, the crack "solution" for different values of crack length is the set of lines between the limit curves of Fig. 27. This solution shows that for a given value of crack length, the crack is stable over a range of external forces, and for a given F_0, a number of crack lengths have stable solutions. This result is contrary to the continuum solution, Eq. (19.4), where there is only a single stable solution (crack length) at

[48] R. Bullough and V. K. Tewary, "Dislocations in Solids" (F. R. N. Navarro, ed.), Vol. 2, p. 1. North Holland Publ., Amsterdam, 1979.
[49] C. Hsieh and R. Thomson, *J. Appl. Phys.* **44**, 2051 (1973).
[50] D. Esterling, *J. Appl. Phys.* **47**, 486 (1976).
[51] R. Thomson and E. Fuller, *in* "Fracture Mechanics in Ceramics" (R. Bradt *et al.*, eds.). Plenum, New York, 1982.

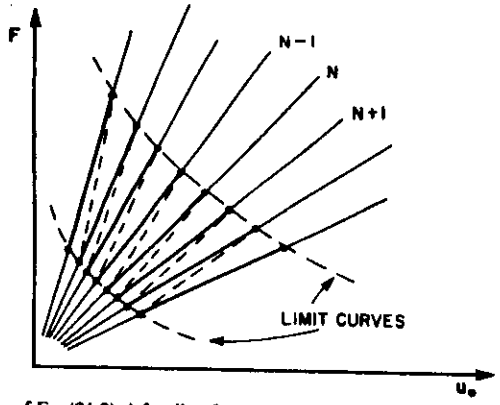

FIG. 27. Solution of Eq. (21.2). A family of compliance curves is generated for various values of crack length N. The curves are limited at a maximum displacement by the bond strength at the tip, and at a minimum displacement by reconnection of the first broken bond at the tip. At the maximum displacement for N, the solution snaps back to $N + 1$ at the minimum, as shown by the dotted lines, provided F can be varied at the same time.

the maximum of a parabola. [The loading conditions of Fig. 3 and for Eq. (19.4) are not the same, but the result is still the same—continuum theory using the loading system of Fig. 3 yields only a unique crack length for any external load, F_0.] When nonlinear bonding forces f_N are postulated at the tips of the crack, then the straight lines of Fig. 27 become the continuous curve shown schematically for a single branch in Fig. 28.

The multiple crack solutions depicted by Fig. 27 are separated by energy barriers, explained as follows. In Fig. 28, the line for constant F_0 crosses the curve at three points. The energy necessary to move from point 1 to point 2 is given by the expression

$$\Delta E_{12} = \int_1^2 F_0(u_0)\,du_0 - F_0\,\Delta u_0. \tag{21.3}$$

The first term is the change in internal energy of the system, and the second is the change in potential energy of the external driving system. ΔE_{12} is the total energy change. ΔE_{12} is thus the cross-hatched area shown in Fig. 28 from point 1 to point 2, and is a positive energy. To go from 2 to 3 is a negative energy. Thus, states 1 and 3 are stable states, and state 2 is a saddle point in configuration space between the two stable states.

This energy is easily calculated if the force law is known, by reference to Eq. (21.2). In this equation, the forces f_N are now assumed to be the actual nonlinear bonding forces exerted by the atoms according to some specified force law, Fig. 29. Since $f_N = f_N(u_N)$ is a nonlinear function of u_N, the set of

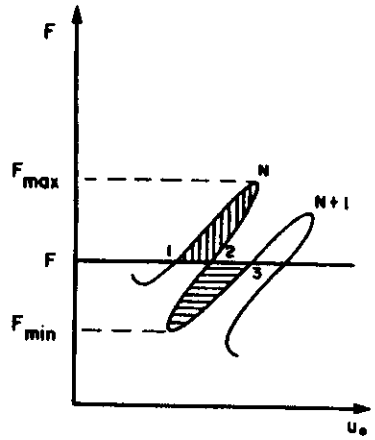

FIG. 28. Crack solution for nonlinear forces for N and $N + 1$. For a given F several discrete solutions are possible. Positions 1 and 3 are stable. Position 2 is unstable. The cross-hatched areas correspond to trapping barriers. That from 1 to 2 is a forward barrier and that from 3 to 2 is a reverse barrier.

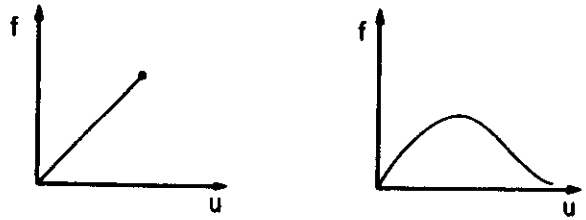

FIG. 29. Bond forces f. A variety of bond forces are discussed. In the left-hand part, the force is a snapping spring. In the right-hand part, a more realistic nonlinear force is shown.

equations (21.2) become a pair of coupled nonlinear equations for the displacements u_0 and u_N in terms of the independent variable F_0. The constants G are still the linear lattice Green's tensor, however. If f_N is eliminated from Eq. (21.2), then after taking differentials,

$$du_0 = \frac{2\,G_{0N}}{G_{NN}}\,du_N + 2\,G_{0N}\left(\frac{G_{00}}{2\,G_{0N}} - \frac{G_{N0}}{G_{NN}}\right)dF. \tag{21.4}$$

Here and later we drop the subscript from F and f because no confusion is possible. Substitution of this expression into Eq. (21.3) yields

$$\Delta E_{12} = 2\int_1^2 \frac{G_{0N}}{G_{NN}}\,F\,du_N - F\,\Delta u_0. \tag{21.5}$$

the term $\int_1^2 F\,dF$ is dropped from Eq. (21.5) because states 1 and 2 have the same value of F. Substituting for F from Eq. (21.2) and for Δu_0 from Eq. (21.4),

$$\Delta E = 2\int_1^2 f(u_N)\,du_N + \frac{1}{G_{NN}}\Delta(u_N^2) - \frac{2G_{0N}}{G_{NN}}\Delta u_N. \tag{21.6}$$

In this equation, $f(u)$ is explicitly the atomic bond function, and is given by the functional form illustrated in Fig. 29. Equation (21.6) exhibits an important theorem for all nonlinear atomic processes at the tip, when the nonlinear process is limited to only one atom, which we will call the decomposition theorem. The activation energy ΔE_{12} is composed of three additive parts. The first is the energy change in the chemical bond at the tip, and is the only term which can reflect the influence of external chemistry. The second is the change in the linear lattice, which is a simple quadratic function of the displacement change at the tip (or alternatively, displacement at the point of force application). The third is the change in the external machinery potential energy which is a negative linear term. The last two terms depend only upon the linear properties of the bulk material. This simple decomposition theorem can be used to deal qualitatively with complicated chemical interactions at the crack tip, even when the nonlinearity is not strictly limited to a single bond. The decomposition theorem is graphically depicted in Fig. 30.

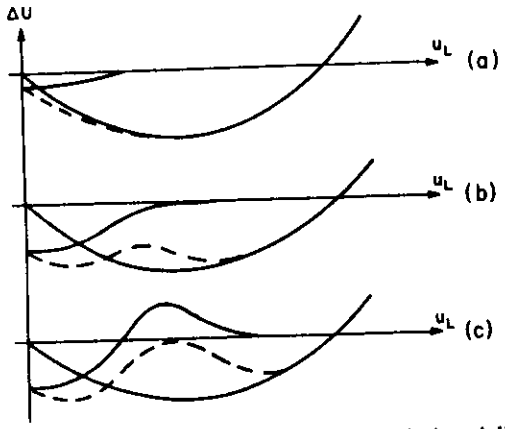

FIG. 30. Diagrams illustrating the decomposition theorem. The broad displaced parabola is composed of the second and third terms of Eq. (21.6). The atomic-bond function is displayed in each of three cases superimposed on the parabola. The resultant is the dotted curve. In (a) the bond function is weak and not near the parabola minimum; no activation energy. In (b), the bond is strong, and has its maximum slope close to the parabola minimum; activation energy. In (c), an additional chemical activation energy is present, which adds a large bump to the total activation energy.

The model above has been pursued more quantitatively by Thomson and Fuller[51] to explore the sensitivity of the energy barriers to force-law form, and to explore the stress dependence of the barriers. In general, the result is that an extreme snapping force law like Fig. 29a leads to a maximum trapping, compared to the softer law of Fig. 29b. This result and that of other discrete crack theories, suggest that for realistic force laws in materials, the 2D energy barrier will lead to a trapping stress range which will be small compared to the Griffith stress. The energy dependence of the energy barriers is found to depend on the type of force law, and

$$E_{12} \propto (k - k_c)^n$$
$$n = \begin{cases} 2, & \text{snapping bond (Fig. 29a),} \\ \frac{3}{2}, & \text{inverted parabola.} \end{cases} \tag{21.7}$$

k_c is a constant, and is the value of k when dynamic cleavage occurs. The 2D mathematics above does not account for the fact that the real crack will make use of its third degree of freedom in moving from one atom row to the next. In particular, just as for dislocations, any crack limited by the lattice barriers will traverse the barriers by nucleation of a double kink of finite length, so the energy to cross traversing the barrier will be finite. Such kinks were proposed by Hsieh and Thomson,[49] and have been discussed semiquantitatively by Esterling,[50] Sinclair[52] for simulated Si, and by Lin and Hirth[53] in a quasicontinuum model.

The only other fully published work with the lattice statics approach is that by Esterling,[50] who explored a variety of force laws at the tip, and who first pointed out that nonsnapping force laws were accessible with the lattice-statics approach. He also made some estimates of kink configuration in a quasi-3D calculation. All such work done by the authors,[49–51] however, was performed in simple square lattices, and was limited to nonlinear forces restricted to the tip bonds. As such, this work is only of very rough qualitative significance. However, the analysis is actually entirely general, and in principle can be applied to any lattice structure and to any number of nonlinear forces at the tip. For other lattices, the Green's tensor would be more difficult to calculate than for the square lattices, but the strategy outlined in Hsieh and Thomson[49] for generating the Green's tensor is applicable using the general theory given in Bullough and Tewary.[48] In addition, if more than one nonlinear bond is contemplated at the tip, then additional terms, f_j and u_j at the tip, must be included in Eq. (21.2). Counting the displacement u_0, Eq. (21.2) becomes a set of $(L + 1)$ equations for $u_0, u_N, u_{N+1}, \ldots, u_{N+L}$ in terms of F_0,

[52] J. Sinclair, *Philos. Mag.* 31, 647 (1975).
[53] I. H. Lin and J. P. Hirth, *J. Mater. Sci.* 17, 447 (1982).

$f_N(u_n)$, etc. This is now a set of $(L + 1)$ nonlinear equations which will require numerical techniques to solve, but poses no further analytic difficulties. Thus, the extended lattice statics approach as outlined here is a very powerful method for obtaining general quantitative results. Once the Green's tensor has been calculated for a given lattice (for a given crack length), then the generalization of Eq. (21.2) can be solved for any arbitrary set of force laws (or chemical interactions), and much insight into the various fracture configurations could be gained. It is to be emphasized that the analysis is not in any way limited by considerations of whether the set of atoms in the discrete lattice is large enough (because it is ∞), or by considerations about boundary conditions between some internal discrete enclave and an outer infinite crystal, because there is no such arbitrary boundary in the problem. Sinclair[54] has reported some initial results on such a program relating to the problem of dislocation emission, but this work is still in progress at the time of writing.

22. Discrete-Enclave Method

A second method for studying the atomic configurations of cracks embeds a finite discrete set of atoms within a surrounding continuum. The configuration is then found numerically by successive approximation of a self-consistent displacement field in the discrete set and in the continuum. This method has a long history for all sorts of defect calculations, and has been used to simulate cracks in real materials. The first such attempts were made by Gehlen and Kanninen[55] using the Johnson[56] potential for iron, and these authors in various combinations with A. Markworth and J. Hirth gradually improved the early computer model over a number of years, in part with a continuum Green's function technique of J. Hirth[57] so that a flexible boundary is allowed between the continuum and discrete regions. In addition, an attempt was made to model the effects of hydrogen on the configuration. Results of this work, together with references to prior work, are given in the paper by Markworth *et al.*[58] The reader is also referred to the paper by Sinclair *et al.* [59] for details on the flexible boundary method (Flex II) as it has been developed for simulation calculations using two embedded regions inside an

[54] J. Sinclair, to be published (1986).
[55] P. C. Gehlen and M. F. Kanninen, *in* "Inelastic Behavior of Solids" (M. Kanninen *et al.*, eds.), p. 586. McGraw-Hill, New York, 1970.
[56] R. A. Johnson, *Phys. Rev.* **134**, *A* 1329 (1964).
[57] J. Hirth, *Scripta Metall.* **6**, 535 (1972).
[58] A. J. Markworth, M. F. Kanninen, and P. C. Gehlen, *Proc. Int. Conf. Stress Corrosion Cracking, France* June 12 (1973); see also, P. C. Gehlen, G. Hahn, and M. F. Kanninen, *Scripta Metall.* **6**, 1087 (1972).
[59] J. Sinclair, P. C. Gehlen, R. G. Hoagland, and J. P. Hirth, *J. Appl. Phys.* **49**, 3890 (1978).

outer continuum. In part, this work has been aimed at simulating cleavage in iron and Fe/H, but it has also been used to study the dislocation emission problems, as discussed in the next section.

Sinclair[52] has used Flex II to simulate a crack in Si, using a directed-bond noncentral force, and has studied how the lattice trapping varies with choice of the radial part of the force law. In addition, he has estimated the kink motion and formation energies for Si with these laws, and finds that the kink motion energy is in the range 0.01 eV, and that the kink pair-formation energy is of the order 0.1 eV. The estimate of formation energy, however, is very crude, and based on a quasicontinuum string model of the crack. The interesting conclusion from this work, however, is that even in this most favorable case, the lattice trapping barriers are estimated to be small, though the actual numbers involved must be considered very rough estimates for the 3D quantities because of uncertainty in the force law.

Most recent work with this method has been an extensive study of simulated Fe with the Johnson potential and simulated Cu with the Morse potential by de Cellis *et al.*,[60] with the intent to study the dislocation emission question of Part VI. The new mathematical development in this work is to derive a boundary condition between the discrete enclave and the continuum which is sufficiently flexible as to allow a dislocation to penetrate it. The iron cleavage plane was found to be {100}, and unlike the earlier work of the Battelle group, the critical k for cleavage is essentially the Griffith value. Other points discussed by these authors are the effect of isotropic/anisotropic elastic solutions in the continuum, and the effect of size of discrete enclave on the accuracy of the results.

Mullins[61] has also recently analyzed simulated iron with the Johnson potential to study dislocation emission and crack branching under mixed loading, with results to be discussed in Part VI.

23. Molecular Dynamics

Straightforward molecular dynamics has been applied to the crack problem by Ashurst and Hoover[62] and more recently in a series of papers by Paskin, Dienes, and collaborators.[63–66] In these calculations, 2D simulations are

[60] B. de Cellis, A. Argon, and S. Yip, *J. Appl. Phys.* **54**, 4864 (1983).
[61] M. Mullins, *Int. J. Fract.* **24**, 189 (1984).
[62] W. T. Ashurst and W. G. Hoover, *Phys. Rev.* **1314**, 1465 (1976).
[63] A. Paskin, D. K. Som, and G. J. Dienes, *Acta Metall.* **31**, 1253, 1841 (1983).
[64] A. Paskin, K. Sieradsky, D. Som, and G. J. Dienes, *Acta Metall.* **30**, 1781 (1982).
[65] A. Paskin, D. K. Som, and G. J. Dienes, *J. Phys. C* **14**, L171 (1981).
[66] G. J. Dienes and A. Paskin *in* "Atomics of Fracture" (R. Latanision and J. Pickens, eds.), p. 671. Plenum, New York, 1983.

made with the largest number of atoms which are practicable in the computer ($\sim 10^4$). The Lennard–Jones 6/12 power-law potential, truncated to include only the nearest neighbors, is assumed. Such a force law does not simulate any particular material, but these authors have very astutely used the model to study a variety of general phenomena to be expected at the crack tip, and as a test bed for investigating the limit of applicability of quasicontinuum calculations. It has also proved possible for these authors to study both static and dynamically moving cracks by varying the external load. The results principally relate to dislocation emission effects, which are the subject of Part VI.

24. Force Laws for Defect Calculations

Clearly, the calculations of crack structure depend in a crucial way on the validity of the force laws which are used. In ionic crystals, the Born–Mayer type of theory can lead to defect calculations for the simple ionic materials possessing a fair degree of accuracy.[67] No crack calculations have been made in those materials, however, because the potential is long ranged, and this would lead to special problems with present techniques.

In the case of the simple metals, pseudopotentials have been used extensively for defect calculations.[68] However, pseudopotentials in their standard form require that the volume change be small, and stacking faults are the only defects where the dilatation distortion is truly negligible. Since the crack involves an incipient surface, there is no hope that standard pseudopotentials can yield suitable force laws for crack calculations.

Another approach which has been used is the molecular cluster quantum chemistry approach. For example, charge distributions have been calculated for small clusters intended to simulate the vicinity of an impurity on a grain boundary, which are then used to rationalize what types of atoms will weaken or strengthen a boundary.[69] But the number of atoms needed to simulate the properties of a crack are well beyond current capabilities.

A third approach is completely heuristic, in which a spline or other function is constructed which is consistent with known material properties.[48] The Johnson potential[56] for iron is such an example. However, there is no reason to believe that such an approach can yield any more information than is fed into it, so far as making predictions for a particular material is concerned.

Thus, the crack poses the same challenge as any defect, to calculate the absolute energy of a configuration from first principles, which is still one of the

[67] M. P. Tosi, *Solid State Phys.* **16**, 1 (1964).
[68] D. Esterling, *Comments Solid State Phys.* **9**, 105 (1979).
[69] C. Briant and R. P. Messmer, *J. Phys. Colloq.* **43**, 255 (1982).

most difficult things to do in theoretical condensed matter physics. But it also goes one step further, and adds a highly distorted surface, where the perturbation of the lattice (the volume-dependent term) is not weak. Hence, the crack is likely to be the last defect for which reasonable force laws can be obtained.

In the opinion of the author, interesting progress is being made on two fronts. In the first, the tight-binding method has recently attracted considerable interest for calculating defect structures, and has the advantage that noncentral forces can be derived for the *d* shells.[70]

The second approach has been an intensive effort by Barnett and Landman[71] to calculate the configuration of a surface in the simple metals. The result is a set of pair potentials which are structure dependent. Unfortunately, the volume- and structure-dependent effects are not always small.

Where do we stand? Clearly, for the near term, there is not likely to be a first-principles calculation of a crack tip. The best we are likely to have is some guidance from theory on general rules about what the "force laws" are like, and how to use them in a qualitative sense. But the crack will probably be the last defect for which a configuration calculation will be attempted which represents an actual solid. Thus, we are left only with the simulation of the general properties of cracks, and the rationalization of findings in terms of "green thumb" chemistry. But these efforts, as already shown by the work of Paskin *et al.*, and Michalske and Freiman (see Part V,26) are likely to be very fruitful in terms of physical and chemical insight, until more quantitative help is available from first principles.

25. Chemical Kinetics

The general results above which show that discrete atomic effects at crack tips lead to energy barriers to crack motion are important for the interpretation of a variety of kinetic effects of fracture. Although, strictly speaking, the mathematical model in Part V,21 only addressed pure lattice effects, the discussion of the decomposition theorem in Fig. 30 shows that external chemical agents which can affect the bond breaking will conform to the same general conceptual framework. Likewise, although the barriers described above were those generated by the discreteness of the lattice, chemical attack at the tip will be discrete in the same way. Furthermore, it is a common occurrence for chemical reactions in the gas phase to have energy barriers to

[70] D. G. Pettifor, *in* "Atomistics of Fracture" (R. Latanision and J. Pickens, eds.), p. 281. Plenum, New York, 1983.
[71] R. N. Barnett and U. Landman, *Phys. Rev. Lett.* **51**, 1359 (1983).

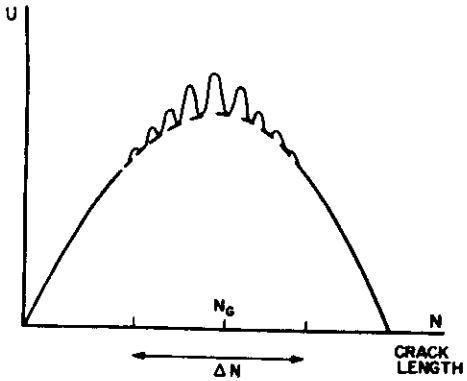

FIG. 31. Modified Griffith energy function. The smooth parabolic curve corresponding to Eq. (19.4) (- - -), becomes a "dinosaur back" function. The trapping occurs over the range ΔN about the central maximum.

the reaction, and the highly constrained region of the crack tip will certainly enhance this possibility. Thus, barriers of one kind or another can be expected to show up for crack growth near the Griffith stress. Figure 31 is a schematic drawing of the modification which the energy barriers make in the continuum energy function, Eq. (19.4).

Physically, the energy barriers will give rise to a thermally activated crack growth (or, according to theory, to regression) near the Griffith point. The rate of jumping the barriers according to chemical reaction rate theory is[72]

$$v^* = \frac{k_B T}{h}\frac{Z^*}{Z} = \left(\prod_{i=1}^{N} \nu_i \Big/ \prod_{i=2}^{N} \nu_i^*\right) e^{-E_{12}/k_B T} \tag{25.1}$$

Here the * represents the 3D saddle configuration, Z is the partition sum, ν_i is a frequency of the system, and E_{12} is the energy of the double kink. In the activated state, there is one fewer vibration frequency than in the stable state. When chemical reactions are taking place, the pre-exponential is modified from that of the simple lattice by incorporation of the appropriate partition sums for the gaseous and adsorbed chemical species.[72] The activation energy (even that for a 3D kink pair), should show the salient features of the 2D calculations, such as its k dependence.

When forward rates of motion for the crack equal the reverse rate, a condition for equilibrium between two stable states, 1 and 3, can be written

$$v_{13} = v_{31}, \qquad \text{or} \qquad Z(1) = Z(3), \tag{25.2}$$

[72] R. Thomson, *J Mater. Sci.* **15**, 1014 (1980).

which, in terms of the standard expressions relating the partition sums to the free energy F, becomes equivalent to $F(1) = F(3)$.

This general condition for equilibrium does not mean that the rates are equal when the forward barrier in Fig. 28 or 31 is equal to the reverse barrier, because the states 1 and 3 are not equivalent states. State 3 differs from 1 by the addition (in 2D) of one surface pair. Thus, the vibration structure of the crystal with one additional surface pair is different from the initial state, and entropy contributions must be counted in setting up the free energy balance, $F(1) = F(3)$. Hence, at $T \neq 0$, there are subtle differences between forward and reverse barriers. Similar results are, of course, valid in the case of chemical adsorption during crack growth.

When the microscopic analysis is translated into the appropriate thermodynamic and mechanical variables, it can be shown[72] that $F(1) = F(3)$ leads to the general law

$$f = 2\gamma, \tag{25.3}$$

where f is the force on the crack derived in Part IV. γ is the temperature-dependent surface energy as defined by Gibbs. This equation remains valid in the case of chemical interactions at the crack tip, and γ in that case depends in the standard way on the surface coverage of the external chemical species. Equation (25.3) was first suggested by Petch and Stables[73,74] on thermodynamic grounds for hydrogen embrittlement in Fe.

An interesting question arises when internal chemistry is combined with external chemistry, for example when a crack runs down a grain boundary with a concentration of solute impurity. If the initial grain boundary distribution is in thermal equilibrium with the dispersed impurity in the bulk solid, then, as the crack opens, the solute on the newly opened cleavage surface will usually not have time to come into equilibrium with the internal solute distributions. This problem has been analyzed in terms of a constrained equilibrium by Hirth and Rice,[75] with the result that when such a grain boundary opens, the γ criterion is modified to be

$$\gamma \to \gamma - \tfrac{1}{2}\gamma_{GB} \tag{25.4}$$

where γ_{GB} is calculated for the boundary covered in such a way as to be consistent with the diffusion off the boundary which will be possible under the circumstances. That is, the energy and vibration entropy will be of the appropriately specified covered surface.

[73] N. J. Petch and P. Stables, *Nature (London)* **160**, 842 (1952).
[74] N. J. Petch, *Philos. Mag.* **1**, 331 (1956).
[75] J. P. Hirth and J. Rice, *Metall. Trans. A* **11**, 1501 (1980).

26. Slow-Crack-Growth Observations

Although lattice trapping is a predicted result for a crack in any lattice, the magnitude of the effect depends on the details of the "back side" of the force law and on its range. Theoretical estimates do not suggest it should be a ubiquitous and easily observed effect, and, indeed it seems to have been observed unambiguously as a slow crack growth in vacuum only in silicate glasses. Even in these systems, the crack-growth curves are very steep, and thus hard to observe. Such slow crack growth has been looked for in Si, where the calculations of Sinclair[52] reported above suggest an observable activation energy, but so far the material has not been studied in a sufficiently high vacuum for the result to be conclusive.

When it comes to chemically enhanced fracture, however, thermally activated slow crack growth is very widespread. However, only in the brittle systems is there general agreement about the effect of the chemistry. In glasses, where slow crack growth has been most extensively studied, the results have been reviewed recently by Wiederhorn *et al.*[76] and Lawn.[77] Briefly, chemically enhanced crack growth in glass is characterized by three regions as shown for H_2O in Fig. 32. Region I depends on the H_2O vapor pressure, and the stress intensity factor, as the general reaction-rate theory suggests. At a certain velocity, Region II, the crack outruns the adsorption rate on the crack tip, and the velocity is independent of stress. Then when the crack reaches the intrinsic fracture stress, the velocity curve (Region III) is similar to that in a vacuum. Stage-III fracture still exhibits some atmosphere-dependent effect which is thought to be a dielectric effect on the bonds at the tip by the water.

Michalske and Freiman[78] have proposed that the water reaction features both hydrogen and electron donors in the reaction, leading to enhanced crack growth. Consistent with this proposal, they have also shown that molecules with a similar capability such as NH_3, N_2H_4, and CH_3NO have similar crack growth curves. The crucial role of hydrogen is confirmed by the fact that D_2O has a slower growth than H_2O.

In further work[79] to explore the effect of direct chemical attack at the Si–O bridging bond in simple glasses, SiO_2 doped with network modifiers (Na and Li) have been cracked in a variety of environments. The effects of the network modifiers have also been studied in molecular-orbital calculations to find the effect of both the bonding and nonbonding Si–O orbitals.[80,81] Although the work is still in progress, it appears that the simple ideas expressed in the decomposition theorem above are correct, and can be used to interpret the results.

[76] S. Wiederhorn, E. Fuller, and R. Thomson, *Metall. Sci.* **14**, 450 (1980).
[77] B. Lawn, *J. Am. Ceram. Soc.* **66**, 83 (1983).
[78] T. Michalske and S. Freiman, *Nature (London)* **295**, 511 (1982).
[79] G. White, D. C. Greenspan and S. Freiman *J. Amer. Cer. Soc.* **69**, 38 (1986).
[80] B. de Jong and G. Brown, *Geochim. Cosmochim. Acta* **44**, 491 (1980).
[81] B. de Jong and G. Brown, *Geochim. Cosmochim. Acta* **44**, 1627 (1980).

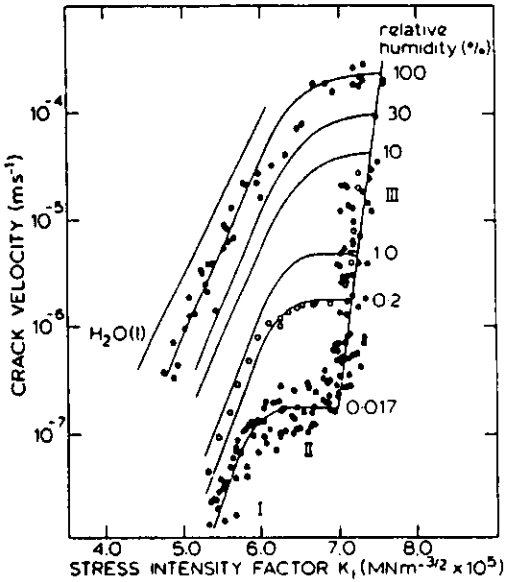

FIG. 32. Slow crack growth of glass in water. Three regions are observed. Region I corresponds to the chemically enhanced growth theory displayed here. In Region II, the external environment is outrun by the crack. Region III is the intrinsic region (after Wiederhorn *et al.*[76]). (Courtesy of S. Wiederhorn.)

VI. Dislocation Emission from Cracks

27. Introduction

According to Part II, one of the two ways to realize a ductile material is if the underlying crack emits dislocations before it cleaves as the external stress is raised. In this section this emission–cleavage dichotomy will be explored.

Historically, this subject was first addressed by Kelly *et al.*,[82] who pointed out that at the tip of a sharp crack, when the K level is high enough to generate cleavage, it is also in the range to initiate spontaneous shear breakdown in the vicinity of the tip. Thus, which event occurs first will depend on the relative

[82] A. Kelly, W. Tyson, and A. H. Cottrell, *Philos. Mag.* **29**, 73 (1967).

magnitudes of the ultimate strength of the material against tension or shear. Rice and Thomson[22] analyzed the problem in terms of dislocation emission from the crack tip, because if shear breakdown occurs at the tip, the result is dislocation emission. However, both descriptions are physically equivalent, as has been pointed out by Lin.[83] Both of these arguments, however, deal with an essentially atomic property of the tip by quasielastic means, and more exacting attempts have addressed the problem via computer simulation with two-dimensional atomic models. However, since only inadequate force laws exist for atoms in the vicinity of such a severe distortion as a crack, these calculations also have major limitations. Thus, the current theoretical situation is not satisfying from a quantitative point of view, though considerable qualitative insight is available. Experimentally, both stable and unstable cracks have been demonstrated, as explained in Part II, and evidence has also been presented there showing that at least under certain conditions dislocation emission and cleavage can coexist in the same material.

In this section, the current status of these effects will be presented. We will begin by reviewing the continuum/cutoff theories, then present the computer-simulation results, and close with a discussion of the experimental findings.

28. Elastic Estimates for Sharp Cracks

Suppose a slit crack in the configuration of Fig. 16 exists, and that no dislocations exist out to a distance large compared with a lattice spacing. Then, a k field can be defined in the vicinity of the crack tip. Assume next that in the two-dimensional configuration a dislocation is emitted from the crack tip. As a result of the emission (Fig. 33), a ledge is formed at the tip, and an elastic force is exerted between the crack and the emitted dislocation, as calculated in Part IV. For the moment, all effects of any other dislocations in the far field are neglected.

In two dimensions, the total force on the dislocation emerging from the crack is composed of a linear combination of the Mode-I, -II, and -III forces. From Eqs. (15.7), (16.8), and (16.10), the force component in the slip plane is

$$\mathrm{Re}(\bar{f}_d^{sp}) = \frac{k_{III} b_s}{\sqrt{2\pi r}} \cos(\theta/2) + \frac{b_e}{2\sqrt{2\pi r}} [k_I \sin\theta \cos(\theta/2) + k_{II}(2\cos(3\theta/2) + \sin\theta \sin(\theta/2))] - \frac{\mu}{4\pi r}\left(b_s^2 + \frac{b_e^2}{1-\nu}\right). \quad (28.1)$$

The expression breaks down into terms bilinear in b and K (direct k-field force), and other terms quadratic in b (image terms). For a positive b which

[83] I. H. Lin, *J. Mater. Sci. Lett.* **2**, 295 (1983).

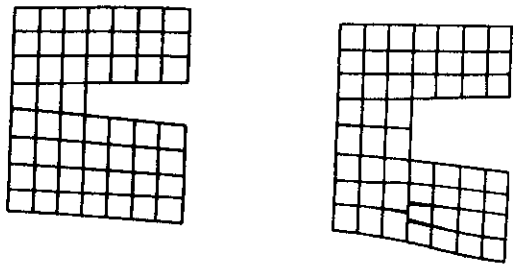

FIG. 33. Crack-tip breakdown in shear by dislocation emission.

blunts the crack, these forces oppose one another, as graphed schematically in Fig. 34. We have used the lower-case k in Eq. (28.1) because it refers to a bare crack without other dislocation effects. According to this result, there is always an attractive force for sufficiently small values of r, and a repulsive force for sufficiently large values of r, because of the different functional dependence on r of the image and k-field forces. Thus, on the basis of purely elastic effects, a crack will always be mechanically stable against the spontaneous emission of a dislocation. But for values of r smaller than the core size of the dislocation and crack, the elastic approximation breaks down. Thus, if the zero in the function of Eq. (28.1) occurs for values $r_0 > r_c$, where r_c is a measure of the effective core size, and r_0 is the radius for which $\bar{f}_d^{sp} = 0$, then emission will occur spontaneously, because by the time a dislocation is "well formed," it already sees a repulsive elastic force, and it never traverses an attractive regime. In other terms, when $r < r_c$ one might assume the emerging dislocation has a Burgers vector which is proportional to r, and in this regime, the repulsive force becomes dominant until the dislocation is formed. Again, if $r_0 < r_c$, then the net force is always repulsive.

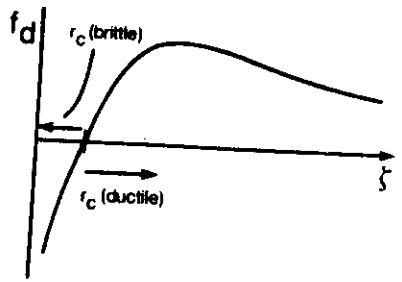

FIG. 34. Force between a crack and a dislocation as a function of the distance ζ between them. The core size of the dislocation r_c is shown in relation to the null point of the force for brittle and ductile cases.

If $f = 0$ in Eq. (28.1), a condition is obtained for r_0 in terms of k, and if r_0 is set equal to the core size r_c, then, from the discussion above, an equation is obtained for values of k which must be exceeded in order to emit a dislocation,

$$\frac{\mu}{2\sqrt{2\pi r_c}}\left(b_s^2 + \frac{b_e^2}{1-\nu}\right) = k_{IIIE} b_s \cos(\theta/2) + \frac{b_e}{2} k_{IE} \sin\theta \cos(\theta/2) + \frac{b_e}{2} k_{IIE}(2\cos(3\theta/2) + \sin\theta \sin(\theta/2)). \quad (28.2)$$

The added subscript E, on k refers to the critical values for emission.

Equation (28.2) yields a criterion for emission of a dislocation, and the cleavage/emission criterion is obtained by comparing Eq. (28.2) with the Griffith criterion for cleavage. For simplicity, we first consider the simple case $k_{II} = k_{III} = 0$. Then Eq. (28.2) becomes

$$k_{IE} = \frac{\mu}{\sqrt{2\pi r_c}} \frac{b_s^2 + b_e^2(1-\nu)}{b_e \sin\theta \cos(\theta/2)}. \quad (28.3)$$

The Griffith criterion for cleavage is

$$k_{Ic} = 2\sqrt{\mu\gamma/(1-\nu)}. \quad (28.4)$$

The combined criterion for cleavage/emission in pure Mode I then becomes

$$k_{IE} < k_{Ic}, \quad \text{emission}, \qquad k_{IE} > k_{Ic}, \quad \text{cleavage}. \quad (28.5)$$

This form of the cleavage–emission criterion was first given by D. Mason.[84]

In their original paper, Rice and Thomson[22] included heuristically in the k_E calculation, a force to produce the ledge. Since the ledge will be fully formed when $r > r_c$, any function such as a $\tan^{-1}$ function which cuts off at r_c and makes an addition to the surface energy equal to the ledge area will suffice. However, since this term is small compared to the others and is purely heuristic, it will not be included here.

Lin[83] has shown that the criterion [Eq. (28.5)] for cleavage–emission is physically equivalent to that proposed by Kelly *et al.*[82] In the latter paper, the cleavate dominance criterion is given as

$$\sigma_{max}^{tensile}/\sigma_{max}^{shear} > \sigma_{theor}^{tensile}/\sigma_{theor}^{shear}. \quad (28.6)$$

$\sigma_{max}^{tensile}$ refers to the maximum stress developed in the tensile direction on the atom bonds at the crack tip, $\sigma_{shear}^{tensile}$ refers to the similar quantity for shear,

[84] D. D. Mason, *Philos. Mag.* **39**, 455 (1979).

$\sigma_{theor}^{tensile}$ is the theoretical tensile strength of the bonds of the atoms of the material, etc. Lin shows that by applying the simple Orowan estimate[85] of the theoretical strength of materials in terms of γ and μ, that Eq. (28.6) is equivalent to

$$\mu b/\gamma > 10. \quad (28.7)$$

This estimate for cleavage stability can be obtained from Eq. (28.4) by setting $b_s = 0$, the angular factors to $\frac{1}{3}$, and using $r_c \sim b_e$.

Weertman[86] and, much earlier, Armstrong,[87] have also discussed spontaneously generated ductility in the presence of a crack in terms of the stresses necessary to form dislocations outside the crack. Armstrong was led to consider the parameter $\mu b/\gamma$ in his discussion, and Weertman's results are generally consistent with the criterion Eq. (28.7).

A detailed discussion of the predictions contained in Eqs. (28.3)–(28.5) will be found in Rice and Thomson.[22] Ohr and Chang[88] have applied the same analysis to Mode-III cracks and compared the results with Mode-III thin-foil experiments. (Since the Mode-III experiments involve analysis of dislocation pileups, the full discussion of this paper will be found in Part VII.) The results of these two papers are shown in Table I.

The most clear-cut interpretation of Eq. (28.2) in terms of emission is in terms of a pure Mode-I crack discussed above. However, an important question relates to how a mixed-mode loading might change the results. The first question, however, to be explored is whether the Griffith criterion, Eq. (28.4), is modified by mixed loading. Sinclair and Finnis[89] have indeed suggested without justification that Eq. (28.4) should be replaced by

$$[1 - \nu/2\mu](k_{Ic}^2 + k_{IIc}^2) + k_{IIIc}^2/2\mu = 2\gamma \quad (28.8)$$

when all modes of loading are present. (We have added the term in k_{III}, which was not in their paper.). Presumably the reason for considering such a generalization of Eq. (28.4) is that (28.8) represents a balance between total elastic force on the left with surface tension on the right, and that k_{II} and k_{III} contribute to the elastic force on an equal footing with k_I.

But Eq. (28.8) is not physically correct, because when $k_I = 0$, no surface is created at all! What is involved is a rather subtle core effect at the crack tip as cleavage takes place under mixed loading. The situation is depicted in Fig. 35.

[85] E. Orowan, *Rep. Prog. Phys.* **12**, 185 (1949).
[86] H. Weertman, *Philos. Mag.* **43**, 1103 (1981).
[87] R. Armstrong, *Mater. Sci. Eng.* **1**, 251 (1966).
[88] S. M. Ohr and S. Chang, *J. Appl. Phys.* **53**, 5645 (1982).
[89] J. E. Sinclair and M. W. Finnis, *in* "Atomistics of Fracture" (R. Latanision and J. Pickens, eds.), p. 1047. Plenum, New York, 1983.

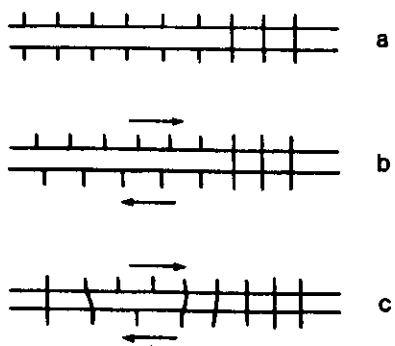

FIG. 35. Mode-II fracture as dislocation formation. In (a) a crack is formed by making a slit in a lattice. In (b), Mode-II forces are applied, and in (c), the bonds are allowed to reweld, because no vertical displacement occurs.

Shown there is a Mode-II crack which moves to the right by one lattice spacing. The result when the bonds facing one another on the cleavage surface are allowed to reweld is a dislocation. If sufficient k_I loading is present to separate the crack to the left of the dislocation core region, a crack can result. Since the core region of the dislocation is always of order b, the presence of k_{II} loading cannot have lowered the critical k_I needed to hold the crack open much below its Griffith value, Eq. (28.4). Thus the effect of mixed loading on the Griffith condition is expected to be minor, but to depend quantitatively in a complex way on the details of the atomic bonding in the tip region. For our purposes, it will be sufficient to retain the form of Eq. (28.4) as the cleavage criterion, but remember that the critical k_I value will depend (only slightly) on k_{II} and k_{III}. Of course, if cleavage and emission are closely balanced in Eq. (28.5), mixed-mode loading could affect this balance for emission in Mode I (see Part VII). We note in passing that lattice trapping could be drastically altered by mixed loading, because that is a property also dependent on the details of the atom bonding.

The effect of mixed loading on emission can now be divided into two separate categories. In the first, emission will be considered onto the crack plane itself where $\theta = 0$ (Fig. 36b,c). Such emission will not blunt the crack. In the second, emission is on a plane inclined at a finite angle to the crack plane, as in Fig. 33.

When emission is on the crack plane, then the elastic forces from k_{II} and k_{III} are at their maximum values, while the k_I elastic force is zero. Thus, for a pure edge on this plane, the condition for emission is

$$k_{IIE} = \frac{\mu}{\sqrt{8\pi r_c}} \frac{b_e}{1-\nu} \sim \frac{\mu}{1-\nu}\left(\frac{a_0}{8\pi}\right)^{1/2}, \tag{28.9}$$

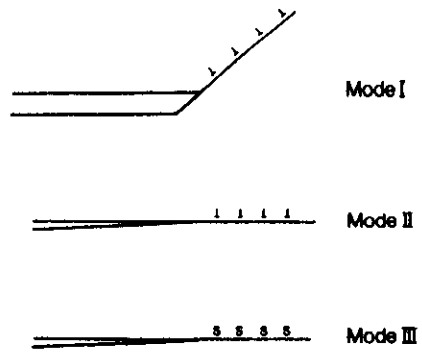

FIG. 36. Emission in Modes I, II, III. In Mode I, the emission force is on an edge on a plane at an angle to the crack, while in Modes II and III the maximum emission force is on the crack plane. A separate requirement is that slip planes exist in these directions.

and for a pure screw,

$$k_{IIIE} = \mu b_s/\sqrt{8\pi r_c} \sim \mu\sqrt{a_0}/8\pi. \tag{28.10}$$

In these equations, a_0 is a number approximately equal to a lattice spacing.

These equations describe a condition in which the tensile and shear loadings are independent of one another. Remembering that the role of k_I is simply to hold the crack open, once that is assured, then emission on the crack plane is simply a matter of building up the k_{II} or k_{III} loadings to their critical values.

In the second case, when emission of the dislocation corresponds to the blunting configuration of Fig. 33, then the full generality of (28.2) is required. Now, k_{II} and k_{III} loadings either lower or raise the value of k_I required to emit the dislocations depending on the sign of k. k_{III} loading acts on the screw component, and k_{II} on the edge. In many cases, simple materials have sufficient symmetry in the cleavage and slip systems available that for a given slip system, such as shown in Fig. 36a, another equivalent slip plane exists mirrored in the cleavage plane. Also, screw components can often be either $\pm b$. Hence, mixed loading will in general break the degeneracy in the emission, and favor one system over the others. Quantitatively, the critical value of k_I from Eq. (28.2) becomes

$$k_{IE} = k_{IE}^0 - \frac{2k_{III}}{\sin\theta}\frac{b_s}{b_e} - k_{II}\frac{2\cos(3\theta/2) + \sin\theta\sin(\theta/2)}{\sin\theta\cos(\theta/2)}. \tag{28.11}$$

k_{IE}^0 is the value of k_{IE} without k_{III} and k_{II}, ie., given by Eq. (28.4).

Equation (28.11) poses a critical problem to the theory of the cleavage–emission balance, because in the simple criterion, Eq. (28.5), both k_{Ic} and k_{IE} are modifed by mixed loadings. We have argued that k_{Ic} is not changed in a

TABLE I. k_e, k_c, AND E_{act} FOR SELECTED MATERIALS[a]

	k_{IC} Eq. (28.3) Ref. 22	k_{Ie} Eq. (28.2) Ref. 22	k_{IIIe} Eq. (28.10)	k_{IIIe} Obs. Ref. 100	E_{act}
Cu	6.4	3.21	1.5	0.4	—
Al	3.4	2.17	1.0	0.7	—
Ni	8.4	5.47	2.6	1.4	—
Fe	8.8	9.34	4.2		2.2 (22)
Mo			8.2	9.2	
MgO	8.4	29.1	14	Cleaves	205 (22)[b]
Si	6.4	14.7	8.2		111 (22)
					0.5–1.0 (92)

[a] k in 10^5 N m$^{3/2}$, E in eV.
[b] The numbers in parentheses are references.

major way by addition of k_{II} or k_{III}, but Eq. (28.11) suggests that k_{IE} can be. This situation has not been explored sufficiently, experimentally. It may be connected with the appearance of dislocations at cracks in materials supposed to be brittle on the basis of Table I, or vice versa.

29. THERMALLY ACTIVATED EMISSION

The previous discussion envisioned a 2D crack and emergent dislocation, which was entirely adequate in discussing the mechanical stability of a sharp crack tip against dislocation emission. But as noted in that analysis, the system always has a lower energy when an emitted dislocation is far enough from the crack, because the force is repulsive when $r > r_0$. In two dimensions, of course, total energies of cracks and dislocations are always infinite because of the infinite length of crack and dislocation. In 3D, however, when the sharp crack is mechanically stable, there will always be a saddle-point configuration of a dislocation loop of finite size through which, in principle, the loaded crack can emit a dislocation by thermal fluctuation. In any discussion of crack stability, the activation barriers for emission by mechanically stable cracks will be an important quantity. It will not be surprising that such a 3D calculation has not yet been carried out in a rigorous way, because of the mathematical difficulty. However, estimates have been formed of the energy barriers.

The first point to note is that in isotropic elasticity, and Mode I, the dislocation loop must meet the crack line at a right angle, because there is no lateral force on the dislocation from the crack, and the dominant force near the tip is the attractive image term. Secondly, the maximum in the function of Eq. (28.2) is a broad one, because of the counteracting effects of the $1/\sqrt{r}\,k$ term and the $1/r$ image term.[22] Thus, although the stress or force field near the tip is inhomogeneous, there is a large region near its maximum, where the force is nearly constant. For this reason, Rice and Thomson[22] suggested that a likely estimate of the saddle configuration is a half-circle in the classic Frank–Read[90] configuration (Fig. 37). On this basis, the energy of the dislocation loop in Mode I was calculated, using the 2D force expressions, Eq. (28.1). The energy barriers calculated for circular loops in Table I (those from Ref. (22)) are all very large compared with thermal energies in all materials investigated, except iron, which is considered borderline.

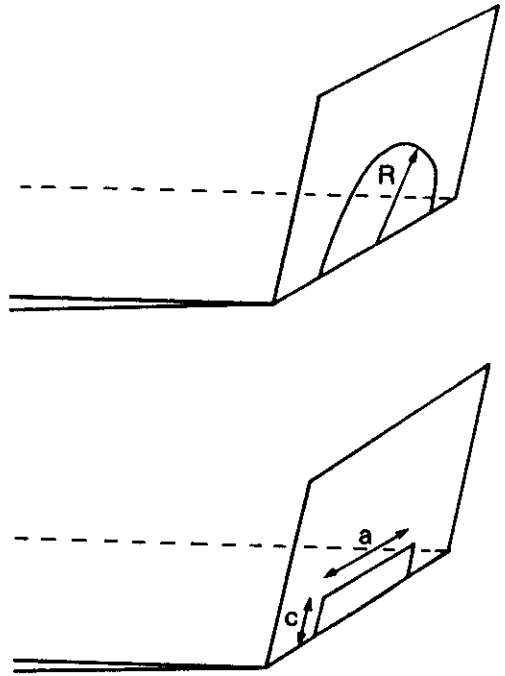

FIG. 37. Mode-I emission in 3D. Dislocations must be nucleated from a mechanically stable crack. In (a) the shape of the critical nucleus is assumed to be a half-circle, and in (b) a rectangle.

Haasen[91] suggested that the earlier values of Rice and Thomson might be too large in the case of Si, because splitting the dislocation lowers its self-energy, and the stacking fault energy in Si is low. He has estimated about

[90] J. Hirth and J. Lothe, "Theory of Dislocations," 2nd Ed. McGraw-Hill, New York, 1982.
[91] P. Haasen, *in* "Atomistics of Fracture" (R. Latanision and J. Pickens, eds.), p. 707. Plenum, New York, 1983.

0.5 eV for the barrier energy of a loop. Lin *et al.*[92] have also carried out an estimate of the loop energy for Si. In addition to allowing the dislocation to split, they also chose a rectangular configuration "loop" with variable size and aspect ratio. Again, the energy barrier for Si is dramatically lowered over the value of Rice and Thomson, as shown in Table I. The decrease in activation energy calculated by Lin *et al.* was about equally due to the altered shape of the loop, and to the dislocation splitting.

All these calculations use the 2D force expressions, and are therefore not self-consistent 3D elastic calculations. Because of the relatively large loop sizes estimated in these calculations, the elastic estimate of the energy barrier does not suffer from the atomic cutoff limitation which the 2D stability calculation of Part VI,28 does. Hence, the energy-barrier calculation is apparently one which can be performed legitimately in the elastic approximation. In view of the apparent sensitivity of the estimates to the details of the calculation, a more ambitious rigorous 3D calculation of a suitable crystal is needed. Further, the mixed loading effects discussed in the previous section have not been investigated, and undoubtedly would be of interest as well.

30. Atomic Calculations

Extensive atomic simulations have been carried out for 2D crack-dislocation configurations. Such simulations relate directly to the most crucial issue regarding dislocation emission, namely the crack stability; so they have an important place. Fortunately, as noted in the previous subsection, atomic effects apparently are not germane to the problem of the energy barrier, because 3D simulations are not currently practicable.

We have already dealt in Part V with the general theory of discrete calculations, and report here simply the results. Dislocation effects in simulations were first observed in the work of Wiener and Pear,[93] who found that in the limit of very high driving forces, and velocities, dislocation emission was enhanced by the higher stress required to move the crack at a high velocity. A series of simulations of iron using the Johnson[56] potential were carried out by the Battelle group[58] in various ways, showing that simulated iron was borderline between cleavage and emission. De Cellis *et al.*[60] have simulated iron (i.e., bcc metal) with the Johnson potential and copper (i.e., fcc metal) with a Morse potential in a calculation with improved treatment of the boundary conditions, and have concluded that these simulated materials have cracks, respectively, stable and unstable against dislocation emission.

[92] I. H. Lin, T-Z Chuang and R. Thomson, to be published (1986).
[93] T. H. Wiener and M. Pear, *J. Appl. Phys.* **46**, 2398 (1975).

Mullins[61] has performed similar calculations on simulated iron under mixed loading conditions, and finds that the general predictions of the continuum theory is correct. That is, the crack can be made to change its cleavage plane abruptly by addition of Mode II, and the emission criterion is altered by mixed loading. A "phase diagram" from his work, showing how the emission criterion changes under mixed loading, is given in Fig. 38.

All previous calculations have attempted to simulate a particular material by choice of a suitable force law, and they all embed a discrete lattice within a surrounding continuum, with boundary conditions set on the interface between the two regions. In a series of papers, Paskin, Dienes and co-workers[63–66] have taken a different approach to the simulation problem. Realizing that no adequate force laws yet exist for real materials, they have carried out a series of molecular-dynamics calculations on a large 2D array with up to 10,000 lattice points using the Lennard–Jones potential. The points in the array form a triangular lattice. The point of view of these investigations is thus to model general fracture phenomena, rather than to make predictions for particular crystals. They have shown that under static conditions, their model will barely support a sharp crack, and that the criterion of Eqs. (28.3)–(28.5) is satisfied. This simulated material thus provides a sensitive test for the validity of the continuum approach, which is encouraging. In their simulations, when the external stress is raised, the crack propagates, and under these

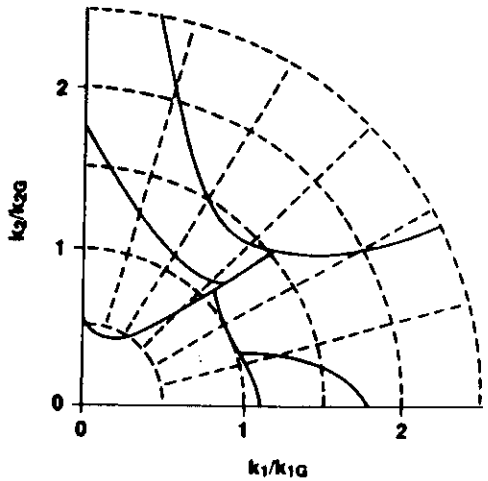

FIG. 38. Results of computer studies in simulated iron for mixed loading A — no fracture, B — (010) cleavage, C — non-(010) cleavage by branching, D — dislocation generation at tip, E — dislocation generation combined with twinning, and F — dislocation generation and/or twinning followed by crack branching.

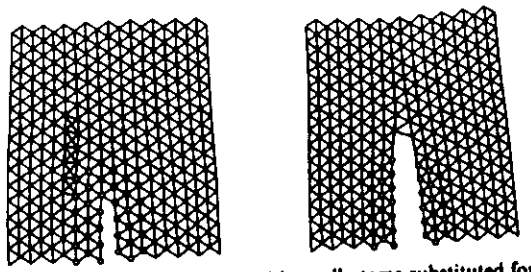

FIG. 39. Results of a computer simulation with small atoms substituted for initial atoms at the surface, as shown by circles. The initial model was ductile. After substitution, dislocation generation is followed by initiation of a new crack (after Paskin *et al.*[64]).

conditions, as in Wiener and Pear,[93] the crack emits dislocations as it cleaves. In the simulations, furthermore, it is observed that virtual emission of dislocations take place. That is to say, when the crack is moving rapidly, an emitted dislocation does not move far after emission, and the dislocation falls back into the cleavage plane after the crack moves on.[63] Such virtual emission was first proposed by Knott[94] in order to explain why the "Griffith γ" for brittle fracture as measured in iron is nearly an order of magnitude higher than the true γ is believed to be. If virtual emission occurs during cleavage, it will be an energy-dissipation mechanism, which will add to the measure of γ in the Griffith criterion.

Finally, Paskin *et al.*[64] have studied the modification of the fracture processes in their model when the atoms in the tip region possess altered bonding properties. Figure 39 shows simulation results when "small" and "large" atoms are substituted at the crack tip, simulating the formation of a surface film at the crack tip. In the one case, dislocation emission is enhanced by the film; in the second, the material is embrittled by the additional stresses induced by the film. In effect, what transpires when a film forms is that the stress singularity at the crack tip is no longer characterized entirely by a local k field, but by the stress field of a precipitate particle. Thus, the discussion of dislocation emission leading up to Eqs. (28.3)–(28.5) no longer applies. The modified analysis using continuum ideas has been carried out by Sieradsky.[95] We will return to additional discussion of the embrittlement question in Part VII.

In a completely different approach, Sinclair[54] has used the lattice-statics discrete-Green's-function approach to study the problem of dislocation emission. Preliminary results only have been reported at the time of printing,

[94] J. Knott, *Proc. Int. Conf. Fract., 4th* **1**, 61 (1977).
[95] K. Sieradsky, *Acta Metall.* **30**, 973 (1982).

but this powerful approach is being used to explore the effect that force law and crystal symmetry have on the emission criterion to gain some perspective on how these factors affect the emission criterion in a general law.

31. Experimental Investigations

The direct and unambiguous experimental demonstration of dislocation emission and the quantitative study of the dislocation phenomena associated with atomically sharp cracks is exceedingly difficult, even with modern techniques. The clearest examples of rigorously brittle cracks have been provided by the observations of B. Hockey[96] in Si, Ge, Al_2O_3, and MgO, all relatively brittle materials. The technique used is to indent the surface of a single crystal by a sharp point, and induce local damage. Cracks thus formed then propagate into relatively undamaged portions of the crystal, where they form isolated entities. The tip region is then cut out of the sample and thinned for transmission electron microscopic examination. In the case of Si, when fracture is induced at low temperature, the final crack tip is completely clean (see Fig. 9b), with no dislocations present at all. In some cases (Fig. 9c) after the crack has moved to a certain position, it retreats presumably because of stress relaxation. In these cases, the former cleavage surface is manifested by a network of misfit dislocations because the surfaces have not come back together in perfect registry. At temperatures above that where dislocations are mobile (Fig. 9b) the cracks are found to be associated with dislocation atmospheres. In Hockey's Si observations, detailed slip-plane analysis is lacking, but the observed dislocations may have been emitted after the crack arrested, or they may have been carried along by the crack stress field as the crack grew from the region around the indenter, where intense deformation has occurred.

In other experiments with bulk samples of Si, Champier[97] has analyzed the deformation fields produced by a stationary crack in a technique first used by St. John.[98] In these experiments, analysis of the dislocation loops formed around the crack shows that only a small fraction of the loops are in the blunting configuration depicted in Fig. 36. That is, the majority of loops are on slip planes which are not parallel to the crack line. Although such loops might also have nucleated spontaneously from the crack line, the activated state would have to be a complete circle instead of a half-loop, and it would appear that the barrier would be larger than for the blunting configuration. The most attractive possibility for the origin of the dislocations constituting the

[96] B. Hockey, unpublished; see also Lawn *et al.*, Ref. 8.
[97] G. Champier, to be published (1986).
[98] C. St. John, *Philos. Mag.* **32**, 1193 (1975).

FIG. 40. Dislocations generated in the vicinity of a crack in MgO. Cracks in MgO appear to generate dislocations from sources close to, but not at, the crack tip. No dislocations are seen which are believed to emanate from the crack itself (after Hockey[96]).

deformation field is thus inhomogeneities in the material whose stress fields are enhanced by proximity to the crack.

In extensive studies of MgO, where deformation accompanies the crack, Hockey[96] has observed many cases where sources of dislocations operate near the crack position (or near a previous crack position), but only a few where the crack itself may have been the source of the dislocation (see Fig. 40).

In summary, for highly brittle materials, the evidence is clear cut that rigorously atomically sharp cracks exist. At elevated temperatures, dislocation emission from these cracks has not been clearly established as yet, although theory suggests that the activation energy may be sufficiently low at least in Si for it to be observed.

In the bcc metals, which are expected to be borderline emitters, the picture is more complex. The most clear-cut experiments have been those of Ohr and co-workers[10,11] using thin film *in situ* electron microscopy, and Vehoff and Rothe,[99] using bulk samples of iron/Si and Ni in hydrogen environments.

The Ohr configuration is shown in Figs. 12 and 13. Cracks are formed when the region near the hole is deformed. Screw dislocations on the slip plane are

[99] H. Vehoff and W. Rothe, *Acta Metall.* 31, 1781 (1983).

responsible for the "sliding-off" deformation, in the foil, and originate at the crack line which is short compared to the width of the foil. The analysis of the configuration requires consideration of the pile-up of dislocations, which is a subject for Part VII. However, the existence of a local k at the crack tip is all that is required to invoke the emission analysis. Ohr and Chang[88] have in fact used this analysis to generate the numbers in Table I. This case must, however, be a mixed-mode situation, because the crack line and cleavage plane are inclined to the tensile axis at about 45°. For the screw dislocations emitted on the crack-slip plane shown in Fig. 13, the mixed-mode analysis of Part VI,29 shows that only the k_{III} part of the loading is involved in the emission, and the analysis of Ohr and Chang[88] only considers this part. For the reasons stated in Part VI,29, the emission of the screw dislocations does not imply that cleavage cannot occur in Mode I. That is, there is no cleavage–emission competition in the k_{III} part of the loading, and emission of screw dislocations will simply take place as soon as the critical k_{IIIE} value is reached. Any growth of the crack is due to the Mode-I loading, which of course is necessarily present in order to hold the crack open. (See Part VII,38 for further discussion of this point.)

In other experiments,[10] when the crack grows into the thicker part of the foil, the fracture mode changes. In Mo, a zigzag configuration develops with the crack propagating in mixed-mode I/II loading on alternating cleavage planes with Mode-II dislocation emission, as shown in Fig. 41. Again, the crack growth shown is, of course, due to the Mode-I loading, and emission occurs when k_{IIE} is exceeded, as discussed in Part VI,29. With the pileup of Mode-II dislocations observed, however, k_{IIE} can be achieved again after a dislocation is emitted only after the pileup moves away sufficiently to allow k_{II} to rebuild, or the crack may branch to another slip plane (see Fig. 41). Unlike the screw-dislocation Mode-III case, here the Mode-I opening interacts with the Mode-II dislocations, as discussed in Part VII.

FIG. 41. Cracks in molybdenum in the thicker part of the foil configuration of Fig. 13. Figure shows cracks growing in mixed mode and oscillating between equivalent slip planes (after Ohr *et al.*[10]).

In Al,[10] a quite different process takes place in the thicker zone. There, an alternating Mode-I cleavage–emission slide-off process occurs. When the Mode-I crack is arrested, emission occurs, to form the classic wedge configuration. Then, as the specimen thins by the continuing general deformation, sudden initiation and propagation of a clean brittle Mode-I crack occurs for a short distance. This Mode-I crack is, of course, not stable in Al, and its appearance as a dynamic event poses a major problem to which we return in Part VII,39.

Experiments on Fe–2.6 at. % Si and Ni single crystals (reviewed by Vehoff and Rothe[99]) have been performed on macroscopic samples which also throw light on the cleavage–emission tradeoff. In these experiments, the materials can be made to shift from a fully ductile wedge configuration with crack growth by pure dislocation emission and slideoff, to a highly brittle (but not pure) cleavage condition by controlling the temperature or hydrogen pressure on the sample (see Fig. 11). These experiments show that cleavage and emission can coexist, and that the fraction of one versus the other is variable over a wide range. Careful experimental analysis shows that the action of the hydrogen is at the crack tip itself. The authors show that the results are consistent with the occupation of the special site at the tip with a Langmuir-type expression for the occupation probability. The site has a trapping depth of 49 kJ/mol H in iron, which is approximately equal to that for chemisorption on the surface. Because the fraction of cleavage saturates with hydrogen pressure before pure cleavage is attained, these authors believe that their results are to be correlated with the simple coverage of the site at the tip rather than γ, because γ does not saturate with pressure. They also reconfirm that addition of O_2 impedes the hydrogen effects (an old result), and interpret this as being due to the adsorbtion of O_2 on the surface, which denies hydrogen access to the tip.

For us, the important results are that intrinsic cracks in both iron and Ni are ductile at room temperature and above. At low temperature, the iron is brittle, suggesting that iron is indeed borderline, as predicted by the theory, and that the activation energy for emission is low. With the addition of H, the Griffith γ is lowered so that emission is less favored. The quantitative results of the experiments are probably interpretable only in terms of a kinetic treatment which predicts how the filling of the sites at the tip, which leads to cleavage, competes with thermally activated emission.

Finally, experiments in ductile materials by Wilsdorf and co-workers, as reviewed by Wilsdorf,[6] have shown that high-purity ductile metals and certain alloys behave almost exactly as predicted. The systems studied were the ductile metals Au, Ag, Cu, and Al, the borderline metal, iron, and the normally brittle Be. All these metals were of high purity, and failure was by fully ductile processes. Under tension, just as the last ligament of a sample is about to pull apart, however, cracks appear in the resultant thin ligament, with the results

shown in Fig. 14. The single-crystal Be samples in these observations are oriented in the easy-glide direction, so that failure is fully ductile. The typical hole-growth process is apparent in the figure, and the only difference between these experiments and hole growth as observed in an engineering material such as in Fig. 6, is that there are no large precipitates for the holes to nucleate on. A new hole is nucleated in these experiments in the dislocation cell walls. After initiation, the crack grows by cleavage (!) to a typical size of the order of a few μm, and then opens in the crystallographic shape shown either by the classic slide-off mechanism, or by the operation of dislocation sources near a tip of the wedge. The major surprise in these experiments is that again, as in the Ohr[100] experiments on Al, a fast-moving cleavage crack has a finite lifetime in a material that in all other ways behaves entirely in a ductile manner.

VII. Dislocation Shielding and Fracture Toughness

32. Introduction

With the help of the ideas and the formalism developed in earlier sections, it will finally be possible to confront here on a fundamental level the central problem of fracture: materials toughness.

This problem has had a long history, in its modern dress stretching back to the classic paper by Griffith[47] in 1920 who worked out the basic overall energy balance between the elastic driving forces on a crack, and the resistive forces against crack advance supplied by the material, as discussed in Part IV,19. In Griffith's work, he identified the resistive forces as the surface tension, γ, of the opening cleavage surface at the crack tip, in the soap-film analogy.

But Griffith's relation, Eq. (19.3), had only very limited applicability to extremely brittle materials such as glass, because of the very weak resistive forces which the true surface tension of solids can supply. Ultimately, Orowan[101] and Irwin[102] independently proposed that Griffith's relations could be generalized to tougher materials if the plastic work γ_p, done by the advancing crack, could also be identified as a resistive term leading to a kind of effective surface energy $\gamma_{eff} = \gamma + \gamma_p$ and incorporated into Eq. (19.3). In cases of small-scale yielding, plastic work done is proportional to the distance moved by the crack, so identifying it as a type of "surface" work is appropriate. With γ in Eq. (19.3) replaced by γ_{eff}, it was found that the modified Griffith relation could, indeed, be applied to the fracture of ordinary tough engineering materials, and the modern field of fracture mechanics was founded. Its success

[100] S. M. Ohr, to be published (1986).
[101] E. Orowan, *Trans. Inst. Eng. Shipbuilders, Scotland* **89**, 165 (1945).
[102] G. A. Irwin, *Int. Congr. Appl. Mech., 9th, Univ. Brussels*, **8**, 245 (1957).

in tough materials is possible because the plastic work done during fracture can be several orders of magnitude greater than the work done in simply opening new surface, and thus the vastly different fracture resistance in materials such as glass and steel can be encompassed.

The term toughness has been used here several times in a descriptive way. Quantitatively, it may best be identified with the resistive force which the material is able to exert against crack advance, and a measure of it would be γ_{eff}. But K_c and J_c at the critical crack condition are also often identified with toughness, and a fourth measure, to be discussed in a later subsection, is the "crack-opening displacement" (COD) measured on the crack at a suitable point. Note that these quantities are not dimensionally equivalent to one another, and are defined in different ways. But relations between them can be obtained by theoretical models; so the four quantities do collectively provide a rather loose operational basis for the general concept of material toughness.

Since the pioneering work of Orowan and Irwin, the field of fracture mechanics has progressed by treating fracture as a stress-analysis problem in terms of continuum elasticity and plasticity. The point of view of this article is quite different, however, because, when continuum fracture mechanics is used to address the question of how the forces are transmitted to the crack tip to open the atomic bonds there, a fundamental difficulty is met. This difficulty is expressed in the Rice theorem[32,46] already mentioned in Part IV,18. According to this theorem, in continuum elasticity and plasticity, when a crack advances, the work done by the machines supplying the external stress is absorbed entirely by the plastic processes in the medium, and none is left over for the surface energy of the opening crack. This result depends upon the assumption that the stress at the tip saturates to a finite value, as it must for any realistic plastic yield constitutive law for a material.

At first glance, because of the smallness of the true surface energy γ, relative to γ_{eff}, this may not seem like a serious problem. However, the point is that there is in this approach no way to model the opening of the atoms at the crack tip as in Part V. This paradox will be further illuminated from the standpoint of dislocation theory in Part VII,34. It will be shown there that, if the dislocation shielding zone (treated as a continuum) goes right down to the crack tip, that the local k is strictly zero, and the crack is completely shielded. The stress at the tip is then given by the finite dislocation friction stress, σ_f, which is always less than the bond-breaking stress required at the crack tip. This prediction is thus inconsistent with the existence of a cleavage crack at the tip. Hart[103] has found conditions, however, under which a continuum theory can be developed, but, as discussed in Part VII,39, these conditions relate to behavior near the tip.

[103] E. Hart, *Int. J. Solids Struct.* **16**, 807 (1980).

In continuum mechanics, it has been popular to postulate the existence of a "process zone" near the crack tip where the continuum theory breaks down and events transpire which open the crack. It will be our purpose in this section to highlight this zone, and show how the crack-tip stress field interacts with the dislocations to produce the overall fracture. The complete crack and dislocation configuration must be constructed in a self-consistent fashion taking account of the intrinsic structure of cracks in the material on the one hand, and the dislocation mobility and source distribution on the other. Given the known complexity of dislocation behavior in materials, especially in engineering materials, one can begin to appreciate some of the reasons for the complicated fracture behavior in most materials, and engineering materials in particular.

The plan of this section is to (1) discuss the general conditions for crack equilibrium in terms of the three fundamental crack morphologies, (2) present a one-dimensional Mode-III model of dislocation shielding for brittle materials, and materials whose cracks emit dislocations, (3) discuss mixed-mode cracks, (4) discuss moving cracks, and (5) discuss time-dependent mixed cleaving and emitting cracks.

33. Equilibrium Conditions for the Three Prototype Crack Classes

The observationally based descriptive discussion of Part II led to a qualitative breakdown of cracks into three distinct morphological classes: the slit crack, the wedge crack, and the externally blunted crack. These different morphological classes also correspond to three different broad mechanisms of fracture corresponding to differing regions on the ductile/brittle spectrum of material response. (The reader should note that the crack classes to be described here are based on different physical mechanisms for fracture, and are, categorically speaking, different from the modes of fracture (Modes I, II, III) which relate to the way in which external loads are applied to a crack.

a. Slit or Brittle Cracks

The slit crack corresponds to a crack which is atomically sharp at its tip, as in Fig. 42, and its most important attribute in comparison with the other two types of cracks is its ability to propagate rapidly. This crack may be a purely brittle crack as envisioned in the mathematical description of Part III, or it may be a crack which has absorbed a finite number of dislocations on its cleavage surfaces so that the crack surface behind the tip has a greater crack opening displacement, as shown in Fig. 42b. In either case, because of the atomically sharp tip, from the elastic point of view, this crack is characterized

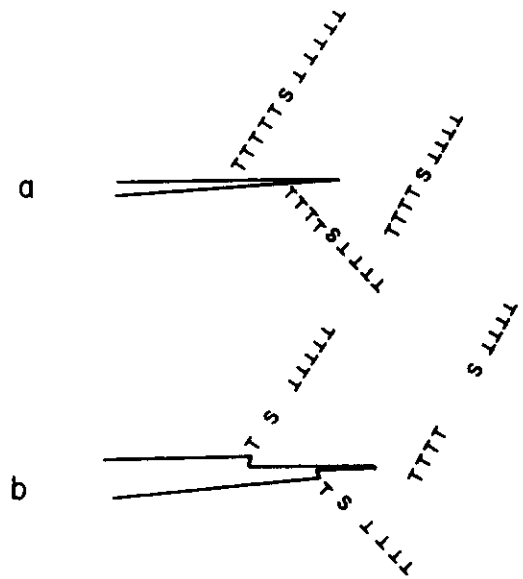

FIG. 42. In (a) an initially sharp slit crack is shown which activates two sources in its neighborhood. When the antishielding dislocations which are attracted to the crack are absorbed by the cleavage surfaces, they create steps which lead to a finite opening of the crack called the COD. The COD is related to the dislocation Burgers vectors absorbed (and to those remaining) by Eq. (33.3). If the source is not precisely lined up with the crack tip, then the tip remains sharp locally.

by a local k field at the tip. The atomic structure at the tip corresponds to the "decohesion" model depicted for the simple cubic lattice in Fig. 3.

It is assumed here that the crack is stable in the lattice in the sense of Part VI, and that the k to which the crack is subjected is less than that at which "decohesion" model depicted for the simple cubic lattice in Fig. 3.

When the criterion for cleavage is met, Eq. (28.5), then the static equilibrium condition for the crack and any associated dislocation cloud (screening and/or antiscreening) is that each defect in the total configuration is subjected to a net zero force. That is to say, the elastic driving forces derived and discussed in Part IV are exactly balanced for each defect by other forces supplied by the material. In the thermodynamic sense, this criterion for the brittle crack is met by the Griffith condition, Eq. (25.3)

$$f_{1c} = 2\gamma. \tag{33.1}$$

In this equation, γ is the surface free energy in the Gibbs sense, and will be a function of the chemical activity of any external chemical species. f_{1c} is given in terms of the local k_1, and when mixed loading is applied, we will assume that only Mode I assists the crack growth, although some assistance from Modes II and III is possible, as discussed in Part VI,28.

For the dislocations in the total configuration, in equilibrium, similar conditions must be postulated:

$$(f_d)_j - b_j(\sigma_f)_j = 0. \tag{33.2}$$

This equation is expressed for the jth dislocation in the cloud in terms of an effective friction stress σ_f at the point j. Typically, this stress might correspond to a Peierls "stress," or interaction with impurities or a grain boundary. They should not refer to interactions with other dislocations, except in special cases, because we shall usually include these interactions in the elastic forces explicitly on the left-hand side of Eq. (33.2).

One of the major difficulties met in applying Eq. (33.2) to real situations is that the interactions envisioned in the second term are usually three dimensional in character, while the formalism adopted here is only two dimensional. Thus, some appropriate averaging process to collapse the third dimension is always envisioned, because the enormity of a full three-dimensional description is far too great to countenance in its entirety.

The coupled equations (33.1) and (33.2) represent a complete set of conditions for two-dimensional equilibrium. A direct attack can be carried through when the number of dislocations is small or other simplifications are made, but generally speaking, successful attacks on the problem involve rather drastic approximations.

b. Wedge Cracks and Slide-Off

The wedge crack in its pure form is one where the crack is unstable against dislocation emission, and its characteristic shape is determined by the geometry and symmetry of the dislocation slip planes at the crack tip. In this case, the crack advance is not by opening of bonds, but by ledge formation as the dislocation is emitted. Thus one dislocation must be emitted for each Burgers vector increment of crack advance. The wedge is formed therefore by alternate "sliding-off" on the equivalent slip planes at the crack tip, as in Fig. 43. This crack morphology was first recognized conceptually by Cottrell[104] and is best confirmed observationally in the work of Vehoff and Rothe,[99] as shown in Fig. 11. Cottrell believed that the slide-off mechanism would not be observed commonly because the crack can only continue to advance without limit if the dislocations continue to advance toward the external surfaces until they exit from the material there. This is exactly what Vehoff and Rothe observe, of course, in their single crystal specimens.

[104] A. H. Cottrell, *Proc. R. Soc. London Ser. A* **285**, 10 (1965).

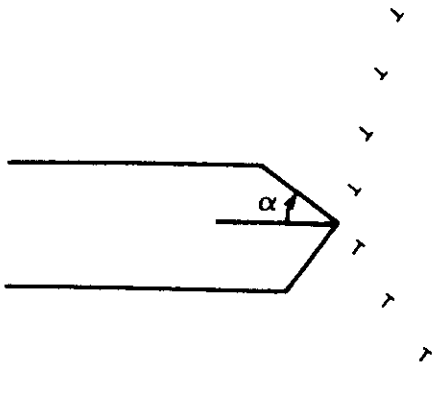

FIG. 43. In an initially sharp slit crack, when $k_e < k_c$, as the stress is raised, alternate emission from the tip on equivalent slip planes intersecting the crack create a wedge crack whose opening angle α is complementary to the angle between the two slip planes. Whether slip occurs on slip planes one or many atom planes separated from one another makes no difference to the final result.

c. *Externally Blunted Crack*

When a crack exists in a material containing bulk sources of dislocations, then as the external stress is raised, these sources may be activated. Figure 42 illustrates what happens to such a crack. In the two-dimensional description, dislocations are always produced from a source in pairs of opposite Burgers vector. By reference to the relevant force expressions in Part IV, it will be found that the dislocation attracted toward the crack is also the antishielding dislocation. In the formalism of Part IV, this corresponds to a negative Burgers vector. On the other hand, the shielding dislocation (positive Burgers vector) of the pair is repelled when the distance to the crack tip is beyond the range of the image force. Generally, then, one will expect that many of the antishielding dislocations will be absorbed in the open (cleavage) surface of the crack. Starting with a slit crack, the result is a crack with a finite opening called the "crack-opening displacement" (COD) given by the total absorbed Burgers vector. Given that the total Burgers vector is conserved during source operation, i.e., by production of compensating pairs, the COD, aside from a cosine factor, is just equal to the remaining total shielding Burgers vector,

$$\mathrm{COD} = \sum_j b_j \cos\theta_j. \tag{33.3}$$

θ_j is the angle made between the crack plane and the Burgers vector. Note that the COD by this definition does not include the elastic part of the crack opening which even a slit crack has by virtue of Eqs. (9.13)–(9.15). This

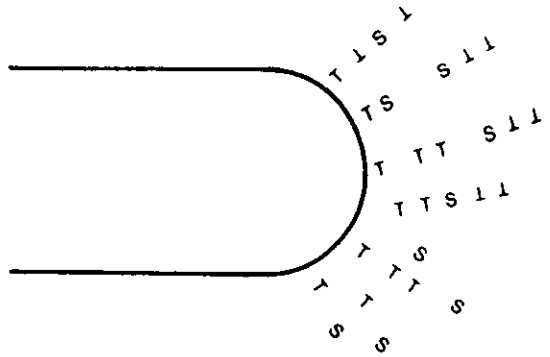

FIG. 44. When a slit crack is blunted continuously by external sources, the crack tip eventually takes on a rounded macroscopic shape because of the randomness of the plastic process. The rounded crack is then best treated from a continuum approximation.

expression is also valid, of course, if the source of dislocations is the crack tip itself.

If the material surrounding a crack is sufficiently soft, then, as the external stress is raised, it may transpire that neither k_{1E} nor k_{1c} is ever reached, and continued operation of the external sources progressively blunts the crack, as discussed in Part II. Figure 44 (and Fig. 7) is a schematic drawing of successive blunting and hole formation, in the way presumed to lead to fully ductile fracture. Wilsdorf's observations in Fig. 14 of very clean thin films, although showing highly crystallographic features, is apparently also an example of the same process. Crack advance in the ductile case is possible only because of the nucleation and coalescence of new holes, and the COD is controlled by the distance between the large holes. Otherwise the material will simply neck to rupture on a macroscopic scale, as in Fig. 1.

Analysis of this case is obviously very complicated, and much effort has been expended on it in the continuum mechanics and materials communities. Although this work will not be reviewed here, the major result is that the maximum triaxial stress in front of a blunted crack occurs at a distance in front of the crack roughly equal to the radius of curvature of the tip. When this region of maximum stress reaches out to precipitate particles in the bulk, they fail, and a new hole forms, as shown in the figures of Part II. For a general review of this subject, see Knott,[105] and Rice.[32]

In principle, the processes of ductile fracture have little to do with fracture as we have described it in this article, because only in the early stages of hole formation do any events involving bond breaking occur. However, on a gross

[105] J. Knott, *Proc. Int. Conf. Fract., 4th* **1**, 61 (1977).

macroscopic level, the failure is cracklike because the COD is given by the hole size, and this of course is on a scale given by the material microstructure. But even on an atomic scale, the hole-growth mechanism can switch over to cleavage when conditions at the tip change, as for example by chemical embrittlement. Thus the important conclusion is that it is the relative size of k_E, k_c, and k_S which governs which of the physical classes of fracture occurs. (Here k_S is a measure of the k necessary to activate sources in the medium in a continuous manner.)

d. Mixed Fracture Classes

The previous discussion has arbitrarily separated the three classes for didactic reasons, when the more usual case, and the more interesting one, involves a mixture. Thus, very few materials are so brittle that no dislocations are emitted, or created by external sources. Indeed, one of the major purposes of this article is to consider the shielding provided by such dislocations, and the source of these dislocations must have been either the crack tip or external sources. If the conditions at the crack tip do not turn decisively in only one direction, so that for example alternating emission and cleavage can occur, or alternating cleavage and external source activation, then significant toughness can be generated for a crack which remains atomically sharp (or nearly so) at its tip. It is toward such a crack and the conditions for its existence that the main discussion of this section will be directed.

In the same way, the careful distinction made here between the externally blunted and wedge cracks is also probably not a sharp dividing line in real materials. In the thin-foil experiments of Wilsdorf (Fig. 14), emission and external dislocation generation are observed in the same specimen. Also, the double-wedge configuration taken by the "holes" of Wilsdorf generate long-range stress not unlike that of a smoothly rounded crack, so that hole generation ahead of the crack is to be expected (and is observed!). Thus it is probably moot whether the typical hole-growth mechanism in its later stages as seen in ductile polycrystalline materials is due primarily to dislocations emitted from the crack itself or to external sources.

On the other hand, in the opinion of the author, the crucial question of whether a material will be capable of sustaining a brittle crack stably in a cleavage mode, without blunting the tip and arresting the bond-breaking process, will be determined by the emission of dislocations at the tip rather than by absorption of externally generated dislocations. The reason is that the externally generated dislocations must collide exactly with the tip in order to blunt it, which is an unlikely event, whereas dislocations emitted from the crack blunt the tip by definition. However, the precise conditions under which external sources can halt a cleaving crack are important and unknown at the time of writing.

34. One-Dimensional Dislocation Distribution

If dislocations are distributed along the cleavage plane in front of the crack in a one-dimensional array, the problem of finding the equilibrium distribution is amenable to analytic treatment, if the number of dislocations is large enough to be considered from a continuum approximation. The first such treatment was by Dugdale (Mode I),[106] followed shortly by Bilby *et al.* (Mode III),[107] hereafter called simply BCS. In the BCS theory, the crack is considered to be a continuum distribution of virtual screw dislocations whose Burgers vector distribution, $\beta(x)$, is related to the crack displacement u_3 by the equation

$$u_3 = \frac{\partial \beta}{\partial x_1}, \qquad db = \beta(x_1)\,dx_1. \tag{34.1}$$

(See Part II,4.) These virtual or "crack" dislocations are set in equilibrium with each other and with the external stress distribution at the point x on the cleavage plane. The resultant distribution thus gives zero stress on the cleavage plane, and therefore "solves" the crack problem. The stress external to the crack is then just that provided by the "crack" dislocations, and the results are equivalent to that of Part III. BCS, however, go further and let a distribution of "real" dislocations be placed on the external cleavage plane, and then solve the total equilibrium problem of "crack" plus "real" dislocations. The external dislocation distribution is presumed to start at the crack tip. The BCS theory has been used extensively to interpret the plastic zone of cracks, because its results are analytic and easy to understand.[108] The BCS theory is a direct extension of dislocation pileup theory to a situation where the stresses are inhomogeneous, and, because of this simple picture, the BCS description has thus been very appealing to those familiar with dislocation theory.

An extension of the BCS model was developed by Chang and Ohr[88,109,110] to explain the experimental results by Ohr and co-workers[10,111–117] and

[106] D. S. Dugdale, *J. Mech. Phys. Solids* **8**, 100 (1960).
[107] B. A. Bilby, A. H. Cottrell, and K. H. Swindon, *Proc. R. Soc. London Ser. A* **272**, 304 (1963).
[108] E. Smith, *in* "Dislocations in Solids" (F. R. N. Nabarro, ed.), Vol. 5, p. 364. North Holland Publ., Amsterdam, 1979.
[109] S. Chang and S. M. Ohr, *J. Appl. Phys.* **52**, 7174 (1981).
[110] S. Chang and S. M. Ohr, *Int. J. Fract.* **23**, R3 (1983).
[111] J. Narayan and S. M. Ohr, *Proc. Int. Conf. Electron Microsco, 9th* **1**, 580 (1978).
[112] S. Kobayashi and S. M. Ohr, *Proc. Annu. Meet. EMSA, 37th* p. 424 (1979).
[113] S. M. Ohr and J. Narayan, *Philos. Mag.* **A41**, 81 (1980).
[114] S. Kobayashi and S. M. Ohr, *Philos. Mag.* **A42**, 763 (1980).
[115] S. M. Ohr and S. Kobayashi, *J. Metall.* **32**, 35 (1980).
[116] S. Kobayashi and S. M. Ohr, *Scripta Metall.* **15**, 343 (1981).
[117] J. Horton and S. M. Ohr, *J. Mater. Sci.* **17**, 3140 (1982).

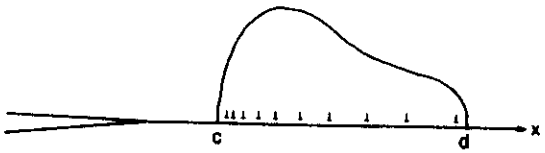

FIG. 45. Dislocation shielding configurations. (a) A Mode-III slit crack is depicted with a distribution of screw dislocations on its cleavage plane. The solid curve represents a continuous distribution function of the same set of dislocations, on the interval from $x_1 = c$ to $x_1 = d$.

Chia and Burns[118] on dislocations emitted from cracks which showed a dislocation-free zone near the crack tip. The path to be followed here is a further simplification of their work, published independently by Majumdar and Burns[119] and by Weertman *et al.*[120] Starting with BCS, all the mathematical developments make essential use of the Muskhelishvili integral equation of the Appendix.

In the following, the description will be a Mode-III crack in antiplane strain, but the analysis is also applicable to Mode I with edge dislocations with Burgers vectors perpendicular to the cleavage plane or Mode II with Burgers vector in the cleavage plane. To make the transition from Mode III to Mode I or II, simply make the substitution $\mu \to (1 - \nu)\mu$ in the equations. In Mode III and II, the cleavage plane is a glide plane, while in Mode I, the dislocation motion in the cleavage plane is by climb.

Consider a semi-infinite Mode-III crack with its tip at the origin, and a distribution of screw dislocations on the x_1 axis as shown in Fig. 45. For such a distribution on the x_1 axis, Eq. (15.7) becomes

$$f_d = \frac{K_{III}b}{\sqrt{2\pi x}} - \frac{\mu b^2}{4\pi x} + \sum{}' \frac{\mu bb'}{2\pi} \frac{1}{x - x_j}\left(\frac{x_j}{x}\right)^{1/2}. \tag{34.2}$$

The subscript on x has been dropped here and subsequently where the meaning is clear.

Making the continuum approximation,

$$db = \beta(x)\,dx. \tag{34.3}$$

Then

$$df_d = \frac{K_{III}\beta\,dx}{\sqrt{2\pi x}} - \frac{\mu(\beta\,dx)^2}{4\pi x} + dx\int_c^d \frac{\mu\beta(x')\beta(x)}{2\pi(x - x')}\left(\frac{x'}{x}\right)^{1/2} dx'. \tag{34.4}$$

[118] K. Y. Chia and S. J. Burns, *Scripta Metall.* **18**, 467 (1984).
[119] B. Majundar and S. Burns, *Int. J. Fract. Mech.* **21**, 229 (1983).
[120] J. Weertman, I. H. Lin, and R. Thomson, *Acta Metall.* **31**, 473 (1983).

If the distribution is in equilibrium, then from Eq. (33.2)

$$\frac{df_d}{dx} = +\beta(x)\sigma_f(x), \tag{34.5}$$

and the equilibrium equation (34.5) can be written

$$\frac{2\pi}{\mu}\left(-\sqrt{x}\sigma_f(x) + \frac{K_{III}}{\sqrt{2\pi}}\right) = -\int_0^d \frac{\sqrt{x'}\beta(x')}{x - x'}dx'. \tag{34.6}$$

The term in $(\beta^2 dx^2)$ is of course dropped because it is a higher-order differential.

Equation (34.6) has the canonical form of the Muskhelishvili integral equation, (A.44), and its solution is given by (A.45),

$$\beta(x) = \frac{2}{\pi\mu}\left(\frac{(x - c)(d - x)}{x}\right)^{1/2}\int_c^d \frac{g(x')dx'}{(x' - x)\sqrt{(x' - c)(d - x')}}, \tag{34.7}$$
$$g(x') = -\sqrt{x}\sigma_f(x) + K_{III}/\sqrt{2\pi}.$$

Because β is assumed to be zero at infinity, all polynomials in (A.45) are zero. If $\sigma_f(x)$ is a constant, the solution of this equation can be written in terms of elliptic integrals[109] (Fig. 45). The general form of β, however, is seen from the square-root factor in front of the integral in Eq. (34.7). There is thus a sharp maximum near the front edge at c, and a decrease to zero at point d. A solution can also be given numerically[121] for an arbitrary function $\sigma_f(x)$.

The continuum solution is only useful when $c \ll d$, and for this case when σ_f is a constant, a very simple set of relations can be written[120]

$$k = \frac{3}{\pi}\left(\frac{2}{\pi}\right)^{1/2}\sigma_f\sqrt{c}\left(\ln\frac{4d}{c} + \frac{4}{3}\right), \tag{34.8}$$

$$K = 2\left(\frac{2}{\pi}\right)^{1/2}\sigma_f\sqrt{d}, \tag{34.9}$$

$$\beta = \int_c^d \beta(x)\,dx = \frac{K}{\mu}\left(\frac{2d}{\pi}\right)^{1/2}. \tag{34.10}$$

Strictly speaking, in these equations, in Mode III, σ_f must correspond to a friction force on the dislocations, which in the simplest terms would be the Peierls force of the lattice against the dislocations. More generally, though, it could be any other resistive force in the lattice, such as interactions with impurities, or grain boundaries. Such resistance terms are usually thermally

[121] N. Louat, unpublished results.

dependent, however, and are not entirely consistent with the time-independent model assumed here.

In Mode I, the stress is usually interpreted as the yield stress, and the reason for this is best seen from Dugdale's original figure (Fig. 46). In a thin plate with a crack under tensile load, the deformation zone is concentrated ahead of the crack because of the tendency of the plate to thin down in this region. The overall effect is that of a distribution of edge dislocations running parallel to the crack tip, and with Burgers vector perpendicular to the crack plane. The opening of the crack, COD, is given by the relation, Eq. (33.3). Since the dislocations are produced by localized yielding in the deformed region, the stress in this region is given by the yield stress σ_y. Without work hardening, σ_y is a constant. Thus, depending upon the details of the modeling, σ_f in Eqs. (34.8)–(34.10) and the equations leading to it, may variously take on the meaning of a static yield stress, or a friction force. If the dislocations are thought of as being created by sources in the region of a static crack, then their local density will be fixed self-consistently by that value of σ_f which gives a local stress equal to the yield stress. If, on the other hand, the dislocations have been created, for example out of the crack tip in Mode III, or Mode II, and are mobile, they will move into a configuration consistent with the local frictional resistance forces. These two cases will be discussed in detail in Part VII,35.

When $c \to 0$ in Eqs. (34.6)–(34.10), the BCS or Dugdale limit is obtained. In that case β is given by an analytic function,[122] and for a finite crack with tips at $x = \pm a$, β is

$$\beta = \frac{2\sigma_f \alpha}{\pi\mu} \ln \left| \frac{x\sqrt{d^2 - a^2} + a\sqrt{d^2 - x^2}}{x\sqrt{d^2 - a^2} - a\sqrt{d^2 - x^2}} \right|, \qquad (34.11)$$

$$\alpha = \begin{cases} 1, & \text{screw} \\ (1 - \nu), & \text{edge.} \end{cases}$$

This distribution contains a singularity at the crack tips, $x = \pm a$. Equations (34.9) and (34.10) are still valid.

Dai and Li[123] have carried out numerical calculations for the equilibrium of a discrete set of dislocations, with Eq. (34.2) directly, with much the same results as shown for the continuum analysis.

The most important result in the BCS limit, however, is that the local k disappears, and the crack is completely shielded from the external stress. This result was already anticipated in Part VII,32 in the introductory comments. The point of view expressed in this article is that without a local k at the core crack, the stress environment there cannot be adjusted to the requirements of

[122] J. Weertman, *Int. J. Fract. Mech.* **2**, 460 (1966).
[123] S. H. Dai and J. C. M. Li, *Scripta Metall.* **16**, 183 (1982).

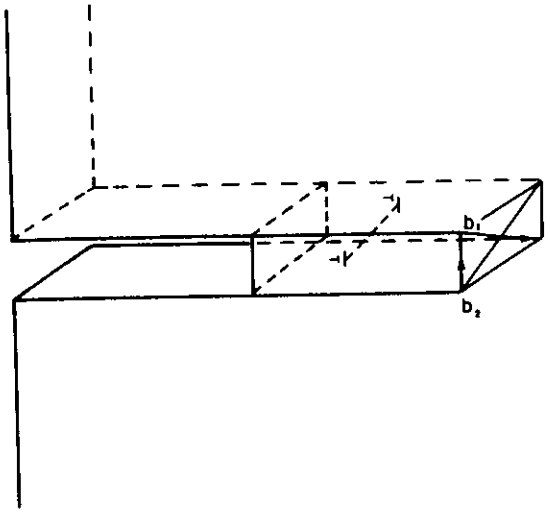

FIG. 46. Dugdale configuration. If a thin plate containing a crack is pulled in tension, the plate will slip ahead of the crack on planes through the thickness as shown, leaving edge dislocations running on the inclined planes through the specimen. The two dislocations, however, have the overall effect of a single edge dislocation with Burgers vector normal to the cleavage plane.

local equilibrium for the core crack. That is, if the crack is a cleavage crack, the local k must reflect the requirements of the bond strengths of the atoms at the tip (k_c), and if it is an emitting crack, the local k must do the same for emission. On the other hand, if the crack is completely shielded, the stress at the tip is given by the limiting value of σ_f, which is a parameter describing some kind of plastic response of the material, such as the yield stress, and does not provide a value of the ultimate bond strength. Thus a completely shielded crack is an inconsistent solution of the total problem. Nevertheless, Eqs. (34.9) and (34.10) do not contain the crack-tip parameters c and k, and are predicted correctly by the BCS continuum solution. These results are useful by themselves, and indeed, books on fracture such as the classic one by Knott,[124] and the reviews such as the excellent recent one by Smith,[108] make much worthwhile use of the BCS theory and these last two relations.

35. The Fracture Criterion in Cleavage

As promised in the introductory subsection, Eqs. (34.8)–(34.10) provide a rudimentary form of a fracture criterion. A fracture criterion should predict K_c

[124] J. Knott, "Fundamentals of Fracture Mechanics." Butterworths, London, 1973.

in terms of intrinsic materials variables for crack equilibrium. If σ_f is a true friction stress, and independent of the properties of the dislocation shield, then Eq. (34.8) is decoupled from the other two in the sense that then the first equation relates only to the crack tip region. The weak dependence on d in the logarithm can be safely ignored in first approximation. In effect, Eq. (34.8) sets c and k so they are consistent with one another, independent of the magnitude or extent of the shielding zone. In a sense, there is no predicted K_c, because it depends on B or d, which can be set at will. Then, Eqs. (34.8)–(34.10) are underdetermined until some additional information is provided, such as a law giving the magnitude of the shielding charge B.

One way to provide the missing information is to identify σ_f as a yield stress, and link it to the local dislocation distribution β by a work hardening law. Such a law, however, would change the character of the integral equation, (34.6), and the solution, Eqs. (34.8)–(34.10) would not be valid. Weertman *et al.*[120] have proposed that another, less satisfactory constitutive law can be obtained by linking σ_f to the total B by an equation such as

$$\sigma_f = \sigma_0(B/B_0)^m. \tag{35.1}$$

With this equation, the set of equations (34.8)–(34.10) is fully determined, and the critical k is given as[120]

$$K = \kappa(k_c^2/c)^{(1+m)/4m},$$
$$\kappa = \left(\frac{\pi^3}{18}\right)^{(1+m)/4m} \frac{\sqrt{2B_0\mu}}{\sigma^{1/2m}\left(\ln\dfrac{4d}{c} + \dfrac{4}{3}\right)^{(1+m)/2m}}, \tag{35.2}$$
$$k_c^2 = 4\mu\gamma.$$

In this equation, κ depends primarily on macroscopic quantities, while k and c are tip region parameters. k_c is the critical k for crack advance, and is given here in terms of the Griffith relation and γ. In this form, one sees that, in spite of the large shielding which might be provided by B, the entire fracture process is very sensitively controlled by the conditions of atomic bonding at the tip because of the overall balance and equilibrium which is required. The appearance of c in this relation is interesting. In Eqs. (34.8)–(34.10) σ_f has been identified as a yield stress, but the model does not let local sources of dislocations operate within the elastic enclave $x < c$, and the physical reason for this is that in real solids, the sources for dislocations are not ubiquitous on an atomic scale. In this picture, then, c is the distance to the first *source* of dislocations, a parameter which is linked back to the inhomogeneity or graininess of the scale of plasticity in a real material. Without this plastic

"grain size," of course, the crack would be fully shielded again, and all the objections already voiced about that situation would pertain.

Equation (35.2) shows qualitatively the required dependence on the physical parameters μ, σ_0 (which is the initial yield stress), work hardening parameter, etc. However, it is based on a very primitive one-dimensional model. Another relation which uses the inner cutoff idea, but uses a two-dimensional treatment of the plastic region gives a somewhat different and probably better relation[125]

$$K_c^2 = 2\pi\left(\frac{2\gamma\mu}{\pi}\right)^{(1+m)/2m} \Big/ (\sigma_0^2 c)^{(1-m)/2m}. \tag{35.3}$$

In this equation, the work hardening law is written

$$\sigma_f = \sigma_0(\epsilon/\epsilon_0)^m \tag{35.4}$$

in the traditional manner, where ϵ is the strain, and σ_f is a local function of strain, in which the local strain is related to β.[126] Equation (35.3) is a correction of the original expression in Thomson.[126] Equation (35.3) has been tested against steels which have been embrittled with results which are satisfactory, but no intensive effort has been made to validate the prediction. The reader will find additional discussion of the elastic–plastic enclave approach by Weertman[127,128] and Fuller and Thomson.[125]

36. Emission-Controlled Shielding

When $k = k_e$ dislocation emission occurs. This class of fracture has been studied intensively in Mode III by S. M. Ohr and his collaborators at Oak Ridge,[10,111–117] by Wilsdorf and collaborators at the University of Virginia,[6] by P. Neumann and collaborators at Dusseldorff,[9,99] and by Chia and Burns.[118] In a typical experiment, as performed by Ohr, a small rectangular specimen is thinned through its center, as shown in Fig. 12. When stressed in the transmission electron microscope, shear is induced in the thin portion of the foil, as shown in Fig. 13b. If dislocations are injected into the thicker part of the foil from the thin edge, eventually when the total Burgers vector component normal to the foil nearly equals the thickness of the foil, the foil shears apart, and a Mode-III cracklike artifact is formed. From the geometry, in pure shear, the "crack" line would have zero length at its tip, but in the experiments, some Mode I develops because the crack possesses a small finite length at its tip associated with the dislocation free zone. Figure 13 has already displayed results for copper.

[125] E. Fuller and R. Thomson, *AIME Symp. Micro Macro Mech. Crack Growth* 49 (1981).
[126] R. Thomson, *J. Mater. Sci.* 13, 128 (1978).
[127] J. Weertman, *Acta Metall.* 26, 1731 (1978).
[128] J. Weertman, *J. Mater. Sci.* 15, 1306 (1980).

The primary results of these experiments are: (1) the dislocations are emitted on the crack plane (which coincides with a slip plane) from the crack tip as it grows into the foil; (2) there is a significant zone in front of the crack devoid of dislocations, called a dislocation free zone; (3) the number of dislocations emitted is correlated with the thickness of the foil; i.e., COD $\simeq \sum b_j \cos\theta_j$, where θ_j is the inclination angle of the slip plane to the normal of the foil; (4) the distance to the first dislocation is a function of the stress on the crack, such that when the stress is lowered, this distance also decreases; (5) the distribution observed is that of an inverse pileup, with a sharp maximum in the vicinity of the first dislocation; (6) when the crack grows into a relatively thick portion of the foil, it often develops more Mode-I character, so that emission is then observed on slip planes intersecting the crack plane at a finite angle, blunting the crack as discussed in Part VI; and (7) quantitative interpretation of the results can be correlated with the emission criteria of Part VI and the shielding results of Part VII,34, to which we now turn.

Chang and Ohr[109] and Ohr and Chang[88] have interpreted these results in terms of the one-dimensional continuum model of Part VII,34 with a finite value of c in Eqs. (34.8)–(34.10). In the experiments, σ_f and c can be measured. From Eq. (34.8) k_{III} and K_{III} can be calculated. In this case, of course, the critical value of k_{III} in Eq. (34.8) is the critical value for dislocation emission, called in Part VI, k_{IIIe}. The results taken from Ohr and Chang[88] are shown in Table I.

Several comments are in order regarding the validity of the models. First, the experiments are performed in thin foils, and the theory pertains to thick specimens. In the elastic analysis, the stresses on the foil faces must be zero [Eq. (7.3)]. If the crack were normal to the foil surface, and the stress state were Mode I or Mode II, then plane stress (see Part III,9) would apply. However, the crack is primarily a shear crack in Mode III, and the axis of the crack and its associated dislocations is inclined to the plane of the foil at a finite angle. Eshelby and Stroh[129] have analyzed the problem of screw dislocations normal to a surface and shown that screw dislocations in that case have a truncated long-range stress field of the form $r^{-1/2}e^{-r/t}$ (incorrectly quoted in their paper), where t is the foil thickness, because of the image terms in the foil surface. Edge dislocations retain their long-range $1/r$ stress fields, however. For the same reason which leads to the truncated screw stress field, the Mode-III crack if normal to the foil surface would also be expected to have a truncated long-range stress field in a foil. However, the crack and slip plane are at an inclined angle to the foil, so only a portion of the $\sigma_{z\theta}$ and σ_{zr} stress fields will be cancelled by the boundary condition on the foil surface. Thus the inclined crack and dislocation distribution will retain a portion of their long-

[129] J. D. Eshelby and A. N. Stroh, *Philos. Mag.* **42**, 1401 (1951).

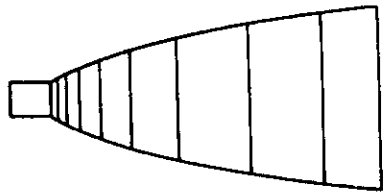

FIG. 47. View of fracture plane for the foil. The crack line is a small fraction of the foil thickness, and the thickness is a function of position in the plastic zone. The stress state at the crack line must possess at least a small amount of Mode I in order to open the crack at that point, but the stress cannot be two dimensional because of the variable thickness of the crack plane.

range interactions and the crack and dislocations will interact with one another at distances well beyond the foil-thickness distance. However, buckling in the foil will still serve to orient the system so that the image terms can operate to some extent, and will tend to decrease the long-range interactions further. Chang and Ohr[130] have studied the effect of finite thickness on the integral equation Eq. (34.6) in Mode III, but because of the inclination of the slip plane to the foil surface, the configuration is not pure Mode III as explained above.

The second point concerns the question of whether the geometry of the sheared foil really represents a two-dimensional Mode-III crack. A view of the crack plane would schematically be that shown in Fig. 47. Because of the variable thickness of the foil in the plastic zone, the stress state cannot be entirely two dimensional. In effect, there must be a higher effective k at the crack tip relative to the two-dimensional k used in the equations, roughly in proportion to the ratio of the crack-line length to the undeformed foil thickness. Thus, the foil geometry generates an inherent uncertainty in the two-dimensional antiplane-strain analysis. However, there is no question that the qualitative picture is correct and the surprising quantitative results shown in Table I indicate that the approximations in the analysis are not serious or that they cancel one another.

It is important to note that these Mode-III experiments do not bear directly on the Mode-I emission–cleavage dichotomy of Part VI. The discussion there emphasized the independence of the modes relative to this question, and emission of screw dislocations in Mode III was shown to be unaffected by cleavage events in Mode I. There is an observable short Mode-I crack in the experiments, as shown in Fig. 47, which coexists with the Mode-III emission, but the value of k_I at the tip has not been calculated. (For self-consistency, of course, it must be at the Griffith value.) The general configuration of the

[130] S. Chang and S. M. Ohr, *Int. J. Fract.* **21**, 3 (1983).

overall loading in the (non-2D) foil dictates that the k_I and k_{III} values must be about equal, but the detailed analysis has not been carried out. Hence, a direct quantitative comparison of k_{IIIE} with k_{IE} based on these experiments cannot be made. It is very interesting, however, to note that in the same configuration, MgO does not emit screw dislocations, but cleaves, showing that the experiments do have a qualitative bearing on the cleavage/emission dichotomy. These mixed mode loading questions are further pursued in Part VII,37.

The Mode-III foil experiments do not relate directly to any perceived macroscopic failure mode in a bulk material, but they throw a very strong experimental light on two general principles in fracture: They confirm direct emission of dislocations from a sharp crack tip in fcc and bcc metals, and they confirm the general proposition of crack tip shielding including the importance of the local k at the crack tip. However, we suggest there is one important mechanism operating in the failure of practical ductile materials where the Mode-III (or its sister Mode-II) crack discussed here could play a role, and that is the observed shear breakdown found to occur between neighboring holes in the later stages of hole growth fracture. (See Fig. 14.)

Experiments reported by Chia and Burns[118] on cracks in LiF do provide general confirmation of the picture presented here in bulk specimens. An additional feature found, however, relates to the effects of nonblunting glide dislocations in shielding the crack. Unloading in their case also had the interesting effect of increasing the deformation zone in a nonlinear fashion, a result of interest for fatigue crack growth.

The experiments of Wilsdorf and collaborators[6] have focussed on the final stage of ductile rupture of a specimen. Some experiments have been performed on macroscopic sized specimens, which neck to a fine chisel edge, as shown in Fig. 5. TEM studies of the thinned neck during final rupture are similar to results of prethinned foil specimens stressed *in situ* in the microscope. Figure 14 shows that, just before final rupture, a ductile "crack" develops composed of a regular series of rectangular holes. The nucleation and growth of these holes has been studied in a variety of ductile materials: Ag, Al, Au, Cu, and Fe and Be in the pure form and stainless steel and Al alloys. Both polycrystalline and single crystals were included. For a general review of the results, see Wilsdorf.[6] The major results were: (1) the voids are nucleated in dislocation cell boundaries; (2) the holes formed take a highly crystallographic shape determined by the operation of dislocation sources either at the sharp corners or from bulk sources very near these corners where stress concentrations are high; the void in other words grows at each of its corners by the slideoff mechanism for an emitting crack; and (3) there is an observable difference when the strain rate is "high" typical of that to be expected in a specimen deformed in an Instron machine, and "low" corresponding to a creep regime. In the "high"-strain range nucleation and growth take place by both dislocation avalanches and twinning, with resultant regular hole formation. At lower strain rates, individual dislocation events are observable, but the overall results are less regular in appearance, corresponding to the ability of the dislocations to achieve lower-energy configurations by strain annealing. The first stage of hole initiations is the growth of a rapid dynamic brittle crack to a length equal to the length of the final void, and then it stops. Blunting then takes place slowly by deformation at the crack tip. The initial fast dynamic growth is not consistent with the subsequent behavior as a ductile process. In Fig. 48, a high magnification micrograph shows the initiation of a hole in a cell boundary.

Analytic treatment of the emitting cracks of Vehoff *et al.* (Fig. 11) and the growing voids of Wilsdorf and co-workers involves the application of the wedge-dislocation interaction analysis of Part III, and has not been carried very far as yet. The reader is referred to the paper of Chang *et al.*[23]

37. Shielding by Externally Produced Dislocations

Even for a stable cleavage crack which does not emit dislocations, external sources for dislocations nearly always exist in a material, and when sufficiently close to the crack, the stress concentration can cause them to operate. Lin and Thomson[131] have investigated the shielding provided by a single external source (Fig. 49) and analyzed the stress on the source and the shielding of the crack tip as a function of the number of dislocations produced. Neglecting the effect of ledge formation by the antishielding dislocations which might be absorbed by the crack, they show that the back stress of the dislocations on the source is stronger than the shielding of the crack tip, because the source is closer to the dislocation pileup than the crack is. Thus, as the external stress of the K field is increased, the cleavage criterion at the crack tip will ultimately be achieved again for a finite number of dislocations produced by the source. Thus, neglecting the effect of crack shape change due to dislocation absorption, the crack will remain brittle in the sense that the sources will provide only a limited and finite shielding for the crack. Brittle crack propagation will then always be possible for some value of external K, which depends upon the source location and source hardening parameters.

This model has not been adequately pursued to explore the toughening properties of a discrete distribution of external sources for dislocations. Crossover to the ductile fracture mechanism is inherent in such a model, however, if the shape change in the crack can permanently lower the local k below k_{IC} while external sources continue to operate. This question is closely

[131] I. H. Lin and R. Thomson, *Scripta Metall.* 17, 1301 (1983).

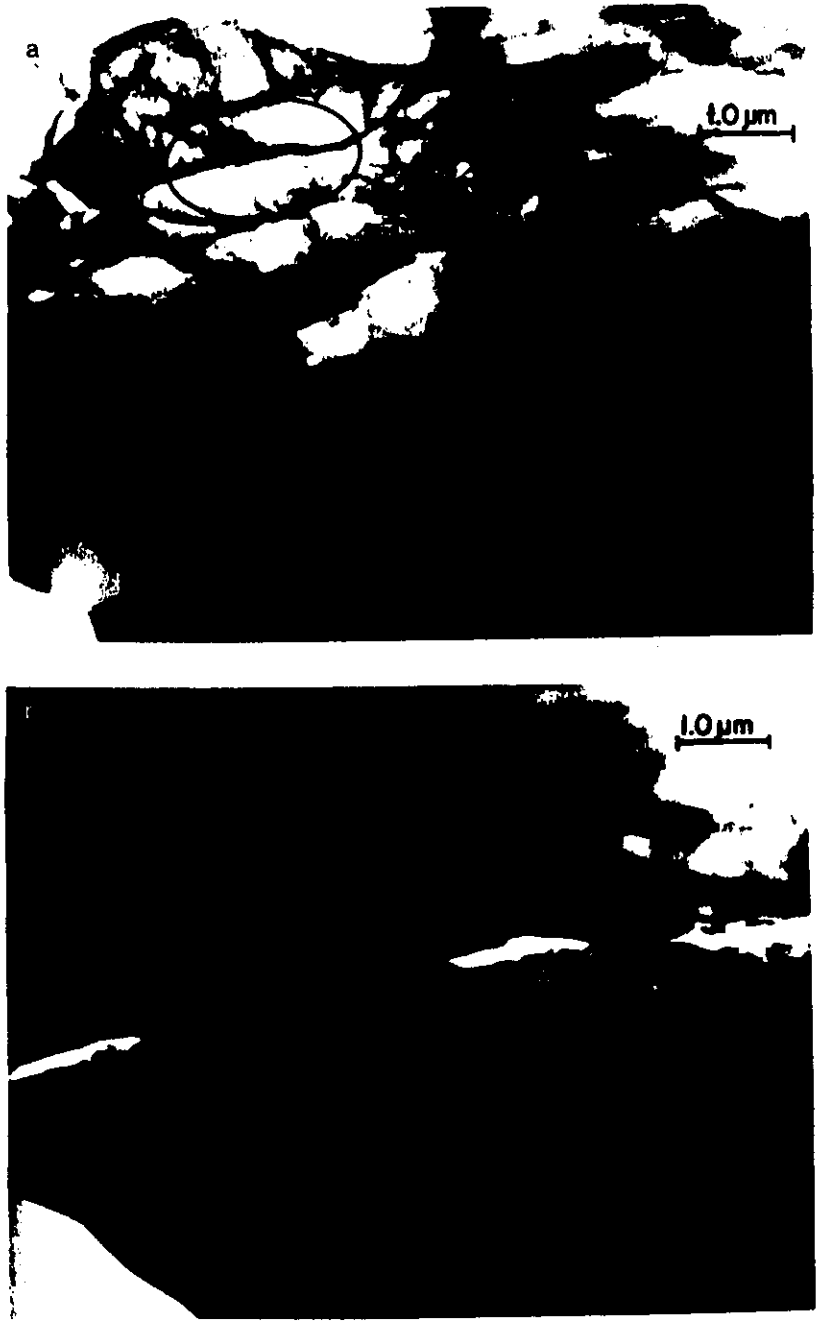

FIG. 48. Initiation of a hole near a crack in the Wilsdorf configuration.[6] (Courtesy H. G. F. Wilsdorf.)

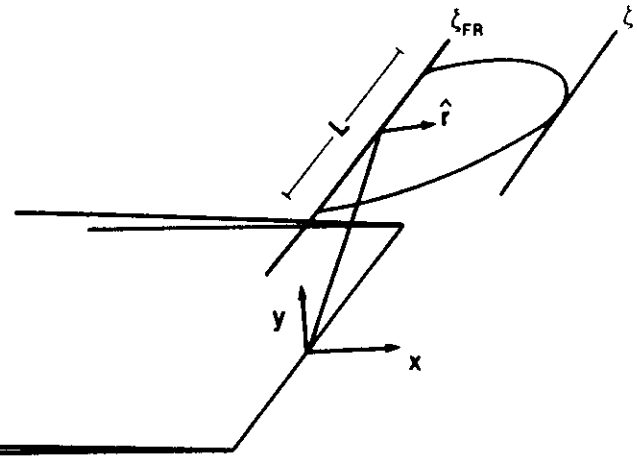

FIG. 49. Operation of a Frank–Read source near a crack tip. ζ_{FR} is the distance to the source and ζ to the dislocation loop tip.

related to the phenomenon of blunting the tip by external sources already discussed in Part VII,33. It is important to find out by further theoretical modeling as well as by experimental investigation if external sources can by themselves provide a path for the cleavage–ductile transition in a material without invoking dislocation emission from the crack tip.

Dislocation shielding of cracks in any real case is probably due to a mixture of external sources as well as emission. For example, any emitted dislocation pileups will certainly interact with sources in the medium, and the overall shielding will be a mixture of the two types. Modeling of such situations probably is best accomplished by material-deformation constitutive laws, which suggests that an ultimate "solution" of the practical problem will probably involve a continuum solution of the outer parts of the deformation field with a discrete approach to the inner region reminescent of the lattice modeling of Part V.

38. Mode-I and Mixed-Mode Problems

The shielding problem in Mode I is sufficiently difficult that relatively little analysis has been carried out for it except for numerical calculations in the 1D BCS approximation. We have given the general 2D results for interactions between cracks and dislocations in Part IV, however, and some general comments can be made here regarding the character of these interactions.

The shielding relation, Eq. (16.7), can be written for the real and imaginary components for the contribution K_d of each dislocation to K as

$$(K_d)_{\mathrm{I}} = \frac{\mu}{(1-\nu)\sqrt{2\pi r}}\left[b_2\cos\frac{\theta}{2} + \frac{\sin\theta}{2}\left(b_1\cos\frac{3\theta}{2} + b_2\sin\frac{3\theta}{2}\right)\right],$$
$$(K_d)_{\mathrm{II}} = \frac{\mu}{(1-\nu)\sqrt{2\pi r}}\left[b_1\cos\frac{\theta}{2} + \frac{\sin\theta}{2}\left(b_2\cos\frac{3\theta}{2} - b_1\sin\frac{3\theta}{2}\right)\right]. \quad (38.1)$$

The overall shielding situation is somewhat complex, because, not only is there an angular dependence in (Eq. 38.1) which changes sign with θ, but for any given crack, there can be a mixed-mode loading. By a mixed mode, we mean that the external loading of the crack can be a combination of Modes I, II, and III. The loading in turn will in general produce the dislocation distributions typical for such loading through dislocation emission.

The characteristic dislocation distributions (from emission events at the crack) will be those depicted in Fig. 50. Figure 51a shows the shielding of a

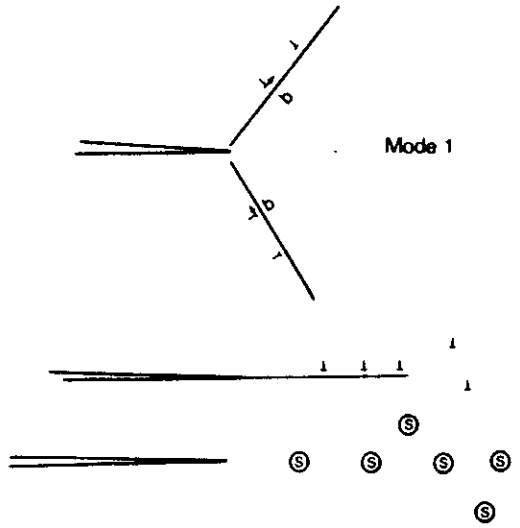

FIG. 50. Typical dislocation configurations for pure loading situations. Mode I produces shielding dislocations on slip planes at an angle to the crack plane. $(b_x)_1 = -(b_x)_2; (b_y)_1 = (b_y)_2$. In Mode II, the dislocations are produced on the plane of the crack, but some cross slip can be expected. In Mode III, no specific slip plane is necessary because of the screw character of the dislocations, but in practice, the dislocations will tend to be formed on the crack plane. In each mode, as the crack moves forward, the dislocations will be left behind as a wake.

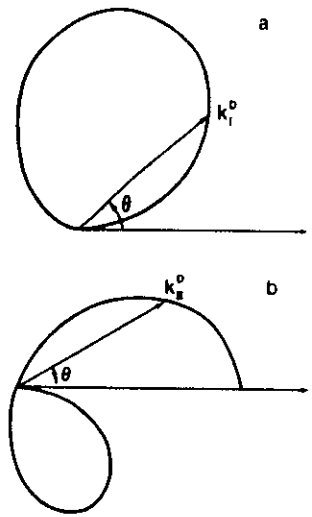

FIG. 51. In (a), the K_d shielding contribution to Mode I of a dislocation with Burgers vector $(1/\sqrt{2}, 1/\sqrt{2}, 0)b$ is displayed as a function of angle θ relative to the crack tip. See Eq. (38.1). In (b) the shielding of a nearly pure edge dislocation in Mode II [$b = (b, 0, 0)$] is shown as a function of angle to the crack tip.

dislocation with Burgers vector $b = b\,(1/\sqrt{2}, 1/\sqrt{2}, 0)$ as a function of angle relative to the tip. Maximum shielding occurs roughly at the $\theta \simeq \pi/2$ point. Dislocations on the two slip planes shown in Fig. 50a contribute symmetrically to K_{I}.

When a Mode-II dislocation interacts with a Mode-I crack, cross slip is assumed to spread the dislocations off their initial slip plane, which is coincident with the crack plane, into a thin region on either side of the crack plane in a symmetrical manner (Fig. 50b). The second term in the first equation of Eq. (38.1) is the relevant one, and it is antisymmetric in θ. Thus no net contribution to K_{I} will be made by a *symmetrical* distribution of Mode-II dislocations.

Figure (51b) shows the shielding of a dislocation in a pure Mode II configuration as a function of angle θ.

When a Mode-II crack interacts with a symmetric pair of dislocations in a Mode-I configuration (Fig. 50a), all three terms contribute in Eq. (38.1), because the Burgers vector has both x_1 and x_2 components. However, the first-term contribution is zero because $(b_1)_{x_1} = -(b_2)_{x_1}$. The second term is an odd function of θ, and hence one dislocation again cancels the other. The third term also contributes zero because $(b_1)_{x_1} = -(b_2)_{x_1}$ and the angular function is an even function of θ.

Mode III is essentially "orthogonal" to the other two modes, and no crossover terms occur.

The overall result is thus that, so far as shielding is concerned, there are no significant cross terms in the shielding contributions, and the modes can be considered individually. This result, of course, depends on the assumption of symmetry. When a single dislocation is being emitted from a Mode-I crack, then there is a contribution to K_{II}, and a reaction in Mode II. This point is further discussed in Part VII,39.

The most interesting mixed-mode crack is one where sufficient Mode I exists to ensure that the crack develops an open surface on the crack plane, but where the primary loading is Mode III (the "Ohr" configuration of Fig. 13) or Mode II. In pure Mode II or III, of course, the bonds are not separated across the crack plane, and no physical crack exists, as discussed in Part VI,28. Suppose initially, then, that a sharp stable Mode-I crack exists so that the Griffith relation is satisfied at the crack tip,

$$k_I^2 = 4\gamma(1 - \nu)/\mu. \tag{38.2}$$

No dislocations are presumed present initially. As Mode-II loading is applied, the local k_{II} starts from zero and increases. Because of the elastic linearity of the Mode-I and -II stress states, the Mode-I stress is not changed by the Mode-II loading. As noted in Part VI,28, the fracture criterion at the tip is slightly modified, because the bonds at the tip will be sheared, and in general, less k_I will be required to hold the atoms open there. However, we expect this effect to be small, as proposed in Part VI,28. Thus, as k_{II} is increased, no additional cleavage occurs, but Mode-II loading can induce dislocation emission, and the standard dislocation emission conditions of Part VI on the crack plane will be valid. We now presume that the crack plane is a slip plane, and the standard one-dimensional dislocation distribution of edge dislocations will be generated, controlled by the local emission criterion in Mode II and the total externally applied K_{II}. In this mixed-mode case, the Mode-II dislocations exert little shielding on K_I of the crack, as explained earlier in this section. So long as the Mode-I-type dislocations are not produced by either emission or external source activiation, the crack can cleave at very low k_I values, yet generate an indefinite number of Mode-II dislocations with large amounts of plasticity. Thus in this mixed-mode case, high ductility and cleavage comfortably coexist.

Lynch[132] has in fact observed phenomena very similar to that described above in chemically embrittled metals. In his experiments, the external chemical environment presumably modifies the Griffith criterion through its effect on γ so that a cleavage crack is stable. Large amounts of deformation are

[132] S. P. Lynch, *AIME Symp. Liquid Metal Embrittlement* (1983).

then observed close to the cleavage plane, as described above for emission in Modes II and III. These ideas suggest in practice cleavage fracture should commonly exhibit this type of shear-mode emission because of the difficulty of ensuring pure Mode-I loading.

An important proposal has been made by Sinclair and Finnis[89] that the cleavage/emission balance can be altered after emission of a group of dislocations has occurred. Their proposal is built on a cleavage criterion like Eq. (28.8) and an assumption that emission occurs in Mode I in an asymmetric manner so that mixed loading at the tip occurs. We have argued that Eq. (28.8) is not the correct cleavage criterion, but there remains the issue mentioned in Part VI,28, where cleavage and emission are finely balanced against one another, that mixed-mode loading might still alter this balance. Indeed, in the "Ohr" configuration of Fig. 13, a small and presumably stable Mode-I crack is observed as schematically shown in Fig. 47. This crack does not emit in the Mode-I configuration of Fig. 50a, as demonstrated in the electron micrograph of Fig. 13, even though the material is the supposedly intrinsically ductile metal, copper, where stable Mode-I cracks are not supposed to exist in pure Mode I. This result has not been analyzed yet in terms of the available slip system geometry and stress state in the films. Two possibilities exist. The first is that some Mode-II loading exists of sign and magnitude sufficient to raise the emission criterion from Eq. (28.2) relative to the cleavage criterion, and the second is that the Mode-III loading changes the cleavage/emission balance at the crack tip. This is an important issue, and requires further study.

Having explored shielding effects on the crack, we turn now to some theorems regarding the forces experienced by the dislocations. The first theorem which can be proved is that in Mode I, for two symmetrically placed dislocations with the configuration of Fig. (50a),

$$(\bar{f}_{dd'})_{\text{slip plane}} = 0. \tag{38.3}$$

The second theorem of interest relates to the relation (15.10). In the deformation theory of cracks using the J integral, it is shown that in the limit of small-scale yielding where the region of deformation is small compared with the crack size and the specimen size, the force on the total configuration is given by the generalization of Eq. (15.10); that is,

$$\text{Re}(\bar{f}_{\text{tot}}) = \frac{(K_I^2 + K_{II}^2)}{2\mu}(1 - \nu) + \frac{K_{III}^2}{2\mu}. \tag{38.4}$$

This theorem is also valid when the deformation field is composed of singular dislocations. The reason is that the far-field asymptotic form of the stress in Mode III and the potential functions in plane strain are all dominated by the $1/\sqrt{z}$ term given by the far-field K field in each case. (See Eqs. (10.3), (10.11), and (10.12).) The next term in the expansion at infinity is not the simple

dislocation term in $1/\sqrt{z}$, but a higher-order term in $1/\sqrt{z^3}$. In the limit of large $|z|$, the integration of these $z^{-3/2}$ stresses around a contour where $|z| \gg |\zeta_j|$ on the contour (ζ_j is the position of any shielding dislocation) in either the J-integral expression, or the Eshelby theorem [Eq. (14.8)], contributes a zero contribution to f. The reason, of course, is the image that the dislocation develops in the open crack which cuts off its long-range $1/z$ field.

Using Eq. (38.3) and the shielding results of Eqs. (15.6) and (16.7), some simplification in the force equations is possible. Writing

$$K = k + K_D, \tag{38.5}$$

which will be valid for each mode, then *for each mode*,

$$\begin{aligned} \mathrm{Re}(\bar{f}_{tot}) &= \mathrm{Re}\, f_c + \mathrm{Re}\sum_j (f_d)_j = \frac{K^2}{2\chi}, \\ \chi &= \begin{cases} \mu & \text{Mode III} \\ \mu/(1-\nu) & \text{Mode I, II.} \end{cases} \end{aligned} \tag{38.6}$$

Using Eq. (38.5), Eq. (38.6) becomes

$$\mathrm{Re}\sum (f_d)_j = \frac{KK_D}{\chi} - \frac{K_D^2}{2\chi}. \tag{38.7}$$

Since the first term is linear in K, it represents the direct force term on the dislocations, while the second term is the combination of image and dislocation–dislocation interactions. Using the shielding relations, Eqs. (15.6) and (16.7), these become in turn for each dislocation

$$\mathrm{Re}(f_{cd})_{tot} = K_{III} b_3 \,\mathrm{Re}(1/\sqrt{2\pi\zeta_j}), \qquad \text{Mode III}$$

$$\mathrm{Re}(f_{cd})_{tot} = \frac{+K_I}{\sqrt{2\pi r_j}}\left[b_{2j}\cos\frac{\theta_j}{2} + \frac{\sin\theta_j}{2}\left(b_{1j}\cos\frac{3\theta_j}{2} + b_{2j}\sin\frac{3\theta_j}{2}\right)\right], \qquad \text{Mode I}$$

$$\mathrm{Re}(f_{cd})_{tot} = \frac{K_{II}}{\sqrt{2\pi r_j}}\left[b_{1j}\cos\frac{\theta_j}{2} - \frac{\sin\theta_j}{2}\left(b_{1j}\sin\frac{3\theta_j}{2} - b_{2j}\cos\frac{3\theta_j}{2}\right)\right], \qquad \text{Mode II} \tag{38.8}$$

The term in K_D^2 is a double sum over the dislocation distribution. The terms in $b_j b_i$ represent dislocation–dislocation interactions. The b_j^2 term represents the self-image term. These expressions are not written here, but are explicit manifestations of the more general expressions in Eqs. (16.13) and (16.16), which can be useful.

In the only serious attempt at Mode-I shielding calculations to date, the BCS model has been extended by Riedel[133] and Vitek[134] to the Mode-I crack with a pair of slip planes intersecting the crack tip at an angle of $\pm\theta$. The resulting singular integral can be converted to one of Fredholm type which can be numerically integrated. The numerical results compare in all major aspects to the full two-dimensional continuum plastic-deformation theory results; so the approximation that slip only occurs on two symmetrically oriented slip planes is apparently a good one. This work, however, did not include considerations of the local k and local crack equilibrium. The results suggest that including such a dislocation-free zone in these calculations would lead to a quite satisfactory description of shielding in Mode I, and hence to a realistic toughness relation. Sinclair[135] has carried the problem one step further, and made a numerical calculation for a wedge crack created by emission of a symmetrical distribution of dislocations on symmetrical slip planes making angles of $\pm\theta$ to the symmetry plane of the wedge. In all these cases, one of the important results is the generation of a maximum dilatation at some distance ahead of the crack tip, which is thought to be correlated with the generation of new cracks in the hole-growth model.

39. Growing Cracks

A growing crack differs from a static one in two important respects. A growing crack has a past history in the sense that its deformation zone has passed through the specimen and left behind a wake of work-hardened material extending some distance on either side of the open flanks of the crack. Secondly, a growing crack is also a time-dependent phenomenon, and will involve rate-dependent dissipation processes in any plastic response of the material, and may also involve dynamic or inertial effects as well. Both of these aspects of moving cracks lead to important physical effects different from static cracks.

a. Quasistatic Cracks

In the quasistatic case, inertial effects are neglected. Hart[103] has treated this problem in an elegant approach using a continuum (but two-dimensional) form of the shielding theory in Mode III. In his work, the crack is assumed to move with constant velocity, and the dislocation density is generated by a

[133] H. Riedel, *J. Mech. Phys. Solids* **24**, 277 (1976).
[134] V. Vitek, *J. Mech. Phys. Solids* **24**, 67, 273 (1976).
[135] J. Sinclair, *Nucl. Metall.* **20**, 388 (1976).

deformation-rate constitutive law which is consistent with laws describing creeping materials, but is not a strain-hardening law. In his earlier work, the deformation zone is also assumed to move with the crack, and the problem of the wake is not addressed. In later work, yet to be published, however, the wake is included, so that a true dissipation takes place. The feature of Hart's work which will be familiar to the reader of this article is that a local k is derived. For a moving crack, even in a continuum theory, this is possible so long as the creep deformation near the crack tip is sufficiently slow so that the crack tip is not completely shielded. This requirement becomes an assumption for Hart's treatment, and it turns out to be attainable provided the creep law,

$$\dot{\epsilon} = A\sigma^n + \dot{\sigma}/\mu, \tag{39.1}$$

in the vicinity of the tip has an exponent, $n < 3$ and far from the crack tip, $n > 3$. Hui and Riedel[136] have published a general analysis of the asymptotic forms of the stress fields at the crack tip and at large distances with creep laws of the form of Eq. (39.1). When $n > 3$ near the crack tip, no k field is possible, and the field is dominated by the plasticity. That is, the crack tip is essentially fully shielded, even though it has a stress singularity.

The interesting predictions of Hart's analysis are that (1) the crack must have a finite velocity, or the creeping material at the crack tip will completely shield the tip and destroy the crack k field, and (2) that for high velocities a breakaway phenomenon occurs corresponding to the crack outrunning the ability of the material to form a significant shielding charge of Burgers vector. In the analysis, this breakaway actually corresponds to an analytically double-valued solution (Fig. 52).

The work of Hart and of Hui and Riedel is of considerable interest, because it shows that, when the crack is moving, rate-dependent continuum solutions can be constructed which are not limited by the Rice theorem[32,46] discussed in the introduction, Part VII,32. When $v \to 0$, as Hart shows, the creeping material at the crack tip will eventually damp out any static stress concentration, and the k field will be destroyed. Then no atomic-bond-breaking process at the tip can be invoked, because at best the stress field is restricted to the much lower stresses allowed by deformation processes, and Rice's theorem applies. When v is greater than some critical value, *and when* $n < 3$, then the plastic creep does not have time to fully shield an atomically sharp crack when it moves into a new region of the material. Then a local k can be sustained, and the bond-breaking stresses at the tip can be achieved. But if $n > 3$, then these results are no longer possible, and the atomic crack breaks down. One might say the physical reason for this breakdown is that the condition described in Part VII,33 leading to Fig. 44 obtain, and Rice's theorem takes over.

[136] C. Y. Hui and H. Riedel, *Int. J. Fract.* 17, 409 (1981).

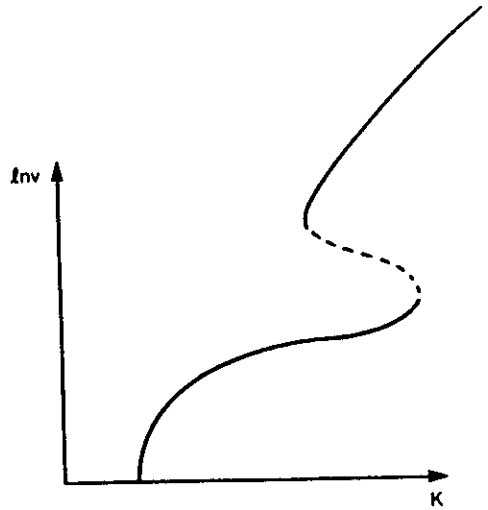

FIG. 52. Predicted form of $K(v)$ for a creeping crack after Hart.[103] The curve stops at the lower limit for v and has a branch with negative slope corresponding to dynamically unstable states.

These rate-dependent results for moving cracks are closely related to the general point of view of this article, that conditions in the near tip region of a crack involving the distribution of dislocation sources and their ease of operation determine whether the sharp crack can be sustained. The condition $n < 3$, physically, is another statement of the same general type. Indeed, as we will show below, one can derive some analogous moving-crack behavior on the basis of the shielding ideas developed here in Part VII,34.

Imagine that a brittle crack is moving at velocity v, and that a dislocation cloud has been attached to the crack by some prior event which will not enter further into the analysis. Suppose the slip plane for the dislocation is parallel to the crack plane, that the Mode-III analysis applies, and that the entire configuration is in steady-state motion with velocity v. With the use of Eqs. (34.8)–(34.10), the configuration is consistent with a steady-state velocity if the friction stress is determined by the stress–velocity law for the dislocations, $\sigma_f(v)$. For a given B, and K, the size of the pileup, d, is determined by Eq. (34.10). The velocity is then determined by Eq. (34.9). Equation (34.8) is a relation between k and c, because all the other parameters in Eq. (34.8) have been determined by the external conditions or by Eqs. (34.9) and (34.10). Thus if the crack local k is a function of v, or in a quasistatic limit simply given by the Griffith relation, $k^2 = 4\mu\gamma$, Eq. (34.8) sets c so this local k can be maintained. Hence a $K(v)$ law is generated consistent with the dislocation $\sigma_f(v)$ law and the

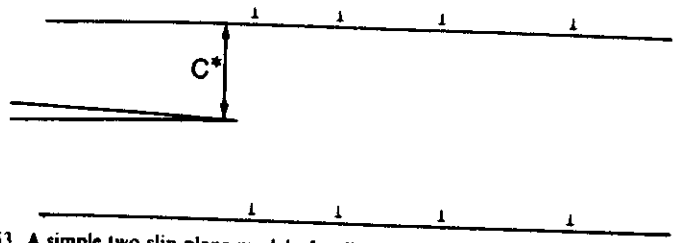

FIG. 53. A simple two-slip-plane model of a dislocation shielding configuration. The closest approach of the first dislocation to the crack is c^*.

shielding relations for all velocities v. However, unless the dislocation slip planes are exactly coincident with the crack plane, there is a lower limit to c, and a maximum limit to K or v. This configuration is shown in Fig. 53, and is due to the fact that when the closest dislocation is on a slip plane a distance c^* above or below the crack plane, the lower limit of c in Eq. (34.8) is c^*. For k values above this initial point, the shielding of the crack tip "runs out of steam," and the crack breaks away from its dislocation shield.

An actual physical situation approximating the above description is that found in LiF in early experiments on dislocations interacting with cracks by Burns and Webb.[137] In their case the slip planes of the dislocations were inclined to the plane of the crack (in the x_3 direction), so that the dislocations wrapped around the crack to form a hairpin shape. The limiting value of c in this case would correspond to the distance between neighboring dislocations in the x_3 direction, and σ_f would be the sum of the actual σ_f for the part of the dislocations looping around the crack and the line tension of the straight segment forming the wake. The interpretation and analysis originally given by Burns and Webb is not inconsistent with this picture, and their experimental results showed the kind of breakaway proposed above.

If, on the other hand, the crack generates new dislocations from sources in the medium as it moves along, a shielding charge is built up and then left behind as a wake as the crack moves on. Speaking physically, the shielding charge generated would again lead to relations between the external K, σ_f (or yield stress), and the size of the deformed region satisfying Eqs. (34.9) and (34.10) provided the system is steady state. Again, the conditions on the local k would involve the distance to the first shielding dislocation. This distance will always be greater than zero, because sources of dislocations are always distributed in the bulk matrix on a very heterogeneous scale. Since k is determined by this close-in dislocation distribution for steady-state shielding, there will again be a limiting lower bound for c associated with the dislocation

[137] S. J. Burns and W. W. Webb, *J. Appl. Phys.* **41**, 2078, 2086 (1970).

source distribution. Since B is a decreasing function of V because of the rate dependence of dislocation generation, there will always be a limiting velocity where the required shielding at the crack tip cannot be achieved, and the crack will break away from its shielding charge.

Thus the shielding relations of Part VII,34 lead to the same breakaway physics as Hart's continuum analysis. However, the shielding relations show that the breakaway is intimately connected with the dislocation structure close to the crack tip, whereas the physical basis for breakaway is less clear in Hart's analysis.

The prediction by Hart that the crack will be completely shielded in the creep regime at very low velocities so that stationary cracks are impossible is a statement which should be taken seriously for some cases. It suggests that a material can behave in a brittle way for sufficiently high strain rates, but blunt out any brittle crack at low strain rates by deformation in the bulk. Materials which are brittle at room temperature (even though some deformation may be present), but ductile at very high temperatures for ordinary testing machine strain rates, suggest this behavior. On the other hand, of course, there are many cases where a static description of a shielded stationary crack is a valid picture.

The discussion of this subsection raises an important property of moving cracks, namely that when shielding dislocations are present, and the crack moves, then a wake is left behind as the crack moves. For purposes of modeling the toughness of the material, the existence of the wake is a crucial factor, because it represents a part of the dissipation, and it contributes to the overall stress. Hart has dealt with this term in an analytic way in work yet unpublished for the Mode-III continuum solution, but Hirth *et al.*,[138] and Thomson and Sinclair[33] also discuss the problem from the standpoint of the forces on the total configuration. This problem has also been extensively investigated in the continuum plasticity approximation.[139]

b. Inertial Effects

The mathematics of time-dependent crack motion is subtle and fascinating. This result will not be surprising to those familiar with the analysis for dynamic dislocations.[20] For a recent review of the elastic problem, the reader is referred to an excellent paper by Freund.[140]

The steady-state stress problem is relatively easy to solve, and complex function methods quite similar to those of Part III lead to the result that the

[138] J. P. Hirth, R. G. Hoagland, and C. H. Popelar, *Acta Metall.* **32**, 371 (1984).
[139] J. Rice, *in* "Mechanics of Solids" (H. Hopkins and M. Sewell, eds.), p. 539. Pergamon, Oxford, 1982.
[140] L. B. Freund, *Mech. Today* **3**, 55 (1976).

moving crack is again characterized by a K field, but that the value is decreased by comparison to the static value. Thus

$$K(v) = \sqrt{\frac{2}{\pi}}\, h(v) \int_0^{vt} (vt - x)^{-1/2}\, \sigma(x)\, dx, \tag{39.2}$$

in complete analogy to the static semi-infinite crack, but where h is a nearly linear function of v given in Fig. 54 for Mode I. In Mode III, the Lorentz contraction comes into play on the displacement and stress functions in the expected way on the x axis. Thus, the complex function, $\eta(z)$, of Eq. (8.2) becomes

$$\eta(x - vt) = \left(\frac{1 - v/c}{1 + v/c}\right)^{1/4} \eta_0\left(\frac{x - vt}{\sqrt{1 - v^2/c^2}}, y\right), \tag{39.3}$$

where η_0 is the static crack function and c is the shear sound speed. In this case, the function $h(v)$ becomes simply

$$h(v) = \left(\frac{1 - v/c}{1 + v/c}\right)^{1/4} \left(1 - \frac{v^2}{c^2}\right)^{1/4}. \tag{39.4}$$

Further, the instantaneous force on the crack tip can be found (140) and is given in Mode I by the result

$$f = (K_0^2/E)(1 - v^2)g(v), \tag{39.5}$$

where K_0 is the static value of K_I and $g(v)$ is again shown in Fig. 54. This result states that, when a fracture criterion such as $f = 2\gamma$ is given and γ is a constant, then the external load as specified by K_0 must be increased to supply the energy to open the crack surface. The extra energy input is, of course, put into the radiation field of the crack.

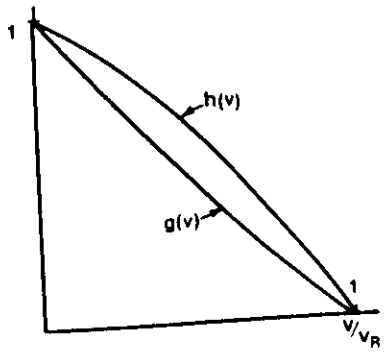

FIG. 54. Functions $g(v)$ and $h(v)$ for Eqs. (39.5) and (39.2).

The startling result for non-steady-state motion is that an elastic crack has no inertia. As a source of stress in a medium governed by a wave equation, one would expect a radiation resistance inertia for the crack such as exists for the classical electron and for the dislocation.[20] In Mode III, the solution has been discussed by Eshelby, and in an elegent paper,[141] he shows that the lack of inertia follows from the fact that the Mode-III crack solution is a "distortionless" solution of the wave equation. That is, a general solution of the wave equation in two dimensions exists of the form

$$\sigma = \frac{1}{z^{1/2}} f(r \pm ct), \tag{39.6}$$

$$z = re^{i\theta},$$

from which a crack solution can be constructed for arbitrary motion. The characteristic crack $1/z^{1/2}$ function is thus a fundamental form for the two-dimensional wave equation. The result which can be constructed easily from Eq. (39.6)—and the argument is almost transparent from Eq. (39.6)—is that a crack can be stopped suddenly from a state of uniform motion, and the precise steady-state stress distribution is radiated out from the center with velocity c. Since the radiated solution is precisely the static solution, no radiation resistance is exerted on the crack. This surprising result is true even though the crack is equivalent to a virtual dislocation distribution over the cleavage surface, and these dislocations, singly, do possess an inertia. The point is that the coherent interaction between the crack dislocations cancels the inertia of the collective motion when they move as a crack.

Freund has shown[140] that the full static solution is not radiated when a crack is stopped similarly in plane strain (Mode I or II) for all angles. However, the static solution is generated along the crack line in front of the crack, and this is sufficient for the Mode-I and Mode-II cracks to possess zero inertia also.

The foregoing results are valid only for semi-infinite cracks. Freund shows that for finite cracks interactions between the crack tips modify the non-steady-state character of crack motion in an essential way.[140]

40. Time-Dependent Cleavage/Emission Considerations

There has already been occasion to note that several cases exist where brittle cleavage cracks appear to be observed running at high speed in materials which are demonstrably ductile in the sense of the criterion, Eq. (28.5).

[141] J. D. Eshelby, *in* "Physics of Strength and Plasticity" (The Orowan 65th Anniversary Volume, A. Argon, ed.), p. 263. MIT Press, Cambridge, Mass., 1969.

Pugh[142] has shown that a crack in brass started at an embrittled site is able to propagate for a distance of the order of tens of micrometers in fast cleavage before coming to rest. There are similar findings in pure copper under corrosion conditions.[143] After nucleation at sites in dislocation cell boundaries, Wilsdorf finds that fast cleavage occurs in foils of copper and gold under stress for distances of the order of a few to 10 micrometers.[6] Ohr *et al.*[10] report that cleavage is initiated in Al in the configuration of Fig. 13 and again runs as a fast cleavage crack through the foil for a distance of micrometers before arrest. Gerberich[144] has shown that cracks in Fe/Si single crystals can be made to propagate as cleavage cracks at high velocities with some, but small dislocation activity, whereas stationary cracks in this material take the wedge shape, according to Vehoff and Rothe.[99] The observations in thin films may be affected by the thin-film geometry, e.g., by rapid slideoff, but the results in thicker specimens are not subject to this objection.

These results suggest that the competition between cleavage and emission is velocity dependent, and proposals along this line have been made by various authors. Jokl *et al.*[145] proposed a model of combined emission and cleavage, where shielding of the crack plays a part in the emission criterion. Rather crude assumptions are made, however, about the basic mechanisms competing at the crack tip. Knott[146] has proposed a very interesting model for virtual dislocation emission, in which an emitted dislocation falls back into the cleavage surface after the crack moves on. Such a mechanism would lead to an enhanced effective γ for a fast-moving crack, because of the energy dissipation of dislocations popping in and out of the crack, but would yield a clean cleavage crack as a result. Paskin *et al.*[63] have simulated fast moving cracks in materials which are ductile for static cracks, and the cleavage is clean. On the other hand, a paradox exists, because if a crack has zero inertia, an emitted dislocation will stop the crack. Once stopped, of course, by postulate, the crack will simply emit dislocations as the stress builds up. Thus, an adequate understanding of the dynamic crack–dislocation interaction does not yet exist.

Appendix

In this appendix, some essential basic mathematics of elasticity is collected. The Appendix is in three parts. In the first, the governing equations for plane strain are developed in terms of the Goursat potential functions. In the second, a generalized conformal-mapping analysis for these functions is developed. In the third part, the mathematics relevant to the use of Muskhelishvili's singular integrals is presented.

[142] E. N. Pugh, *in* "Atomistics of Fracture" (R. Latanision and J. Pickens, eds.), p. 997. Plenum, New York, 1983.
[143] K. Sieradsky, R. Sabatini, and R. Newman, *Met. Trans. A* **15**, 1941 (1984).
[144] W. Gerberich, unpublished results.
[145] M. Jokl, V. Vitek, and C. J. McMahon, *Acta Metall.* **28**, 1479 (1980).
[146] J. Knott, *in* "Atomistics of Fracture" (R. Latanision and J. R. Pickens, eds.), p. 209. Plenum, New York, 1983.

1. Plane-Strain Field Equations

The mathematical development of this and the following section is based on papers by Stevenson,[147] and Tiffin,[148] but some of the same results will be found in the Muskhelishvili treatise.[15] In plane strain, the displacement u_i satisfies and $u_3 = 0$. u will be taken to be a complex vector

$$u = u_1 + iu_2, \tag{A.1}$$

and

$$\frac{\partial}{\partial x_1} = \frac{\partial}{\partial z} + \frac{\partial}{\partial \bar{z}}; \qquad \frac{\partial}{\partial x_2} = i\left(\frac{\partial}{\partial z} - \frac{\partial}{\partial \bar{z}}\right)$$

Derivatives of u (which is not yet assumed to be analytic) are given by

$$2\frac{\partial u}{\partial z} = \theta + 2i\mathscr{W}, \qquad \theta = u_{i,i}; \qquad \mathscr{W} = \tfrac{1}{2}(u_{i,j} - u_{j,i}). \tag{A.2}$$

θ is the dilatation, and $\mathscr{W}$ the rotation.
The equilibrium equations (7.1) become

$$\begin{aligned} \sigma_{11,1} + \sigma_{12,2} &= 0, \\ \sigma_{22,2} + \sigma_{12,1} &= 0. \end{aligned} \tag{A.3}$$

Multiplying the second equation by i and adding yields

$$\frac{\partial}{\partial z}(\sigma_{11} - \sigma_{22} + 2i\sigma_{12}) + \frac{\partial}{\partial \bar{z}}(\sigma_{11} + \sigma_{22}) = 0 \tag{A.4}$$

This equation states the condition for the existence of a potential function F, such that with Eqs. (A.1) and (7.2),

$$-\frac{\partial F}{\partial \bar{z}} = \sigma_{11} - \sigma_{22} + 2i\sigma_{12} = 4\mu\frac{\partial u}{\partial \bar{z}}, \tag{A.5}$$

$$\frac{\partial F}{\partial z} = \sigma_{11} + \sigma_{22} = 2(\lambda + \mu)\theta. \tag{A.6}$$

[147] A. C. Stevenson, *Proc. R. Soc. London Ser. A* **184**, p129, p218 (1945).
[148] R. Tiffen, *Q. J. Mech. Appl. Math.* V, 352 (1952).

Equation (A.5) is immediately integrable to give

$$4\mu u = f(z) - F(z, \bar{z}) \tag{A.7}$$

Substituting Eq. (A.2) into (A.6) gives

$$\frac{1}{2(\lambda + \mu)} \frac{\partial F}{\partial z} = 2\frac{\partial u}{\partial z} - 2i\theta \tag{A.8}$$

From Eq. (A.6), because θ is real, $\partial F/\partial z$ is real, and Eq. (A.8) is also real. Hence, substitution of Eq. (A.7) into (A.8) leads to

$$\frac{\partial F}{\partial z} = \frac{\lambda + \mu}{2(\lambda + 2\mu)}\left[\frac{\partial f}{\partial z} + \overline{\left(\frac{\partial f}{\partial z}\right)}\right] = 2\varphi'(z) + \overline{\varphi'(z)}. \tag{A.9}$$

The function φ' is defined by Eq. (A.9). This equation is now integrable, giving

$$F(z, \bar{z}) = 2[\varphi(z) + z\varphi^{*\prime}(\bar{z})] + 2\psi^*(\bar{z}). \tag{A.10}$$

The star operator is defined by

$$\varphi^*(z) = \overline{\varphi(\bar{z})}, \qquad \text{etc.} \tag{A.11}$$

and is a convenient way to show explicitly that $\bar{\varphi}$ and $\bar{\psi}$ are functions of $\bar{z}$, not z.

Now Eqs. (A.5), (A.6), and (A.7) take the form

$$\sigma_{11} + \sigma_{22} = 2[\varphi'(z) + \overline{\varphi'(z)}], \tag{A.12}$$

$$\sigma_{22} - \sigma_{11} + 2i\sigma_{12} = 2[\bar{z}\varphi''(z) + \psi'(z)], \tag{A.13}$$

$$2\mu u = \kappa\varphi(z) - z\overline{\varphi'(z)} - \overline{\psi(z)}, \tag{A.14}$$

$$\kappa = 3 - 4\nu \qquad \text{(plane strain)}. \tag{A.15}$$

Equations (A.12)–(A.15) are the new field equations of plane-strain elasticity. They are expressed in terms of the two independent complex functions, $\varphi(z)$ and $\psi(z)$, even though the stresses and the displacement functions are not necessarily complex functions of z. If the displacement is a single-valued function of z (and perhaps $\bar{z}$), then the elastic problem automatically satisfies the incompatibility equations discussed in all elasticity books. In the form of the theory used here, however, they need not be addressed explicitly. For example, if dislocations are present as singularities, then φ' and ψ' have poles at the position of the dislocation, and the u function is multivalued there, with

$$\Delta u\Big|_{z=\zeta} = b = b_1 + ib_2. \tag{A.16}$$

We will not consider continuous distributions of dislocations, but in that case,

the appropriate Burgers-vector density function can be defined. The functions φ and ψ are the standard potential functions of Goursat,[149] e.g., as used in Muskhelishvili.[15] In plane strain, the Burgers vector defined by Eq. (A.3) corresponds to an edge dislocation with components b_1 and b_2, and to a crack in either Mode I or Mode II.

The general elastic solution, combining antiplane strain with plane strain, with a screw component of a Burgers vector as well as edge components, and including mixtures of Modes I, II, and III, is a simple linear combination of stresses and displacements calculated from the three independent potential functions, $\eta(z)$, $\varphi(z)$, and $\psi(z)$ with stresses and displacements given by Eqs. (8.1) and (8.2) and (A.12)–(A.15).

Generally speaking, since φ, ψ, (and η) are complex functions, solutions are obtained for an elastic problem by applying considerations of analyticity and function theory to the potential functions in the light of the boundary conditions set on the problem by the existence of free surfaces, behavior of stress at ∞, multivaluedness of u, etc.

2. Conformal Mapping

One of the important ways to solve two-dimensional boundary value problems is by means of conformal mapping, in which complicated problems are transformed into simpler soluble ones. The same is true of elastic problems, except that in this case, since tensors are involved, the analysis must be generalized beyond that familiar in electrostatics or hydrodynamics.

Consider a coordinate transformation which maps the z plane (the initial problem) into the ξ plane (the simpler problem) and the real coordinates, x_1, x_2, into the new coordinates, y_1, y_2. In real coordinates the transformation law from the tensor $A_{ij\cdots}(x_1, x_2)$ into the new tensor $A'_{pq\cdots}(y_1, y_2)$ is given in standard notation

$$\begin{aligned} A'_{pq\cdots}(y_1, y_2) &= \beta_{pi}\beta_{qj}\cdots A_{ij\cdots}(x_1, x_2), \\ \beta_{pi}\beta_{pj} &= \delta_{ij}, \\ dx_i &= \sum_j \frac{\partial x_i}{\partial y_j} dy_j = \sum_j h_{(i)}\beta_{ij}\, dy_j. \end{aligned} \tag{A.17}$$

Here the β are the rotation matrices, and the tensors are not separated into their contra- and convariant parts. The advantages of this form of the transformation law is that stress tensors do not change their dimensional

[149] E. Goursat, *Bull. Soc. Math France* **26**, 236 (1898).

units when transformed into a new coordinate system. (See Morse and Feshbach[150].) The β are functions of position in general.

A rotation suitable for transforming vectors and tensors which are complex functions is now required. If the mapping of z into ξ is given by the functional relationship

$$z = z(\xi), \tag{A.18}$$

then the rotation angle α of the x_1 coordinate into the y_1 coordinate at the position z is given by

$$dz = \left|\frac{dz}{d\xi}\right| e^{i\alpha}\, d\xi, \tag{A.19}$$

and the transformation law Eq. (A.17) for a complex vector $A(z)$ into the new vector $A_T(\xi)$ is given by

$$A_T(\xi) = e^{-i\alpha} A(z). \tag{A.20}$$

A problem in notation arises here, because the standard notation for a transformed quantity is the prime as used in Eq. (A.17). In the complex plane, however, the prime will be reserved for differentiation with respect to a complex variable. Hence the subscript T will be used to denote a transformed quantity. Since z' in general is a function of position, the rotation angle varies also with position z. The reader is also reminded that the functional form of $A_T(\xi)$ is recovered from the substitution

$$A_T(\xi) = A_T(\xi(z)) = A(\xi(z))e^{-i\alpha} = A(z)e^{-i\alpha}. \tag{A.21}$$

In this article, it will be implied that when the new coordinate ξ is used as an independent variable in a function f, the functional form is defined by $f(\xi) \equiv f(z(\xi))$.

Transformation laws can now be written for the relevant elastic quantities. In antiplane strain, relative to rotation in the x_1, x_2 plane, u_3 is a scalar quantity. Also σ_{3j} relative to the same rotation transforms as a vector. However, since the complex "vector" defined in Eq. (8.2) is related to the complex conjugate of the "true" vector σ_{3j}, the function transforms as follows.

a. Antiplane Strain

$$u_T(\xi) = u(z(\xi)) = u(z), \tag{A.22}$$

$$\sigma_T(\xi) = e^{i\alpha}\sigma(\xi(z)) = e^{i\alpha}\sigma(z). \tag{A.23}$$

In plane strain the following relations hold.

[150] P. Morse and H. Feshbach, "Methods of Theoretical Physics," Vol. I, p. 21. McGraw-Hill, New York, 1953.

b. Plane Strain

$$(\sigma_{11} + \sigma_{22})_T = \sigma_{11} + \sigma_{22}, \tag{A.24}$$

$$(\sigma_{22} - \sigma_{11} + 2i\sigma_{12})_T = e^{2i\alpha}(\sigma_{22} - \sigma_{11} + 2i\sigma_{12})$$

$$= \frac{z'(\xi)}{\overline{z'(\xi)}}(\sigma_{22} - \sigma_{11} + 2i\sigma_{12}), \tag{A.25}$$

$$u_T = e^{-i\alpha}u. \tag{A.26}$$

The first of these equations follows because the contracted stress tensor is a scalar, the second is from direct substitution in the tensor transformation laws, and the third because $u = u_1 + iu_2$ is a true complex vector.

With these transformation laws, the transformed elastic field equations become of the form following.

c. Antiplane Strain

$$u_T(\xi) = \frac{2}{\mu}\operatorname{Im}[\eta(z)] = \frac{2}{\mu}\operatorname{Im}[\eta(z(\xi))], \tag{A.27}$$

$$\sigma_T = e^{i\alpha}\sigma(z) = 2e^{i\alpha}\frac{d\eta}{dz} = 2e^{i\alpha}\frac{d\xi}{dz}\frac{d\eta(z(\xi))}{d\xi} \tag{A.28}$$

d. Plane Strain

$$(\sigma_{11} + \sigma_{22})_T = 2[\varphi'(z) - \overline{\varphi'(z)}] = 2[\Phi(\xi) + \overline{\Phi(\xi)}], \tag{A.29}$$

$$(\sigma_{22} - \sigma_{11} + 2i\sigma_{12})_T = 2e^{2i\alpha}\left(\frac{\overline{z(\xi)}}{z'(\xi)}\Phi'(\xi) + \Psi(\xi)\right)$$

$$= 2\left(\frac{\overline{z(\xi)}}{\overline{z'(\xi)}}\Phi'(\xi) + \frac{z'(\xi)}{\overline{z'(\xi)}}\Psi(\xi)\right), \tag{A.30}$$

$$2\mu u_T = e^{-i\alpha}[\kappa\varphi(z(\xi)) - z(\xi)\Phi(\xi) - \overline{\Psi(z(\xi))}] \tag{A.31}$$

$$\Phi(\xi) = \frac{d\varphi(z(\xi))}{d\xi}; \qquad \varphi(z) = \varphi(z(\xi)) = \int z'(\xi)\Phi(\xi)\, d\xi, \tag{A.32}$$

etc. In these equations, the derivatives of the potentials in the ξ plane are awkward to handle, so for both φ and ψ, the capital functions Φ and Ψ are defined in Eq. (A.32).

The strategy in the use of the conformal-mapping procedure for Eqs. (A.27)–(A.32) is to map the original complicated boundary into a simpler geometry, e.g., a wedge into a half-plane, etc., and solve the new transformed boundary problem in the simpler geometry. There is a "trap" in this strategy, however, when a mapping function is used where the scale factor h is not unity,

then the two coordinate systems are not physically equivalent, since the scale of length is different in the two. Hence, a comparison of two *a priori* solutions in two such coordinate systems without considering the scale factor for length measurements between the two systems will lead to error. For this reason, the strategy here will always be to express the physical problem in the "natural" coordinate system, and use the ξ system only as a mathematical convenience in handling the geometry of the boundary conditions. Note also that in this spirit the potential functions corresponding to the z system are used, exclusively, without ever writing down the transformed potentials. The relations between φ, ψ, etc., and the transformed displacements and stresses are, of course, given by Eq. (A.27)–(A.32). When these potentials are written in terms of the new coordinates ξ, however, it does not mean the new functions are then the new transformed potentials, which would relate to the new stresses by relations such as Eqs. (A.12)–(A.15), etc.

In order for this strategy to work conveniently, it must be true that the boundary conditions are "covariant." That is, if on the initial boundaries,

$$\sigma_{ij} n_j = 0, \tag{A.33}$$

the condition on the new transformed boundary is also given by

$$\sigma'_{ij} n'_j = 0. \tag{A.34}$$

This statement is proved by direct substitution of the transformation laws. If there are external forces exerted on the boundaries F_i, then these are, of course, transformed into the forces F'_i.

3. The Hilbert Problem and the Integral Equation of Muskhelishvili

In treating slit cracks and dislocation pileups in the text, the elegant mathematical theory developed by Muskhelishvili and the Russian school has been invoked.[15] These results will be summarized here. The reader is also referred to an alternative real-variable treatment of some of the same singular integrals by Bilby and Eshelby in the Appendix of their article in "Fracture."[16]

In the fracture problem in Part III, it is desired to find the complex potential function generated from a stress distribution on the crack surfaces. To this end, we write the Cauchy formula for a function $f_0(z)$ at an arbitrary point not on the cleavage surface in terms of an integral over the contour of Fig. 55:

$$f_0(z) = \frac{1}{2\pi i}\int_L \frac{f_0^+(t)}{t-z}\,dt - \frac{1}{2\pi i}\int_L \frac{f_0^-(t)}{t-z}\,dt + \frac{1}{2\pi i}\int_{C_\infty} \frac{f_0(\zeta)}{\zeta - z}\,d\zeta. \tag{A.35}$$

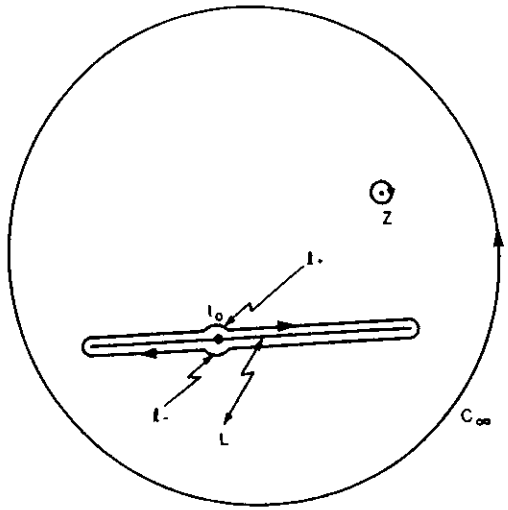

FIG. 55. Contour for integrals in Eqs. (A.35) and (A.43). The contour encloses the cut L. It contains a pole at z for Eq. (A.35), and circles around t_0 for Eq. (A.43).

Mathematically, the cleavage surface is a branch line, and is denoted by L. $f_0(z)$ is assumed to be analytic everywhere in the complex plane except on L, and to approach zero at ∞ in such a way that the integral over C_∞ is zero. f_0^+ and f_0^- are the limiting values of $f_0(\zeta)$ on the positive and negative sides of L. Hence

$$f_0(z) = \frac{1}{2\pi i}\int_L \frac{g(t)}{t-z}\,dt, \qquad g(t) = f_0^+(\zeta) - f_0^-(\zeta). \tag{A.36}$$

This equation is a solution of a form of the Hilbert problem. That is, it gives $f(z)$ in terms of an integral over a boundary. It should be noted that Eq. (A.31) and other similar results in this Appendix are valid only when $f(z)$ is sufficiently continuous on L, and at its end points.

In the fracture problem, the known stress function on the cleavage plane is not $f_0^+ - f_0^-$ but $f_0^+ + f_0^-$. To proceed in this case, a property of the function

$$\chi(z) = [(z-a)(z+a)]^{-1/2} \tag{A.37}$$

is noted. That is, on $-a < t < a$.

$$\chi^+(t)/\chi^-(t) = -1. \tag{A.38}$$

Hence, the ratio $f_0(z)/\chi(z)$ has the property

$$\left[\frac{f_0(z)}{\chi(z)}\right]^+ - \left[\frac{f_0(z)}{\chi(z)}\right]^- = \frac{f_0^+}{\chi^+} - \frac{f_0^-}{\chi^+}\left[\frac{\chi^+}{\chi^-}\right] = \frac{f_0^+ + f_0^-}{\chi^+}. \tag{A.39}$$

Substitution of Eq. (A.39) into (A.36) yields

$$f_0(z) = \frac{\chi(z)}{2\pi i}\int_L \frac{h(t)}{\chi^+(t)(t-z)}\,dt, \qquad h(t) = f_0^+(t) + f_0^-(t). \tag{A.40}$$

In this discussion, the function χ thus serves the role of an integrating factor, and Eq. (A.40) is a solution of a second form of the Hilbert problem, suitable for application to fracture when the function h is known.

The solutions, Eqs. (A.36) and (A.40), are not the most general functions which can be generated, when g and h are known, because analytic functions can be added to them, which are continuous on the boundary L. Thus, when P_n is a polynomial of degree n, a more general solution is

$$f(z) = \frac{\chi(z)}{2\pi i}\int_L \frac{h(t)}{\chi^+(t)(t-z)}\,dt + \chi(z)P_n(z), \qquad h = f^+ + f^-. \tag{A.41}$$

A similar generalization holds for Eq. (A.36). The polynomial is, of course, fixed by the behavior of f at ∞. Further generalization of Eq. (A.41) can be derived when L consists of multiple segments, not necessarily straight.[15] In the special case of a set of segments lying on the x axis, the integrating factor is simply composed of a product of functions, Eq. (A.37), one for each segment. The results for this latter case have been summarized by Head and Louat,[151] but these more complicated cases will not be required in this article.

The second invocation of the Muskhelishvili theory is in Part VII, where the problem of a pileup of dislocations in the presence of a crack is addressed. In this case, it is desired to invert a singular integral equation similar to those above, a solution which was first given by Muskhelishvili.[152] In this development, the so-called Plemelj equations arise, and we begin with their derivation.

Consider the Cauchy integral

$$\int \frac{f_0(\zeta)}{\zeta - t_0}\,d\zeta = 0 \tag{A.42}$$

on the contour given in Fig. 55. In this case, t_0 is on the contour L. Then

$$0 = \frac{1}{2\pi i}\oint \frac{f_0(\zeta)}{\zeta - z_0}\,d\zeta = \frac{P}{2\pi i}\int_L \frac{f_0^+(t)}{t-t_0}\,dt - \frac{P}{2\pi i}\int_L \frac{f_0^-(t)}{t-t_0}\,dt + \frac{1}{2\pi i}\int_{l_1} \frac{f_0^+(\zeta)}{\zeta - t_0}\,d\zeta + \frac{1}{2\pi i}\int_l \frac{f^-(\zeta)}{\zeta - z_0}\,d\zeta + \frac{1}{2\pi i}\int_{C_\infty} \frac{f_0(\zeta)}{\zeta - t_0}\,d\zeta. \tag{A.43}$$

[151] A. K. Head and N. Louat, *Aust. J. Phys.* **8**, 1 (1955).
[152] N. Muskhelishvili, "Singular Integral Equations." Noordhoff, Groningen, 1953.

P (without subscript) denotes the Cauchy principle value, and $f_0(\infty) = 0$ so that the integration over C_∞ is zero. Rearranging terms, Eq. (A.43) becomes

$$\frac{P}{\pi i}\int \frac{g(t)}{t-t_0}\,dt = h(t), \qquad g = f^+(t) - f^-(t), \qquad h = f^+(t) + f^-(t). \tag{A.44}$$

Equations (A.44) are the Plemelj equations,[15] and their inversion is desired for the solution of the dislocation pileup problem. That is, h represents the known external stress on the dislocations, and g represents the dislocation distribution which is sought.

The inversion of Eq. (A.44) is obtained immediately by the application of Eq. (A.41) first to calculate $f^+(t)$ and then to calculate $f^-(t)$. Noting the property, Eq. (A.38), then subtraction of $f^+(t)$ from $f^-(t)$, yields

$$g(t_0) = \frac{\chi^+(t_0)}{\pi i}P\int_L \frac{h(t)}{\chi^+(t)(t-t_0)}\,dt + \chi^+(t_0)P_n(t_0). \tag{A.45}$$

The polynomial is determined once more by the property of f at ∞. Again, though there will not be a need for it in this article, when L consists of a set of segments on the x axis, the solution proceeds from an integrating function composed of products of functions like Eq. (A.39), and a general prescription will be found in Head and Louat.[151]

Acknowledgments

It is a great pleasure to acknowledge my colleagues at NBS for the years we have spent in collaboration in this field. Special thanks are due to E. Passaglia and I.-H. Lin for their careful reading of the manuscript.